Copyright Warning & Restrictions

The copyright law of the United States (Title 17, United States Code) governs the making of photocopies or other reproductions of copyrighted material.

Under certain conditions specified in the law, libraries and archives are authorized to furnish a photocopy or other reproduction. One of these specified conditions is that the photocopy or reproduction is not to be "used for any purpose other than private study, scholarship, or research." If a, user makes a request for, or later uses, a photocopy or reproduction for purposes in excess of "fair use" that user may be liable for copyright infringement,

This institution reserves the right to refuse to accept a copying order if, in its judgment, fulfillment of the order would involve violation of copyright law.

Please Note: The author retains the copyright while the New Jersey Institute of Technology reserves the right to distribute this thesis or dissertation

Printing note: If you do not wish to print this page, then select "Pages from: first page # to: last page #" on the print dialog screen

ABSTRACT

CONTROLLED REDUCTION OF GRAPHENE OXIDE AND GRAPHENE OXIDE-CARBON NANOTUBE HYBRIDS AND THEIR APPLICATIONS

by
Samar Azizighannad

Graphene and graphene derivatives are widely used in diverse research and industrial applications. Graphene production on a large scale is carried out by exfoliating graphite oxide and producing graphene oxide (GO), which comprises of graphene sheets with different oxygen-containing functional groups such as hydroxyl, carboxyl, and carbonyl. GO is reduced to reduced graphene oxide (rGO), which has properties that are closer to graphene. Properties of GO and rGO depend upon the oxygen content, and the effect of reducing oxygen content on the aqueous behavior of rGOs is not well understood.

In an effort to understand how properties of rGO change as GO is reduced, a stepwise reduction of the same GO to rGO containing different levels of oxygen was carried out, and their corresponding chemical and colloidal properties are reported. Starting with GO containing 49 percent oxygen, rGOs containing 31, 19, and 9 percent oxygen were synthesized. The aqueous behavior in terms of solubility and dispersibility is presented.

In the second part, the controlled synthesis of reduced graphene oxide-carbon nanotube (rGO-CNT) hybrids and their aqueous behavior is reported. The CNTs are suspended in an aqueous dispersion of GO, and the GO-CNT hybrids are reduced in-situ in a controlled fashion using nascent hydrogen. Several hybrids with oxygen content ranging from 26 to 2% were synthesized. The properties of the hybrids with a low degree

of reduction were closer to GO, while those with a high degree of reduction were closer to CNTs. Solubility, dispersibility, hydrophobicity, critical coagulation concentration (CCC value), and zeta potential of the hybrids are studied and compared.

Finally, as a major application of some of the above-mentioned materials is the development of polyacrylamide (PAM) gel polymer electrolytes (PGE) with doped nano carbons. Carboxylated CNTs referred to as (fCNTs), GO, and the hybrid of fCNT/GO embedded in the PGE were fabricated as supercapacitors (SC). Thermal stability of the pristine PGE increased with the addition of carbon nanomaterials which led to lower capacitance degradation and longer cycle life of the SCs. The fCNT/GO-PGE showed the best thermal stability, which was 50% higher than PGE. Viscoelastic properties of PGEs were improved with the incorporation of GO and fCNT/GO into the PGE structure. Oxygen-containing groups in GO and fCNT/GO formed hydrogen bonds with polymer chains and improved the elasticity of PGE. Yet, fCNT-PGE showed a slightly lower viscous strain modulus due to its ununiform distribution in the polymer matrix and the defects that were formed within. Furthermore, ion diffusion between GO layers improved in carbon-based composites, which was enhance in fCNT/GO-PGE because fCNTs decreased the aggregation of GO sheets and enhanced the ion channels, thus increasing the ionic conductivity from 41 to 132 mS cm^{-1}. Finally, MnO_2-based supercapacitors containing PGE, fCNT-PGE, GO-PGE, and fCNT/GO-PGE electrolytes were fabricated, and their performances were examined. This research demonstrated the effectiveness of carbon nanomaterials as dopants in polymer gel electrolytes for property enhancements.

CONTROLLED REDUCTION OF GRAPHENE OXIDE AND GRAPHENE OXIDE-CARBON NANOTUBE HYBRIDS AND THEIR APPLICATIONS

by
Samar Azizighannad

A Dissertation
Submitted to the Faculty of
New Jersey Institute of Technology
in Partial Fulfillment of the Requirements for the Degree of
Doctor of Philosophy in Materials Science and Engineering

Department of Physics

May 2021

APPROVAL PAGE

CONTROLLED REDUCTION OF GRAPHENE OXIDE AND GRAPHENE OXIDE-CARBON NANOTUBE HYBRIDS AND THEIR APPLICATIONS

Samar Azizighannad

Dr. Somenath Mitra, Dissertation Advisor — Date
Distinguished Professor of Chemistry and Environmental Science, NJIT

Dr. Nuggehalli M. Ravindra, Committee Member — Date
Professor of Physics, NJIT

Dr. Edgardo T. Farinas, Committee Member — Date
Associate Professor of Chemistry and Environmental Science, NJIT

Dr. Tao Zhou, Committee Member — Date
Associate Professor of Physics, NJIT

Dr. Keun Hyuk Ahn, Committee Member — Date
Associate Professor of Physics, NJIT

BIOGRAPHICAL SKETCH

Author: Samar Azizighannad

Degree: Doctor of Philosophy

Date: May 2021

Undergraduate and Graduate Education:

- Doctor of Philosophy in Materials Science and Engineering,
  New Jersey Institute of Technology, Newark, NJ, 2021

- Master of Science in Nanofiber Structures Engineering,
  Amirkabir University of Technology, Tehran, Iran, 2014

- Bachelor of Science in Textile Technology and Fiber Science Engineering,
  Amirkabir University of Technology, Tehran, Iran, 2011

Major: Materials Science and Engineering

Publications:

Samar Azizighannad, Zhiqian Wang, Zain Siddiqui, Vivek Kumar, Somenath Mitra, "Carbon Nanomaterials Doped Polyacrylamide Gel Electrolytes for High Performance Supercapacitors" - Under review- 2021

Samar Azizighannad, Somenath Mitra, "Controlled Synthesis of Reduced Graphene Oxide-Carbon Nanotube Hybrids and Their Aqueous Behavior"- *Journal of Nanoparticle Research*- 22: 130- 2020

Samar Azizighannad, Worawit Intrchom, Somenath Mitra, "Raman Imaging of Membranes Fouling"- *Separation and Purification Technology*- Volume 242, 116763-2020

Samar Azizighannad, Somenath Mitra, "Stepwise Reduction of Graphene Oxide (GO) and Its Effects on Chemical and Colloidal Properties"- *Scientific Reports*- Volume 8, 10083- 2018

Indrani Gupta, Samar Azizighannad, Somenath Mitra, " Antiviral Properties of Nanocarbons and Their Functionalized Analogs"- Under review- 2021

MohammadSaiful Islam, Faradae Renner, Samar Azizighannad, Somenath Mitra, "Direct Incorporation of Nano Graphene Oxide (nGO) into Hydrophobic Drug Crystals for Enhanced Aqueous Dissolution"- *Colloids and surfaces B: Biointerfaces*- Volume 189, 110827- 2020

Zhenglong Li, Yu Hsuan-Cheng, Lixin Feng, De Felix, Neil Jacob, Reis Pedro Antonio, Juliana Yang, Maryom Rehman, Samar Azizighannad, Somenath Mitra, and Sagnik Basuray, "Electrochemical Impedance Signature of a Non-planar, Interdigitated, Flow-through, Porous, Carbon-Based Microelectrode"- *Journal of The Electrochemical Society*- 166, B1669- 2019

Krishna Prasad Gannavarapu, Samar Azizighannad, Murali Krishna Molli, Meera Pandey, V. Sai Muthu Kumar, Somenath Mitra, Rajesh Babu Dandamudi , "Nanoporous Hierarchical Carbon Structures Derived from Fungal Basidiocarps for High Performance Supercapacitors"- *Energy Storage*- 1:e58- 2019

Krishna Prasad Gannavarapu, Samar Azizighannad, Sai Muthukumar, Somenath Mitra, Rajesh Babu Dandamudi- "Microwave-Assisted Biogenic Synthesis of Metal-Decorated Reduced Graphene Oxide and their Electrochemical Properties"- *ChemistrySelect*- 03420- 2018

Presentations:

Samar Azizighannad, Somenath Mitra, "Synthesis of Reduced Graphene Oxide/Carbon Nanotubes Composites and their Colloidal Behavior " – Oral presentation at 2020 American Chemical Society (ACS) national meeting and expo, Philadelphia, Pennsylvania

Samar Azizighannad, Worawit Intrchom, Somenath Mitra, "Quantifying and Imaging of Membrane Fouling using Raman Chemical Imaging"– Poster presentation at 2020 American Chemical Society (ACS) national meeting and expo, Philadelphia, Pennsylvania

Samar Azizighannad, Somenath Mitra, "Colloidal and Chemical Properties of Graphene Oxide and Step Wisely Reduced Graphene Oxide"- Oral presentation at 2019 American Chemical Society (ACS) national meeting and expo, Orlando, Florida

Samar Azizighannad, Somenath Mitra , "Structure Function Relationship in the Variation of Colloidal Behavior of Reduced Graphene Oxides and Their Fate in Aqueous Environments", Poster presentation at 2017 Annual Meeting of the APS Mid-Atlantic Section- Newark, New Jersey

*"To my parents, **Nasser and Faegheh**, who I could not be where I am without their endless love and support"*

*"To my sister, **Sahar**, who makes me stronger"*

*"Last but not least, to my beloved husband, **Siamak**, who patiently walked with me through this journey"*

ACKNOWLEDGMENT

First of all, I would like to express my gratitude and respect for my mentor and supervisor Dr. Somenath Mitra, and I would like to thank him for his endless help and great support throughout my study. I had a great opportunity by coming to NJIT to improve my research skills and I had the advantage of working in well-equipped NJIT labs under a great mentor and supervisor.

Next, I would like to express my deepest appreciation to my committee members, Dr. N. M. Ravindra, Dr. Edgardo D. Farinas, Dr. Tao Zhou and Dr. Keun Hyuk Ahn for providing valuable advice and useful comments. I am also grateful for Dr. Xueyan Zhang, Dr. Jeon Seop Shim and Dr. Larisa Krishtopa for helping me with the experiments and their technical support. Many thanks to Physics and Chemistry department administrative support from Ms. Christine Oertel, Ms. Leslie Williams and Ms. Genti M. Price for their valuable assistance. Also, my thanks go to my research group members: Dr. Zhiqian Wang, Dr. Sagar Roy, Dr. Worawit Intrchom, Mohammad Saiful Islam, Indrani Gupta, Mitun Chandra Bhoumick and Sumona Paul.

Finally, I cannot begin to express my thanks to my parents enough my parents, Faegheh and Nasser, for their unlimited love, kindness and care. I am extremely grateful to my sister, Sahar, who has been always on my side. And last but not least, I would also like to extend my deepest gratitude to my lifetime partner, Siamak, for believing in me. With all of these supports, I would not have been able to accomplish this dissertation.

TABLE OF CONTENTS

TABLE OF CONTENTS
(Continued)

TABLE OF CONTENTS
(Continued)

Chapter **Page**

LIST OF TABLES

LIST OF FIGURES

LIST OF FIGURES
(Continued)

LIST OF FIGURES
(Continued)

CHAPTER 1

INTRODUCTION

1.1 Background and History of Carbon-based Nanomaterials

Carbon is the base element of different materials and nanomaterials depending on carbon-carbon bonds with sp, sp^2, and sp^3 hybridizations. The very first researches on the chemical and physical properties of graphite started in the 1950s [1]. Fullerene or buckyball is the first carbon nanomaterial discovered in 1985 [2] that is a closed mesh of pentagonal or hexagonal carbon-carbon bonds [3]. A monolayer of the graphene sheet that is sp^2 hybridized hexagonal carbon-carbon bonds was discovered by H. P. Boehm in 1962 [1]. Yet, the study on graphene did not continue due to the lack of characterization techniques. In 1991, carbon nanotubes discovered accidentally while researching on fullerene application, and S. Iijima published a paper named "Helical microtubules of graphitic carbon" as a start to the new era for carbon-based nanomaterials [4]. Iijima referred to carbon nanotubes as needle-like graphitic sheets and inspired research in the 1990s to be focused on carbon nanotubes. Since then, research on nanocarbons and their application has increased due to the fact that synthesis and application of them have been significantly developed. Until 2004, Novoselov and Geim exfoliated graphite and achieved the single layer of graphene and published a paper titled "Rise of graphene" [5].

In the past 20 years, since the "Rise of graphene," there have been numerous studies on the structure, applications, and derivatives of carbon-based nanomaterials. The research continues to develop carbon applications, this fascinating ancient element.

1.2 Objectives of This Study

Graphene and graphene derivatives are widely studied in materials science and condensed materials physics. There is a rising number of research on graphene production and application. Production of graphene in large scales is by exfoliating graphite oxide. Byproduct of this process is graphene oxide (GO) which is graphene sheets with different oxygen-containing groups. GO is reduced to reduced graphene oxide (rGO), which has closer properties to graphene. Properties of GO and rGO highly depend on oxygen content. There is a gap in a basis for accurate comparison as to how properties change with such reduction. In this research, new aspects of graphene-based materials are introduced and analyzed as noted below:

- Control oxygen content in graphene oxide and characterize them
- Study aqueous behavior of step-wisely reduced graphene oxide
- Reduce graphene oxide in the presence of carbon nanotubes
- Study aqueous behavior of graphene oxide-carbon nanotubes composites properties change under *in situ* reduction and with oxygen content.

1.3 Dissertation Outline

This dissertation includes five chapters. Chapters 1 and 2 are introduction and literature review about graphene, graphene oxide, and reduced graphene oxide. A study about the application of carbon nanomaterials in electronic devices is discussed. Chapter 3, in an effort to understand how properties of rGO change as GO is reduced, a stepwise reduction of the same GO to rGO containing different levels of oxygen was carried out, and their corresponding chemical and colloidal properties are reported. The continuing project, Chapter 4, reports the controlled synthesis of reduced graphene oxide-carbon nanotube

(rGO-CNT) hybrids and their aqueous behavior. The CNTs were suspended in an aqueous dispersion of GO, and the GO-CNT hybrids were reduced *in situ* in a controlled fashion using nascent hydrogen. This approach is novel and provides insight into rGO-CNT hybrids, which are very different from those made by mixing CNTs with rGO. This study also provides a basis for true comparison as to how chemical and colloidal behavior of stepwise reduced GO-CNT composites are changing depending on the degree of reduction. Lastly, Chapter 5 presents GO, functionalized carbon nanotubes (fCNT), fCNT-GO hybrids effects on an acrylamide gel electrolyte cast in a three dimensional printed cells to study thermal, mechanical, and electrochemical properties of generated composites. Figure 1.1 shows a graphical abstract for this dissertation.

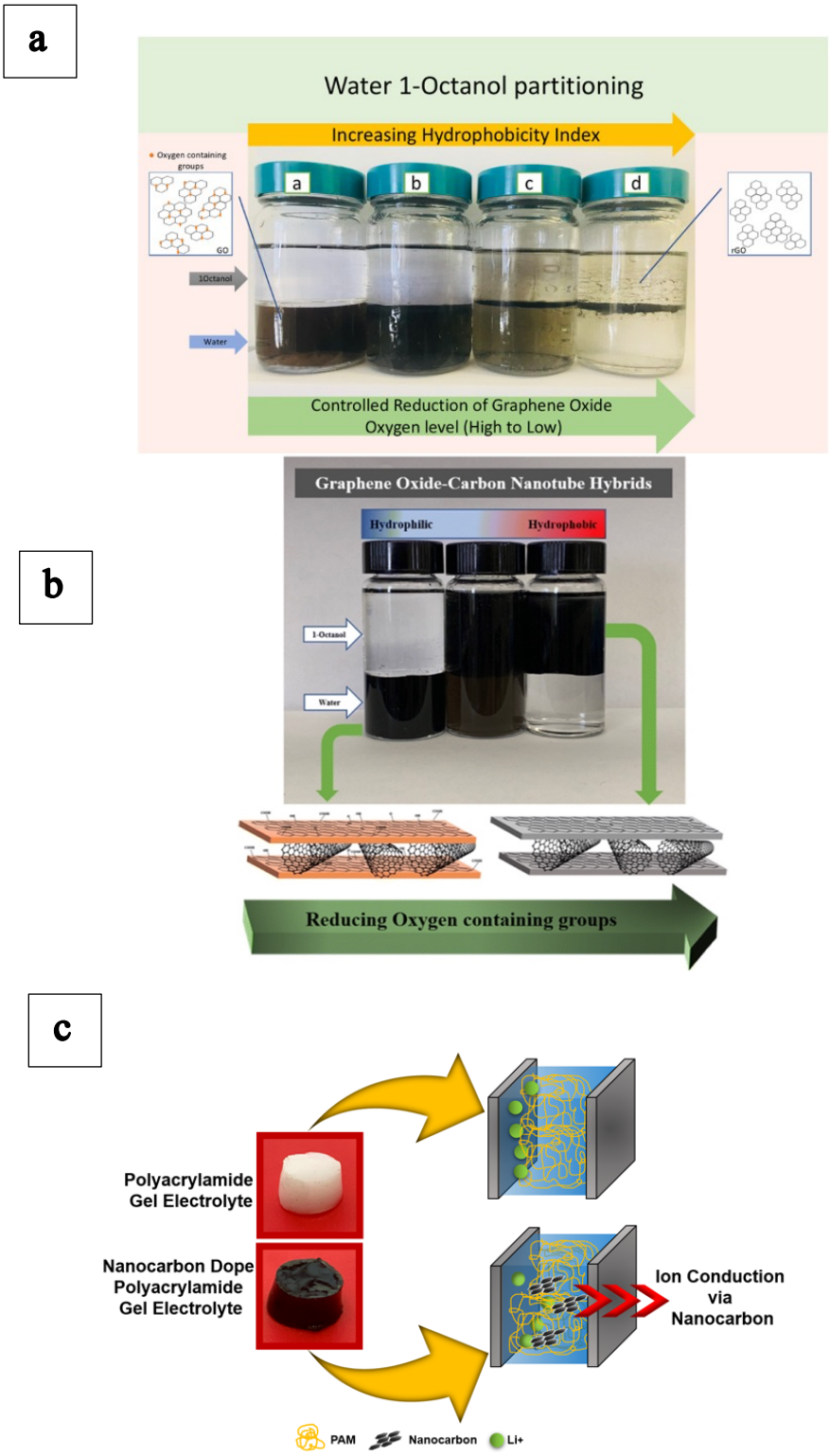

Figure 1.1 **a)** Step wisely reduced graphene oxide, **b)** Controlled reduction of graphene oxide in the presence of carbon nanotubes, **c)** Studying carbon nanomaterials doped gel electrolyte.

CHAPTER 2

LITERATURE REVIEW

This chapter presents an introduction to graphene and its derivatives to explain why there are so many interests in this allotrope of carbon and its unique characteristics. A literature review on several applications for graphene-based nanomaterials as well as distinctive specification that makes them a great candidate research topic is discussed accordingly. After a short introduction to carbon nanotubes, additionally, it demonstrates how carbon nanotubes-graphene alters their effectiveness in different applications. Ultimately, the application of nanocarbon in electronic devices is presented in summary.

2.1 Graphene, Graphene Oxide, and Reduced Graphene Oxide

Since the discovery of fullerene in 1985, there have been numerous studies on various structures of nano carbons [2]. Carbon-based nanomaterials with a variety of nanostructures and morphologies such as nano onions, nanohorns, nanosheets, nanofibers, and nanocages attracted the researcher's attention [2,6]. The most recent allotrope of carbon that has been proposed by computational simulation is Hp-C17 which consists of 17 carbon atoms in a hexagonal cell with an all-sp^3 network [7]. Allotropes of carbon have very different unique properties based on sp, sp^2, and sp^3 hybridizations with different characteristics which make them capacitive for a wide range of applications [6-8]. Carbon attaches to the different elements properly and alters final properties, which makes carbon nanomaterials even more interesting with countless applications in different industries [6]. One of the rapidly

growing research fields is graphene and graphene-based nanomaterials which is a single layer of strongly bonded carbon atoms.

2.1.1 Properties

Graphene is a two-dimensional (2D) structure with a single layer of flat sp^2 carbon sheet with excellent electrical, mechanical, thermal, and optical properties [9-11]. Stacked graphene layers that interact with each other are considered graphite, a very well-known structure of carbon-based materials. Since it was impossible to detect a single layer of atoms in a flake, the discovery of graphene was delayed, and the properties were out of sight for many years after graphite [12]. The numerous weak bonding between the layers prevents the graphene sheets from separating and holds the stack together. Unique properties of a single layer of graphene compared to graphite arise from electron confinement in two dimensions [13,14]. A graphene sheet is a cluster of aromatic macromolecules with a much higher specific area than activated carbon. 2D structure of the graphene is the leading block in producing other hybridized sp^2 structure of carbon atoms [15]; for instance, carbon nanotubes are the rolled form of graphene sheets, and fullerene is the wrapped form of graphene sheet [16-18]. Figure 2.1 introduces the formation of carbon nanomaterials from honeycomb structure graphene sheet. Strong carbon-carbon bonds in the flat configuration are either rolled up in sphere fullerene structure or tubular carbon nanotubes. Properties of carbon nanotubes are discussed in Section 2.1.1.

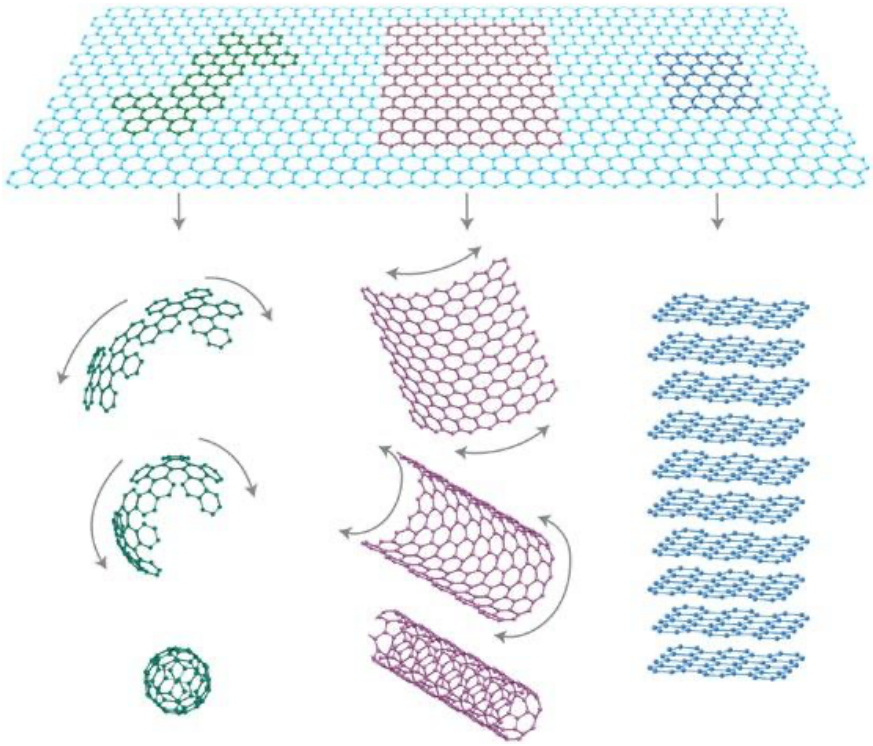

Figure 2.1 Different forms of the graphene sheets.
Source: [19]

Carbons in the honeycomb structure of graphene are connected in sigma bonding and make it hard for other atoms to replace a carbon but, graphene structure includes different kinds of defects, such as topological defects (pentagons, heptagons, or both), impurities, vacancies, displacement of carbon atoms and defects on the edges [10,20,21]. These defects can be observed with transition electron microscopy (TEM) at sub-Ångstrom resolution and Raman spectroscopy [16]. There are two main peaks in the Raman spectrum of graphene: one is at ~1580 cm^{-1} which is according to the G-band, and one is at ~1350 cm^{-1} which is according to the D-band [10,13,16]. G band in Raman spectrum is related to the in-plane optical vibration. D-band in the non-defective graphene will be eliminated. Raman spectrum also can be used to determine the number of graphene layers; for example, increasing the number of layers will cause a downshift in the location of the G-band [22].

There are two approaches to investigate mechanical properties and Young's modulus of a single layer or multilayer graphene sheets: molecular dynamics simulation [16] and atomic force microscopy (AFM) [23]. Mechanical properties also highly depend on defects [16]. Researches have shown that Young's modulus and fracture strength for non-defective graphene are 1 TPa and 130 GPa, respectively [24]. Other important properties of graphene are zero-band gap, large surface area (2630 m^2g^{-1}), high mobility (1.5x104 $cm^2\ V^{-1}\ S^{-1}$), and high thermal conductivity (5000 W $m^{-1}\ K^{-1}$) [25]. It is crucial to study defects and disorders in graphene since it has an important role in the overall mechanical and electrical properties of graphene. Higher disorder and defects in the graphene structure lower the final electrical conductivity [26]. Difficulties in the production process, along with agglomeration and low solubility of graphene, limit the general application of this group of carbon nanomaterials [6]. Impurities, the addition of functional groups, and doping graphene with other atoms will establish a new category of materials with different properties than graphene. Graphene sheets are doped with elements such as Phosphorus [25], Nitrogen [27-29], Boron [30], Sulfur [31], as well as functional groups in order to improve electrochemical properties. Graphene that includes oxygen-containing groups referred to as graphene oxide is one of the most common graphene derivatives that have been widely studied.

Graphene oxide (GO) is also a single layer of sp^2 carbon layer which includes hydroxyl (-OH), carboxyl (-COOH), carbonyl (C=O), alkoxy (C-O-C), and other oxygen-containing groups [32-34]. It mostly contains 45-55% oxygen which makes it highly soluble in aqueous solutions. Compared with pristine graphene, GO contains remarkable structural defects which are related to oxygenated groups [35,36]. The electrical, mechanical, and

chemical properties of GO highly depend on oxygen-containing groups [9]. Polar oxygen-containing groups make GO highly water-soluble and suitable for aqueous phase procedures, for instance, drop-casting, sparing, and spin coating, which need well dispersed, uniform, and stable solutions [37]. Oxygen-containing functional groups are proper sites to modify GO by a variety of functional groups such as metals [38], enzymes [37], DNA [39], and bacteria [40]. Functionalized GO will be a new opportunity to access benefit graphene properties in different divisions [41]. Moreover, the engineering of GO allows reaching insulating, semiconducting, and conducting materials according to the final application. The number of researches on GO is increasing due to its processability, easy synthesis, and versatile properties. An optical image of GO shows wrinkles and folding of the sheets, which shows the flexibility of GOs. The size of the GO flakes depends on the graphite that has been used in the production process, and it varies from nanometer to millimeter scale. Depending on the final application of GO, the size of the flakes can be reduced to a nanoscale by a simple sonication procedure [42]. For instance, in bio-applications and drug delivery systems, nano-size GO is a better candidate [43].

Removing oxygen-containing functional groups in GO will produce reduced graphene oxide (rGO). rGO is a general term that refers to the GO samples that have been in chemical, electrochemical, physical, and other techniques to remove oxygen-containing groups from GO [16]. Properties of rGO are strongly dependent on the oxygen content of the carbon sheets. It starts from 44% to almost no oxygen content which has very similar properties to graphene. Whenever properties of graphene are proper for final application GO will be reduced to generate rGO since GO production is a more simple procedure than graphene production.

2.1.2 Synthesis and Preparation

Preparation of graphene is very critical in order to reach the desired size, number of layers, and purity [12]. Two essential methods to produce nano-scale materials are top-down and down-top paths [44]. Chemical vapor deposition (CVD) [16] is a down-top approach to produce high-quality single-layer graphene sheets. During the CVD process desired structure of graphene is produced by decomposing of selected hydrocarbon and lateral growth on the substrate in a reaction chamber [45]. This is a very low speed with a production rate of a few microns per hour. Down-top methods such as (CVD) and epitaxial growth [46] produce high purity graphene, but they are very complicated methods with high cost and high maintenance processes. There are a few researches about the preparation of graphene out of carbon nanotubes (CNT) which is called un-zipping of CNTs [47]. In this method, CNTs will subject to open up longitudinally by chemically exfoliation, mechanical, electrochemical, and hydrothermal methods [48]. For instance, CNTs in the intercalation of lithium and ammonia continuing process by acid exfoliation will produce nanoribbons and graphene concurrently [49]. Plasma etching is also sufficient to open up CNTs. CNT un-zipping proceeds low quantities of graphene and is not scalable, and methods have been reported earlier [13]. The top priority of graphene production is to make high-quality, scalable sheets in order to be used in large-scale applications. Top-Down methods such as graphite oxide exfoliation are the most common path to produce graphene on large scales. In the very beginning steps, scotch tapes were used to mechanically exfoliate graphite oxide sheets to produce few layers of graphene oxide (GO), which is the oxidized graphene sheet including hydroxyl, epoxy, carbonyl, and carboxyl functional groups [12]. The product was used to fabricate electronic devices, but the applications were

limited due to the insufficient exfoliation process. Hummer's method was developed in 1958, which is a chemical process that starts with oxidation of graphite to increase interlayer distance and proceeds with exfoliation of graphite oxide [6]. In this chemical process, potassium permanganate is added to sodium nitrate and sulfuric acid, including graphite. Organic solvents such as dimethylformamide (DMF), tetrahydrofuran (THF), and ethylene glycol can be used to exfoliate graphite oxide. The product of exfoliation of graphite oxide is GO [50]. Figure 2.2 summarizes the procedure of Hummer's method in a graphical format. Based on Figure 2.2, two steps of GO production are oxidation of graphite sheet and exfoliation of graphite oxide. Hummer's method is the most common approach to produce inexpensive GO on large scales for further application due to the low cost of raw materials and uncomplicated process.

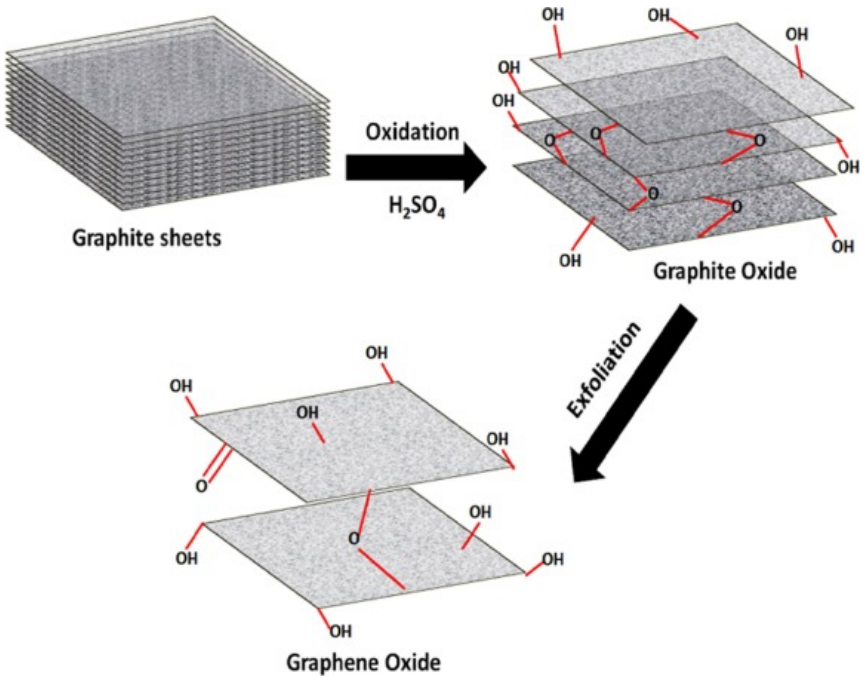

Figure 2.2 Formation of graphene oxide from graphite sheets by Hummer's method. *Source:[51]*

The main disadvantage of Hummer's method is that the oxidation of sodium nitrate emits toxic gasses. There are different studies on modification of Hummer's method, which proposes the replacement of sodium nitrate by sulfuric or phosphoric acids and increasing amount of potassium permanganate [52]. There are also other methods to produce graphene including, micromechanical cleavage, mechanical ablation, etc. [53].

Since Hummer's method and modified Hummer's method are inexpensive and easy, they are the most common procedures to produce insulator GOs which should be reduced to conductive rGOs to become processible in electronic devices. GO, which is the oxidized graphene sheet is the more preferred form for composite applications. Since pristine graphene sheets tend to agglomerate and $\pi - \pi$ stacking occurs in flat graphene sheets, GO is mostly used to produce uniform and fully dispersed nanocomposites, followed by removing oxygen-containing groups to reach rGO properties [54]. Removing oxygen content to produce rGO, which has close characteristics to graphene, brought to attention and, it has been several studies on the reduction of GO. The most effective method to produce graphene in large scales is to remove oxygen content in GO structures. There are numerous researches on effective, low cost, non-toxic and mass production of rGOs [16]. The first approach to determine the effectiveness of reduction method is the color of the colloid state. Brown/yellow (depending on concentration) converts to a blackish solution after reduction, and in the solid-state, the brown color of GO transforms into metallic due to the increment of electrical conductivity [55]. Visual differences of GO and rGO in the solid and colloid state are presented in Figures 2.3 a) and b). Figure 2.3 b) shows the brown color of GO aqueous solution changes to black color after reduction. With even a mild reduction and removing a small number of functional groups, solution color

transition happens in the aqueous suspension. This method has been used to verify that the reduction was processed successfully.

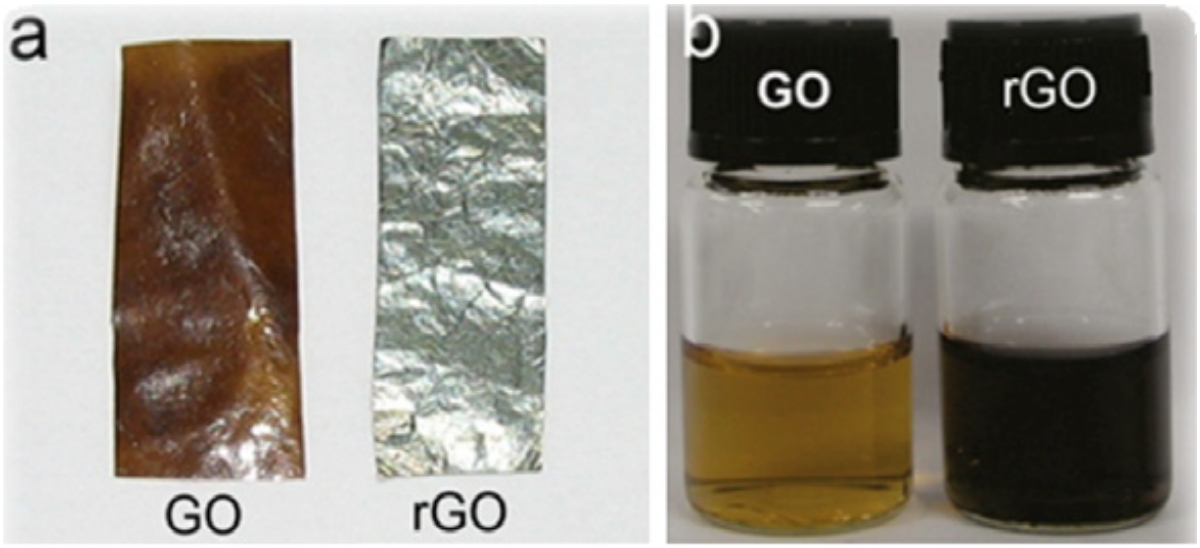

Figure 2.3 Visual differences between GO and rGO.
Source: [16]

Chemical, electrochemical and thermal approaches are used to eliminate oxygen-containing groups in GO. To achieve a high quality rGO, it is important to decrease the reduction process time. As the reduction process time increases, it causes the aggregation of rGO sheets and lower colloidal stability. The most common method that has been used to reduce GO is using hydrazine [9] as reducing agent stirred for 12 hours under 80 ℃. Hydrazine reduced GO shows the closest electrical and structural properties to pristine graphene [54]. A disadvantage of this method is that hydrazine is a toxic agent, and also the process is time consuming, but it is scalable [56]. Other reducing agents that have been used to reduce GO are sodium borohydride ($NaBH_4$) [57], hydroiodic acid (HI) [58], hydroquinone [59], strong alkaline solutions (KOH, NaOH) [16], and hydroxylamine [60].

Among these reducing agents, $NaBH_4$ is mostly used due to the better electrical conductivity of rGO products. The intermediate boron oxide complex acts as an interlayer spacing and prevents stacking of rGO layers [61]. Another chemical reduction route for GO is to use aluminum (Al) or zinc (Zn) in an acidic environment. Al reacts with hydrochloric acid (HCl) and produces hydrogen. Hydrogen reaction with oxygen-containing functional groups generates rGO after 2 hours process [54]. Organic solvents including dimethylformamide (DMF) and alcohols (methanol, ethanol, isopropanol) have been used to remove oxygen content. DMF and GO solution was kept at 153 °C for 1 hour to fabricate a highly conductive (6380 S $m^{-}1$) rGO [54]. Semiconductors such as TiO_2 are used as photocatalysts, and charge separation occurs after UV radiation [62]. Accumulated electrons in this process react with oxygen-containing groups of GO and create rGO. The electrochemical approach to convert GO to rGO occurs in a typical electrochemical cell, including an aqueous buffer at room temperature. Electron exchange between electrodes and GO generates rGO, and there is no need for further reducing agents [63]. Thermal reduction of GO is a heating treatment process at high temperatures, which starts with exfoliating of graphite oxide at the rate of 2000 $℃/min$. High temperature decomposes oxygenated groups attached to carbon into the gas phase [64]. During the rapid exfoliation of graphite oxide, exfoliation, and reduction happen in one step. Yet, it makes wrinkled graphene in very low quantities, and requires specific environment and equipment with high energy consumption. Thermal annealing shows the best electrical conductive rGO among all the reduction methods and in some studies, it has been combined with chemical methods for further oxygen content removal. Furthermore, dispersible GO that has been used in composite production goes under the thermal reduction process to apply *in situ* GO

reduction [54]. There are green approaches to remove oxygen functional groups of GO with no ecotoxicity by using plant extracts such as eucalyptus leaf extracts, green tea, sugar, starch, rose water, pomegranate juice, ganoderma lucidum extract, sugarcane bagasse extract (SCE), lycium barbarum extracts, salvadora persica roots extract, kaffir lime peel extract, spinach leaves juice, asian red ginseng, honeycomb flavone chrysin, caffeic acid, oxalic acid, and gallic acid as reducing agents. rGO produced by this method are colloidally stable in polar and organic solvents, but these are limited sources and reaching large quantities of these materials is the most challenging issue [54]. All mentioned reduction methods can be combined in order to increase efficiency, and reach preferable final product.

Properties of GO and rGO highly depends on carbon to oxygen ratio. Elemental analysis and X-Ray photo electron spectrometry (XPS) are two approaches to determine the C/O ratio. It has been reported that data reached from these two methods are consistent, but the elemental analysis is more useful due to the fact that it presents bulk analysis, unlike XPS, which is more for surface characterization.

2.1.3 Dispersion of Graphene Derivatives in Polar and Non-Polar Solvents

Preparation of graphene and its derivatives in solution form in water or organic solvents plays an essential part in further applications of these nanomaterials. The study of dispersibility and solubility of graphene in water and organic solvents is the first step to prepare uniform solutions. These characteristics highly depend on parameters of graphene derivatives such as functional groups. Oxygen functional groups in the GO increases the surface energy, which leads to the hydrophilicity of GO compared to rGO or pristine graphene. Electrostatic repulsion is the reason that negatively charged GO sheets are

relatively stable in aqueous solutions. However, graphene is highly hydrophobic and instantly agglomerates in the aqueous solutions. Yet, the pristine graphene is more stable in nonpolar solvents compared to GO [18,65,66]. To increase the dispersibility of GO in nonpolar solvents, there are approaches such as functionalization of GO with polymers or other molecules [18]. Studying the aggregation of graphene derivatives in an aqueous solution is also important environmental-wise, and it is essential to understand how nanomaterial particles are transferring in the environment [67]. The dispersibility of graphene nanomaterials can be measured experimentally or using molecular dynamics (MD). MD is an efficient molecular simulation method that uses classical mechanics to anticipate the structure, movement, and geometry of molecules In this case, describes the interaction between solvent molecules on the surface of the nanomaterials [68,69]. MD is a computational approach for having a better understanding of molecular interactions. In one study, Chen et al. used MD and proposed that using a solvent, for instance, dimethyl sulfoxide (DMSO), in aqueous solutions helps with the dispersibility of GO [68]. Figure 2.4 presents MD for GO in DMSO and water solution. Figure 2.4 c) shows water molecules on the GO sheet. And Figure 2.4 b) shows DMSO on the attracted water layer working as a double layer which prevents aggregation of GO sheets.

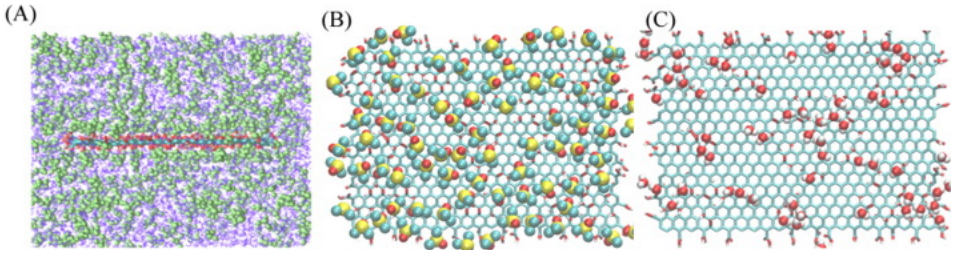

Figure 2.4 Molecular simulations of **a)** and **b)** DMSO and GO in aqueous solutions, **c)** Water layer on GO sheets.
Source: [68]

2.1.4 General Applications of Graphene Derivatives

According to the excellent electrical, mechanical, optical, and thermal properties of graphene, there is a wide range of applications for graphene and graphene derivatives. There are extensive applications from electronics [70] and sensors to biomedicines [71] and environmental sciences for graphene-based materials. Some of the developing applications of graphene are transparent electrodes, electrocatalysts, supercapacitors, fuel cells, and drug delivery systems. Figure 2.5 summarizes the variety of graphene-based applications. The most challenging part with graphene is the size of graphene sheets and the coagulation of them. Also, the insolubility of graphene in aqueous solutions limits some of the applications which can be replaced by GO in order to overcome this dilemma [65,67,72]. Yet, this will cause a lack of fast electron transferring ability in biosensors.

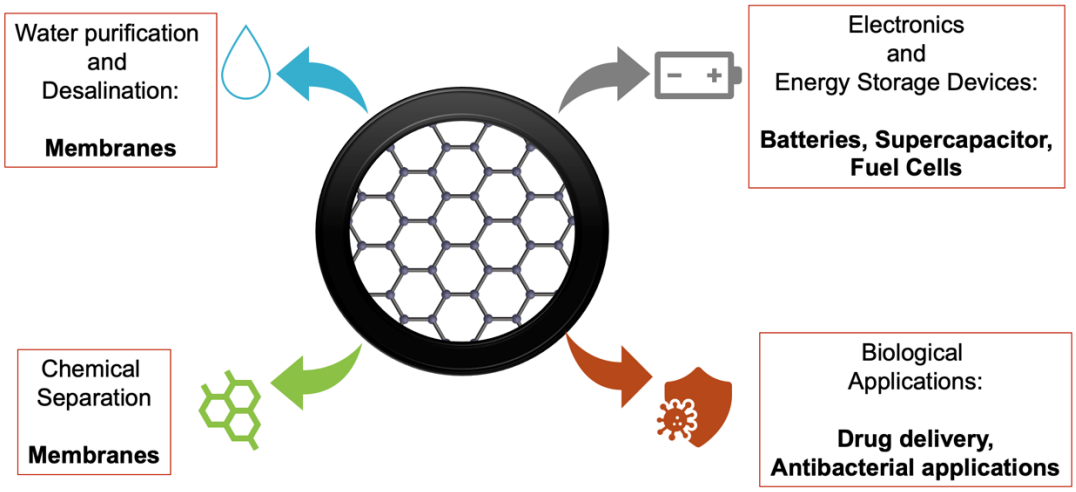

Figure 2.5 Summary of graphene applications.

Graphene has very high mobility, mobility of 200,000 $cm^2\ v^{-1}\ s^{-1}$ [74], mechanical stiffness of 1060 GPa, an excellent light transmittance of 97.7%, a large surface area of 2630 $m^2\ g^{-1}$, and thermal conductivity of 5000 $W\ m^{-1}\ k^{-1}$ [13]. It is also a zero-band gap semiconductor that can be used in nanoribbon form with narrow width and soft edges to reach a sufficient band-gap for transistor applications. Furthermore, engineering band-gap by heteroatomic doping graphene is another approach to fabricate desirable electrical properties for electronic application [75]. Dopants that have been used for graphene are nitrogen [76], boron [77], sulfur [78] and potassium [79,80]. Graphene-based materials have diverse properties from insulators to semiconducting and conducting structures, which broadens the applications in different industries [81]. They also have non-corrosive nature and chemically inert materials [81]. Graphene derivatives are highly used energy storage devices such as batteries, capacitors, and supercapacitors. Details about this category of applications are discussed in Section 2.3.

Applications of graphene-based materials are not limited to electronics, and they can be used for biotechnology and biological studies such as functionalized biosystems. Structural properties, as well as biocompatibility of graphene monolayers, establish a great candidate for biomedical engineering [81]. Figure 2.6 presents the integration of graphene with biological samples in order to improve biocompatibility, solubility, and selectivity. For instance, graphene and GO sheets adsorbed deoxyribonucleic acid (DNA) by $\pi - \pi$ stacking on both sides and used as fluorescence resonance energy transfer (FRET) biosensors and field-effect transistors (FET). FRETs and FETs can be used for living cell detection as well as diagnostics and therapy with excellent selectivity and reproducibility [11,22,81].

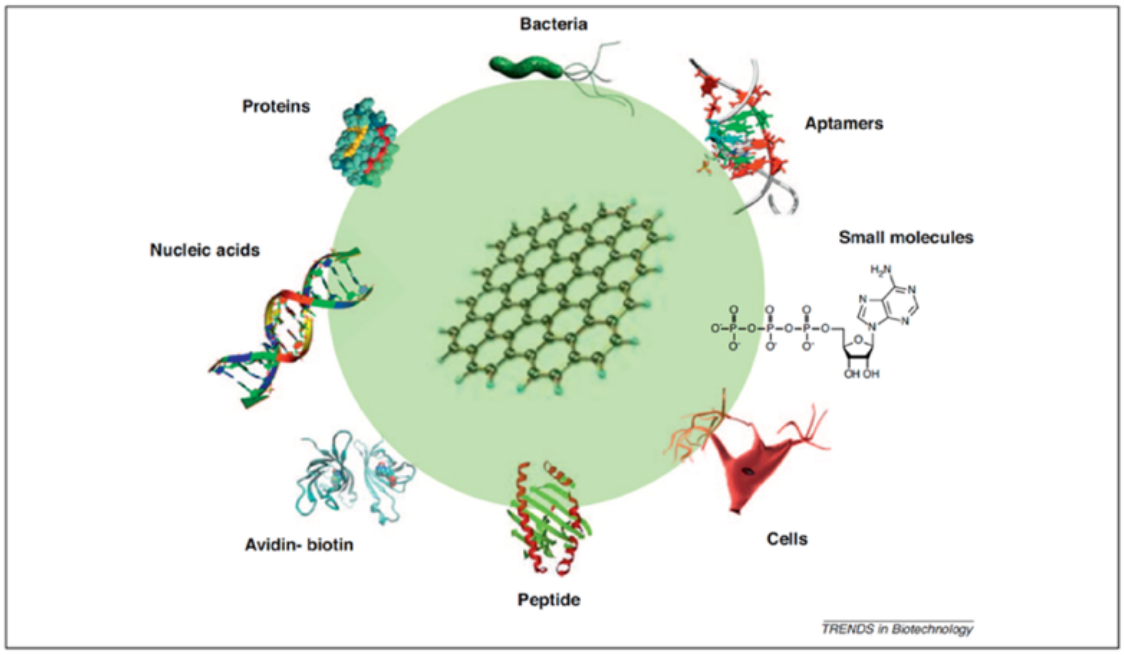

Figure 2.6 Functionalization of graphene with biological samples by physical adsorption or chemical reaction.
Source: [11]

Graphene and its derivatives are proven to be antibacterial with chemical and physical interaction with bacterial cells. Antibacterial mechanisms are the synergy of membrane stress, oxidative stress, and wrapping isolation. But the aggregation behavior of nanomaterials is an important parameter in antibacterial activity. The smaller the size of the nanoparticle, and the higher metallic property show higher cytotoxicity [82,83]. Graphene that has been functionalized with silver nanoparticles, titanium dioxide, zinc, and copper is also studied for its antibacterial properties. In order to functionalize graphene, it should have oxygen-containing groups. Thus, GO or rGO is better candidates for using graphene-based materials along with other antibacterial materials [84]. GO coated polymers are another method to introduce GO to the bacterial environment. Liu et al. used a GO layer

on top of a silicon rubber substrate to reduce the risk of inhalation of GO sheets. This method is easy to recycle and useful in medical instruments [85]. The size of the GO flakes is an important parameter in nano-bio application. Performing ultrasonication of GOs for 1 hour decreases the sheet's size to nanoscale. Incorporation of nano-sized GOs into hydrophobic drugs proposed for fast drug delivery systems [43].

Another application of graphene and its derivates are according to their excellent electrocatalytic properties of them. Graphene/noble metals such as Au, Pt, Pd, and Ru composites are generated by physical vapor deposition, atomic layer deposition (ALD), and wet chemical synthesis. Electrocatalytic-energy-conversion applications, such as the hydrogen evolution reaction and CO_2 reduction was improved in the composites compared to conventionally used methods [86].

Graphene is a useful additive to improve the thermal properties of epoxy resins, such as thermal interface materials (TIM) that are assigned to minimize the thermal contact resistance and improve heat dissipation of electronic devices [87]. The important factor for this application is the high thermal stability of graphene. Graphene, in general, is a great candidate in composite materials in order to increase the overall thermal stability of composites. For instance, in a study addition of 0.05% graphene to polyvinylidene fluoride (PVDF) increased the decomposition temperature by 20°C [88]. Electrical conductivity and thermal conductivity were also surged significantly by introducing graphene to the composite structure.

Besides using graphene in PVDF composite, a thin layer of graphene on top of the PVDF membrane proved a promising nanofiltration system for water purification. The modified membrane showed higher separation rates for organic dyes [89]. There are

difficulties with using graphene-coated membranes since non-defective graphene is a packed layer of carbon and it has impermeable nature [90]. To overcome this issue, membranes coated by defective GO sheets have shown enhanced efficiency in applications of selective ion-transport [91], vapor transport [92], hydrogen separation [93], water transport [94], proton exchange [95], and desalination [96].

The surface plasmon property of graphene and its behavior as a photoluminescence compound make it suitable for the optical sensors, the optical fibers, and photodetectors [73]. Precious metals such as silver and gold can be easily replaced by graphene. Also, it is hard for graphene to be oxidized, unlike silver and gold. In order to reach the photoluminescence properties of graphene, it should be cut in small sheets with 3-20 nm length, and it is called graphene quantum dots (GQD) [97].

Applications of GO are different from graphene since they both have different unique properties. Reactive surface-bound oxygen-containing groups of the GO sheets can be replaced by functional groups and metals in order to reach desirable criteria for further applications. For instance, functionalization of GOs by polymers will make novel composites and, according to selected polymer properties will be different. Electroactive polymers such as polyaniline (PANI) [98], poly- styrene sulfonate (PSS) [99], nafion [100], and poly- diallyl dimethylammonium (PEDOT) [101] incorporated with graphene to enhance electrochemical properties and sensing properties of graphene or polymer sensors. PANI/GO has been used in supercapacitor electrodes and has delivered a uniform structure with higher specific capacitance with better a lifetime of charging and discharging cycle [102]. Both covalent and noncovalent modification of GO has been reported. Electrostatic and hydrogen bonding, as well as $\pi - \pi$ stacking is a noncovalent modification of GOs.

One of the noncovalent methods to generate GO composite is to sonicate functionalization agent and GO in an aqueous or an organic solvent followed by evaporation of the solvent. GO sheets will sandwich polymer between layers. Important parameter in composite applications is the concentration of carbon nanomaterials. Increasing the concentration of graphene-based materials (more than 10%) increases the agglomeration areas and decreases the uniformity of composite [103].

2.1.5 Toxicity of Graphene-Nanomaterials

Increasing usage and applications of carbon-nanomaterials, specifically in biomedicine, increases health and safety concerns. On another aspect, the release of graphene derivatives in the environment and aquatic medium is unpreventable. From a biological point of view, it was demonstrated that highly hydrophobic graphene is toxic due to the accumulation on cell membrane surface followed by DNA damage and oxidative stress [103,104]. Methods to decrease the toxicity of graphene-based materials are surface modification and functionalization as well as composite preparations. A mechanism that was proposed for rGO toxicity in the aquatic environment is that rGO with lower oxygen content on the edges are acting like a nano blade and disturb algal cells [104].

Additionally, the reaction of graphene derivatives with air pollutants and threading human life by migration of particles through inhalation should be studied in detail. Interaction between graphene and air pollutants such as ozone (O3), oxygen difluoride (OF_2), carbon monoxide (CO), phosgene ($COCl_2$), nitrogen oxides, and sulfur oxides was studied by Zhou et al. It was concluded that pristine graphene is weakly attached to the pollutants and there was no significant change in physical and chemical properties of graphene [105].

2.2 Graphene Oxide and Carbon Nanotube Hybrids

2.2.1 Carbon nanotubes, Structure, and Properties

Tubular and rolled-up graphene sheets called carbon nanotubes (CNT) was discovered in 1991 by Iijima [106]. There are two variations of CNTs: single-walled CNTs, and multi-walled CNTs based on tubes with different structural, and slightly different properties [107]. Besides excellent thermal, mechanical and electrical properties of CNTs, the 1D CNT structure brings up new "line-to-point" contact areas between the CNT framework in composites [108,109]. Different functional groups were introduced to carbon nanotubes in order to change some properties such as solubility and dispersibility, as well as expanding the applications of CNTs. Oxidizing CNTs by acid treatment is the most used functionalization process, which will establish the sites for further functionalization. Carboxyl functional groups added inert chemicals and defect-free tubes in sulfuric acid and nitric acid mixture in order to increase the dispersibility and solubility of CNTs [110]. Further functionalization of CNTs with amine, metals, and biological species are also reported in several researches. Based on a study by Zhang et al. amine-functionalized CNT showed better performance in removing heavy metals due to the functional groups coordination with heavy metals [111]. Maleki et al. prepared aminated CNTs to increase dye adsorption in wastewater treatment [112]. The presence of oxygen-containing groups on CNTs increases the interaction of metals such as gold (Au), silver (Ag), and platinum (Pt) with CNT walls and fabricates more stable products for electronic applications [113].

2.2.2 Advantages of Using Graphene and Carbon nanotube Hybrids

Graphene and carbon nanotubes (CNT) are two sp^2 hybridized structures of carbon. CNT is the rolled-up graphene sheet in a single wall and multi wall shape. The high length to diameter ratio, high electrical conductivity, and mechanical strength of CNTs have made them very attractive among carbon nanomaterials. Applications of graphene and GO are increasing due to their unique structure and properties, but it is difficult to maintain the single layer of the sheets [114]. Modification of CNT or GO is a method to improve their properties, yet, some intrinsic properties will change after modification [115]. One method to improve the properties of CNT and GO is fabricating hybrids with these two components followed by combining their properties. Recent studies show altered properties of graphene/CNT and GO/CNT over individual graphene and CNT materials [8,20]. Figure 2.7 represents scanning electron microscopy and transmission electron microscopy of graphene and CNTs. Figure 2.7 e) shows the TEM image of the CNT-GO hybrid that CNT has been distributed between GO sheets. It is proved that the agglomeration of CNTs and GOs will be decreased by using the GO-CNT hybrid over the individual components. GO-CNT hybrids are mostly used in composite materials, and the distribution of fillers in composites is a crucial point in composite production [116]. Band gap and electrical properties of the hybrids change over single materials, and it should be considered in electronic applications [114]. The most important property in the hybrids is the synergetic effect the in their structure which improves the ultimate performance [8].

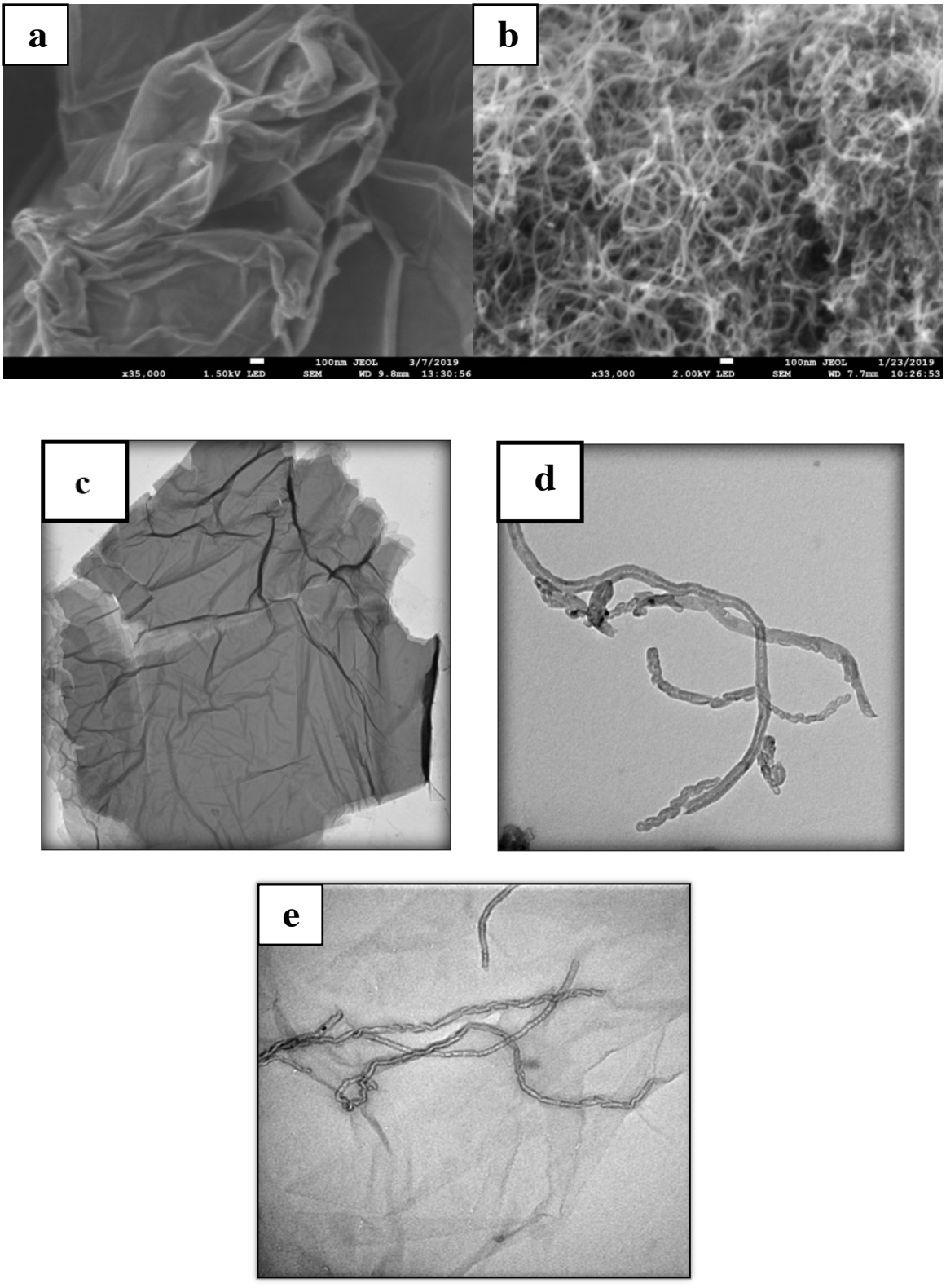

Figure 2.7 Scanning electron microscope images of **a)** Graphene, **b)** Carbon nanotubes, and Transmission electron microscope images of **c)** graphene and **d)** Carbon nanotubes, **e)** Graphene- CNT hybrid.

The main problem with individual CNT and graphene, is low dispersibility in organic and aqueous solvents. CNTs tend to tangle and agglomerate because of the van der Waals forces making them unsuitable for use in composites [67]. The lower dispersibility of CNTs are, the more uneven composite will be produced. Carboxylation of carbon nanotubes is a method to increase the dispersibility of them in the aqueous solutions, but it will affect their properties of them. GO has been used in different studies as a dispersing CNTs in the solutions. GO is an inexpensive, easily produced single layer of oxidized carbon layer that can be used as a dispersing agent for CNTs [117].

However, an important consideration is that aggregation of graphene sheets is often an unwanted process during GO reduction. This is a well-known phenomenon and leads to the formation of hard agglomerates. Processible rGO, which is suitable for further applications, should have minimum interaction between layers. The presence of CNT in GO-CNT hybrids prevents hard agglomeration of GO during the chemical reduction of oxygen-containing groups [118].

2.2.3 Synthesis of Graphene/CNT Composites

The preparation of graphene/CNT hybrids and their applications have been investigated in different studies. CNTs will be distributed in graphene/CNT hybrid in three different orientations. Based on Figure 2.8, in type 1 CNTs will disperse between the layers of graphene sheets, in type 2 will indent in the graphene sheets, and in type 3 CNTs will wrap around GO sheets. Type 1 is the most common form of hybrids, which does not need any specific formation method, and graphene works as a substrate for CNT. Type 2 shows better plane electrical conductivity, and mechanical strength, and CNT grows on graphene sheet by means of catalysts. Preparation of perpendicularly attached CNTs to graphene

sheet is a difficult structure to achieve and it depends on the aspect ratio of each component. This is a unique structure of core-shell complex with an increased oscillating frequency of nanometers and reduced damping coefficient. Formation of graphene/CNT composites consists of the following methods: Chemical vapor deposition (CVD), layer by layer assembly (LBL), vacuum filtration (VF), electrophoretic deposition (EPD), and *in situ* reduction (ISR) [119].

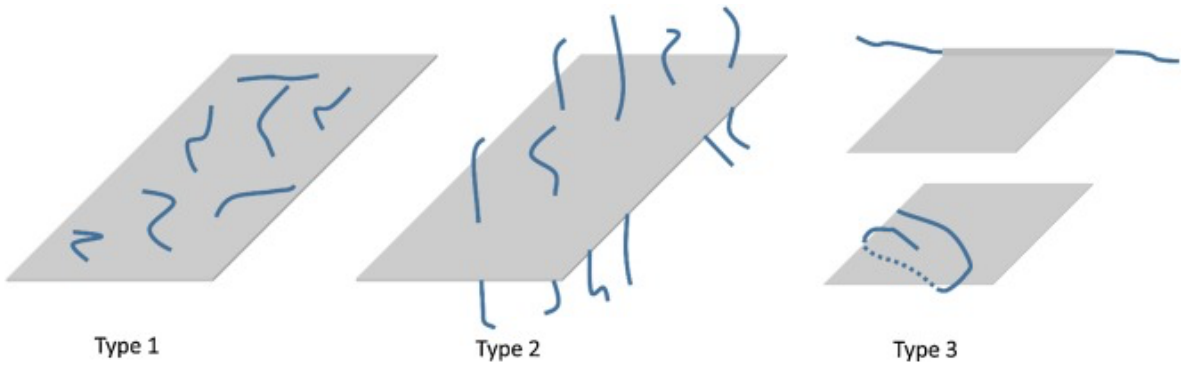

Figure 2.8 Different types of distribution of CNTs in graphene CNT composites. *Source: [119]*

CVD, which is mostly used for thin-film fabrication, has been used to attach CNTs vertically on the graphene from both ends. The idea is the formation of graphene on the substrate and CNT growth on the graphene sheet through catalyst followed by etching of the first substrate. In the next step, CNT will be sandwiched between graphene layers. The length of CNTs is around 100 nm and uniformly distributed between graphene layers [120]. Graphene-CNT-graphene sandwich has a high specific capacity that is suitable for electronic devices [121]. LBL is also two-phase process that is based on oppositely charged components. Interaction between graphene and CNT is formed on electrostatic forces that can be applied in larger areas. Self-assembled uniformly sandwich layers of graphene and

CNT is also used in electronic devices. VF that is a method to separate solids and liquids, is an easy technique to prepare GO-CNT hybrid films. GO, and CNT should be dispersed in a solution followed by VF on a membrane filter. The film will be removed from the membrane and transferred on a proper substrate for further applications. The challenges in the VF technique are selecting a suitable surfactant in order to reach a homogenous solution. Graphene and CNT are both hydrophobic and are not going to disperse in the aqueous solutions, so N-methyl pyrrolidone (NMP), block copolymers, tetra butyl titanate, and gallic acid has been proposed in order to reach a uniform solution. Microporous polyvinylidene fluoride membrane with a pore size of 0.45 has been used to separate solids from the liquid and generate a hybrid film [119].

2.2.4 Applications of Graphene/CNT Composites

Using CNT and GO separately in composites have been extensively studied throughout the years; their effectiveness in altering electrical, thermal, and mechanical properties have been proved. Carbon nanotubes- graphene hybrids also have been used in different areas such as energy storage devices (batteries, supercapacitors) [122-125], sensors, composite materials [24,126] and, water purification [127,128]. A different variation of CNT and graphene have been used based on the final application of the product. Carboxylated and pristine CNTs, along with GO and rGO, have different electrical and ionic conductivity depending on functionalization groups. But for all these variations, there is $\pi - \pi$ stacking interaction between CNTs and Graphene layers which increases synergistic effects in the hybrids and improves overall properties. Synergetic effect in all these combinations is the key parameter that makes CNT-Graphene hybrid so unique for further applications [119]. In a study, Polybenzimidazole composite showed improved electrical conductivity and

tensile strength after reinforcing polymer by GO-CNT in comparison to using GO and CNT separately in the polymer matrix [129]. In another study, Song suggests sandwiching polymer between fCNT and rGO by attaching the polymer chain to fCNT at the first step and attaching the polymer functionalized by fCNT to the rGO at the second step [34]. Improvement of thermal conductivity and mechanical strength of styrene-butadiene rubber was the outcome of this approach. Graphene-CNT was used for fire protection and improving thermal stability as well as water-resistance of the composites [130]. Overall, carbon nanofillers are very effective additives in composite production since they have a higher impact on thermal conductivity and mechanical properties with minimum filler content [131]. CNT-rGO has been used as an additive to ionic liquids in high vacuum to reduce friction and improve wear resistance [119,132]. This idea opens a new class of applications in space. Wimalasari proved in a research that CNTs in GO-CNT hybrid works as a diffusion path for ion conduction and increases the porosity of the structure. This phenomenon increases the specific capacity of the hybrids and makes them beneficiate for energy storage devices [133].

Another application for GO-CNT hybrids is in membrane separation. Polyimide membranes reinforced with the hybrids for gas separation approaches. It was concluded that membranes including GO-CNT showed improved gas sensing and separation performance [134]. Sui et al. used GO-CNT hybrid for water purification approach and proved the potential of hybrids in deionization of light metal salts and heavy metal ions, as well as removing organic dyes [127]. In a study by Liu et al. epoxy reinforced composites with 0.5% GO-CNT for enhancing microwave and electromagnetic absorbing properties [115].

2.3 Application of Carbon-based Nanomaterials in Electronic Devices

2.3.1 Energy Storage Devices

Climate change caused pollutions produced by human being have become an important concern in current days. Fossil energy sources are the main origin of greenhouse gases, mainly carbon dioxide, and also, they are limited resources for consuming energy in future days. Environmental issues and the limitation of fossil energy sources have highlighted the importance of other energy sources such as solar, wind, and electric energy [135,136]. Converted energy from renewable sources such as wind and solar resources needs to be stored effectively to increase efficiency. Energy storage systems have been through so many improvements in the past decades. Performance comparison of different energy storage devices is presented in the Ragone plot in Figure 2.9.

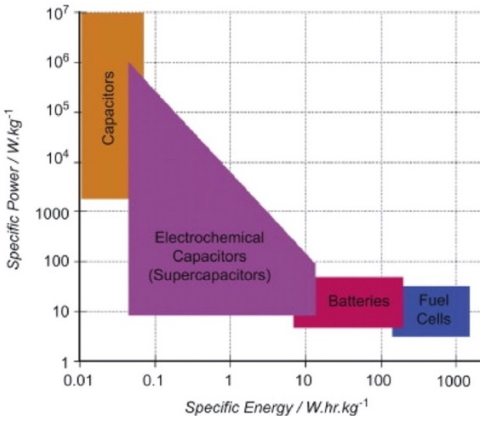

Figure 2.9 Energy storage Ragone Plot.
Source:[137]

Energy storage devices need continuous development and increase overall performance as well as durability. The best energy storage device is the rechargeable one with the highest specific energy and the fastest charging time [138]. Batteries and

supercapacitors are widely investigated to improve overall performance. Electrodes, electrolytes are the main variables that are common in these devices, and the study of their materials is important in order to reach the highest capacity. Next, the most used energy storage devices are discussed.

2.3.1.1 Capacitors, A capacitor is the simple system of using an insulator (dielectric) between conductors (electrodes), but the research to reach higher power density, and the higher energy density continues. Different types of capacitors such as film, ceramic, electrolytic, and double-layer capacitors are available [139]. Investigation on types of dielectrics used in capacitor continues.

2.3.1.2 Supercapacitors, Supercapacitors (SC) have higher specific energy compared to capacitors and they have specific energy close to batteries without any chemical reaction. There is a later of activated carbon on the conductive metal layer of electrodes in SC which makes them double-layer capacitors. Figure 2.10 represents a schematic of double layer electrochemical capacitor and shows the importance of ionic conductivity of electrolytes as well as conductivity of electrode film on current collector [140]. Supercapacitor, along with rechargeable batteries, will increase the battery life and energy recovery efficiency in hybrid and electric cars [141].

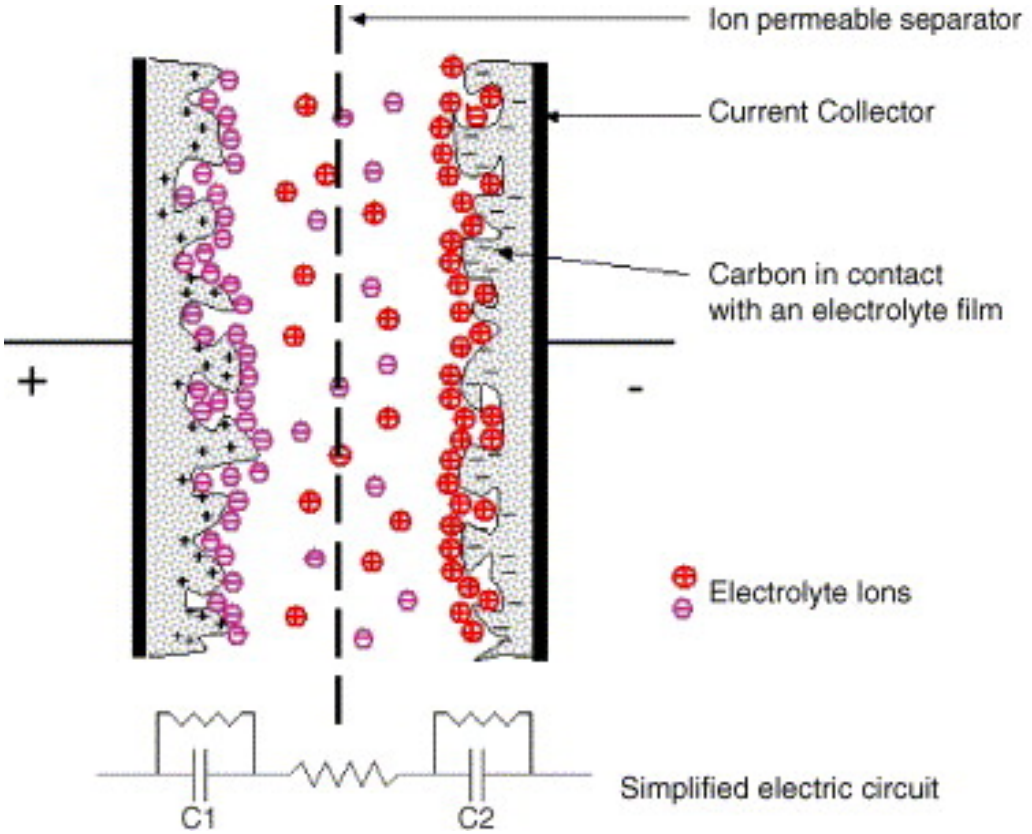

Figure 2.10 Double-layer supercapacitor.
Source:[140]

2.3.1.3 Batteries, Batteries are separated into two main groups as primary and secondary batteries. Primary batteries that cannot be recharged are being used for portable electric devices are Zinc-carbon (Zn-C) battery, Alkaline battery, Lithium primary cells. Secondary batteries that are rechargeable include Lead-acid (Pb-A) batteries, Lithium-ion batteries, Lithium-Sulphur (Li-S) batteries, Nickel-metal hydride (Ni-MH) batteries, Nickel-cadmium (Ni-Cd) batteries, and Nickel-zinc (Ni-Zn) batteries [142]. There are more efforts for optimization of rechargeable batteries since they are more being used in chargeable devices such as phones and electric cars. Commercial lithium-ion batteries (LIB) were first started 30 years ago by Sony Co. in portable electronics with high energy density but low power density [143,144]. LIB is still the most used rechargeable battery in portable devices

such as phones, laptops, and electric cars. Lithium is the key component in LIB batteries which is ionized in the anode and they move through the cathode, and electrically neutralize. Different types of electrodes for anode and cathode, separators, and electrolytes have been used throughout the years to reach the maximum capacity of these types of batteries. But still, there are struggles such as environmental hazards issues as well as cost issues for LIBs [145]. To overcome the deficiency of the LIBs, environmentally friendly alkaline batteries have been developed, which provide high power density due to the aqueous electrolytes [146]. Alkaline batteries use nickel/manganese/zinc-based cathodes. High specific energy and low cost is the advantage of the alkaline batteries [147].

Recently, developing iodine-based batteries have become more interesting due to their high theoretical specific capacity (211 mAh g-1) and fast reaction kinetics.

In another point of view, increasing demand for wearable and flexible technologies is a motivation for numerous researches on light-weighted, flexible energy storage devices, which means using flexible electrodes as well as practical electrolytes [148].

2.3.1.4 Fuel cells, Fuel cells (FCs) with the highest specific energy are the form of energy storage devices that converts different energy of chemical fuels into electrical energy. Advantages of FCS over other energy storage devices are higher energy conversion efficiency and minimum energy loss as heat as well as low carbon dioxide emission [149,150].

2.3.2 Carbon Nanomaterials Incorporated into Batteries

Rechargeable batteries and renewable sources of energy are growing in different industries, specifically using electric cars instead of using fossil energy sources. There are environmental concerns as well as interest in high technology to move from conventional

vehicles to hybrid or fully electric cars [151,152]. Fuel cells and batteries are candidates for new technology vehicles. Lithium-ion batteries are the most common rechargeable batteries for electric cars. As mentioned earlier, the most concerns in the battery industry are higher energy density, specific energy, and low solubility in electrolytes and low self-discharge rate. The number of electron processing is cathode material plays an important role in the specific capacity of the batteries. Among carbon-based materials, the physical and chemical properties of graphene and CNTs are most desirable for active electrode materials due to the high surface area and excellent electrical conductivity. They also improve flexibility and porous structure as well as buffering support for anode electrode. Since GO reduction is the most used method in rGO production and electrical conductivity is the key factor in electrode materials, Table 2.1 summarizes the effect of the reduction method on the electrical conductivity of rGOs. The reduction method is a harsh chemical, thermal or electrochemical method that removes oxygen-containing groups from the surface of graphene sheets that increases the electrical conductivity of the products, and causing unpreventable defects. The reduction method must be selected based on the final application; for instance, in battery applications that electrical conductivity is crucial for the performance of the batteries.

Table 2.1 Electrical Conductivity of rGO Based on Reduction Method

Derivative	**Reduction/modifying agent**	**Electrical conductivity (S.cm−1)**
rGO	KOH	60
rGO	Hydroiodic acid	103
rGO	Hydrazine hydrate	58
rGO	Hydrobromic acid	36
rGO	Sodium borohydride	34
rGO	Dextrose	18
Gr	Hydrazine hydrate	1000
TrGO	Thermal	2.3
Gr	Ammonia and hydrazine	5.5
GNS	Ammonia and hydrazine	7.2
TrGO	Hydrazine and thermal annealing	298
TrGO	Thermal	727
rGO	Hydroiodic acid and acetic acid	304
GNS	Hydrazine	24
fGO	Hydrazine and Pyrene groups	~1000
TrGO	Thermal reduction	80

Source: [103]

Figure 2.11 summarizes the graphene derivatives along with polymers in the form of composites that have been used in electronic devices. Graphene derivatives have

different electrical properties based on structure, functional groups, and defects. Selected graphene material might be modified, doped, or combined with polymers to fit the final application. Determination of the proper nanocarbon, as well as engineering the structure of it, opens a wide range of applications in different energy storage devices. Engineering band gap as well as controlling electrical properties are the most important parameters in battery design.

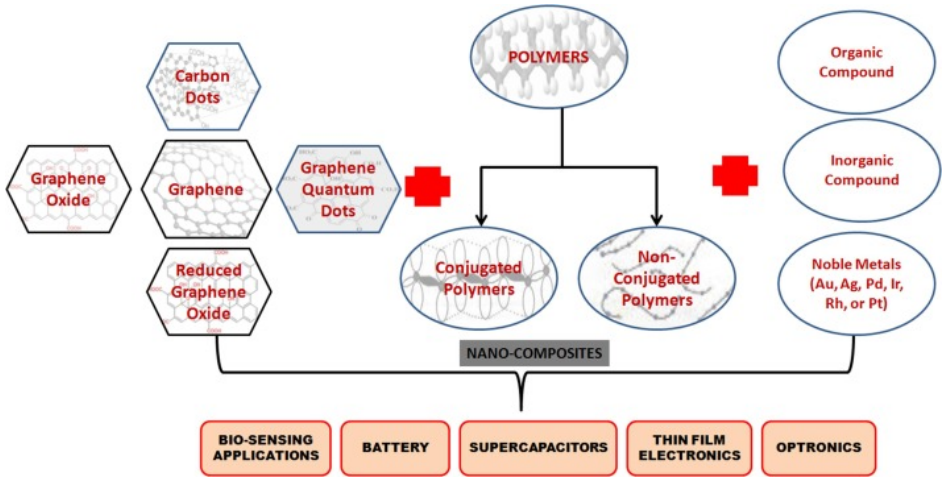

Figure 2.11 Summary of Graphene derivatives and polymers composite. *Source:[51]*

Table 2.1 is a summary of findings in the electrical conductivity of graphene-loaded composites. It was concluded that the electrical conductivity of rGOs enhances significantly after using along with a polymer or filler [103]. As expected, polyaniline, which is a conductive polymer, shows the best electrical conductivity among the composites, and for most of the concentration of the graphene in the samples was kept low. At the higher graphene concentrations, sheets agglomeration occurs, and conductivity decreases [103]

Table 2.2 Electrical Conductivity of rGO and Polymer Composites

Nanocomposites	**Filler loading**	**Fabrication method**	**Electrical conductivity (S.cm–1)**
Polystyrene/Phenyl Isocyanate-functionalized rGO	2.5 vol.%	Melt blending/Solution casting/*In situ*	0.1
Poly(ethylene-2,6-naphthalate)	5 wt.%	Solution casting	0.0004
PET/Graphene	3 vol.%	Melt blending	0.1
Polystyrene/Graphene	2.5 vol.%	Solution casting	0.1
Polystyrene/Graphene	5 vol.%	Solution casting	1
PMMA/Graphene	1-5 wt.%	Melt blending	0.1
Polyurethane/Graphene	0.015, 0.02, 0.025 vol. %	Melt blending/Solution casting/*In situ*	0.0001
Polypyrrole/Graphene	20 wt.%	*In situ*	7.930
PVDF/Graphene	15 wt.%	Solution casting	0.01
polystyrene-co-acrylonitrile (SAN)/TrGO	12 wt.%	Melt blending	0.0012
Polypropylene/TrGO	12 wt.%		0.001
Polycarbonate/TrGO	5 wt.%		1×10^{-5}
Polyamide 6/TrGOH	12 wt.%		7×10^{-6}
PDMS/Graphene	4 wt.%	Solution casting	1×10^{-7}
Natural rubber/Graphene			0.3
Nylon-6/Graphene	1.5 vol.%	*In situ*	0.001
HDPE/Graphene	3 wt.%	Melt blending	2×10^{-11}
Polyphenylene Sulfide/Graphene	4 wt.%		1×10^{-6}
Polyaniline/Graphene	1.5 wt.%	*In situ*	10
Polyvinyl Alcohol/Graphene	0.47 vol.%	Solution casting	1×10^{-7}
Epoxy/Graphene	0.52 vol.%	Solution casting	1×10^{-8}
PLA/rGO	1.25 vol.%	Solution casting	0.022
Graphene/Nano-cellulose	10 wt.%	Solution casting	80

Source: [103]

Lithium-ion batteries (LIB) are the most used rechargeable battery in energy storage devices due to their high power density, high specific energy, and longer cycle life [153]. Previously, graphite anode was used in LIBs, but the charge and discharge capability were low, and the distance between the layers remarkably varied that caused gradual peeling. The research focused on using metals instead of graphite which caused other problems like structural change and deformation during the charge and discharge process or low electrical conductivity. The development of graphene created a new path to carbon-based anodes that have been used as anode additive in LIBs, in pristine form, alloy form or modified by different functional groups such as fluorinated, and sulfonated graphene, or combined with polymers and silica. Graphene sheets with large surface area, wide electrochemical window, excellent electrical conductivity, better theoretical capacity, and high chemical diffusivity are the best candidates for LIB anode materials [26]. Graphene properties highly depend on the production process. Since reduction of GO is the most convenient path to produce graphene; it is important to select a proper process according to the final application, which in this case it is crucial to decrease graphene defects to reach better electrical properties. The disadvantage of using graphene as the anode in LIBs is the agglomeration of lithium atoms and decreasing charge-discharge capacity [26]. In order to overcome the lithium agglomeration, graphene can be modified by doping or using other additives. Heteroatom-doping the most promising approach to improve electrochemical properties of graphene. Nitrogen which is the most popular dopant introduced to the sp^2 graphene layer, generates the chemically active sites for charge transferring and improves final electrical properties [154,155]. There are several methods for nitrogen doping graphene such as CVD, ball milling, plasma, microwave, thermal and hydrothermal procedure [75].

Graphene has also been used as an electron conductive additive in LIB cathode materials. Yet, it is crucial to mix the cathode materials properly to facilitate lithium ion migration [156].

Carbon-based nanomaterials are also used as cathode materials for zinc ion batteries. Zinc ion batteries (ZIB) are low-cost and non-toxic sources of energy storage systems that should be optimized with proper cathode for zinc ions. The essential struggles in alkaline batteries are selecting and optimizing anode to reach high specific capacity, low solubility, low self-discharge rate, and high energy density. MnO_2–Zn [157], Ni–Cd, Ni–MH, and Ag–Zn are the conventional single electron redox that are mostly used in industry [158]. In order to increase the specific capacity of the batteries, it is important to achieve multiple electron redox. In one study, Wang discovered that Carbon nanotubes are promising conductive additive in alkaline batteries according to their high flexibility as well as conductivity [146]. Graphene cathode used in ZIB batteries optimized by coupling with zinc manganate nanodots, polystyrene sulfonate, sulfur, zinc manganese oxide, nitrogen, etc.

In designing anode materials, the addition of conductive material will improve the specific capacity of the anode. Carbon-based materials including graphene, graphene oxide (GO), reduced graphene oxide (rGO), carbon nanotubes (CNT), and amorphous carbon have been used in electrode materials. The main problem with the application of GO or rGO is the aggregation of the sheets, which prevents obtaining maximum surface area. The presence of CNT in the reduction process of GO reduces aggregation and π-π stacking of GO sheets. Kim et al. introduced all graphene batteries using functionalized graphene in the cathode and reduced graphene in anode structure. Similarities chemistry and structure

of anode and cathode materials increased the final performance of batteries. Kim et al. labeled this structure as a bridge between batteries and supercapacitors [159].

2.3.3 Carbon nanomaterials Incorporated into Capacitors

Electrodes play the most important role in energy storage devices to determine energy density and power density [160]. Commercialized supercapacitors mostly use activated carbon over metal oxide, organic metal frameworks, and conductive polymers as electrode material due to their high surface area, and low cost [160]. But there are disadvantages such as limited conductivity that limits the electrochemical performance. CNTs are another candidates for supercapacitors to overcome the low conductivity of activated carbons, but they also have trouble with cost and van der Waals forces between the tubes [141]. Graphene with a high surface area and electrical conductivity is a great candidate for supercapacitor applications [161]. Interlayer distance, specific surface area, pore size distribution, conductivity, edges, and dopants are important parameters of graphene that should be investigated for supercapacitor applications. In order to reach low-cost graphene, GO should be reduced to rGO and used in the electrode structure, and one of the most common problems caused during the reduction process is agglomeration [162]. Graphene and CNTs have been individually used in supercapacitor in a few researches. In one study combination of graphene, CNT showed better specific capacitance. Graphene and CNT properties alter by the combination of these two materials. Graphene would be an electron transferring channel, and CNT would decrease the aggregation of graphene sheets. The specific capacitance of graphene (135 F/g) and CNT (113 F/g) increased to 385 F/g in graphene-CNT composites [2]. The disadvantage of using graphene as electrode materials is the stacking and agglomeration of graphene sheets which is followed by decreasing

supercapacitor performance. Overlapping sheets occur during the reduction process and electrode preparation. In order to overcome this issue, Tang et al. proposed using a composite of conducting polymer such as PANI along with rGO to improve charge-discharge rate of capacitors [163]. Oyedotun et al. suggested using graphene foam with an interconnected hierarchical form to prevent overlapping the sheets and increasing the internal surface area as well as forming diffusion channels for electrons and ions [164]. In another study, Ge et al. fabricated montmorillonite nanosheets (MTs) and rGO aerogel by hydrothermal process and reached the specific capacitance of 275 F g^{-1}. They studied the effectiveness of MTs in preventing agglomeration of graphene sheets during the hydrothermal process [165]. According to Chen et al. continuous reduction of oxygen functional groups on rGO-based electrodes will cause capacitance increment after increasing the cycle numbers until the 2000^{th} cycle [166].

2.3.4 Carbon Nanomaterials Incorporated into Electrolytes

Engineering electrode/electrolytes increase the energy density of batteries and supercapacitors [167]. Improving mechanical properties and thermal stability as well as ionic conductivity plays a key role in designing electrolytes [168]. Tunable structure and compatibility of carbon nanomaterials make them a great candidate in solid-state electrolyte-related researches, and they have been widely investigated as an additive in electrolytes. Excellent mechanical strength and thermal stability make carbon-based nanomaterials more interesting in composite structures. There are two approaches to introduce GO into electrolytes: making a GO film and fabricating polymeric composites [169]. The addition of less than 1% carbon-nanomaterials will make a big difference in overall mechanical and thermal properties [170]. Moreover, carbon-based nanomaterial

introduce pathways for ions or protons to pass through the electrolytes, causing increasing the ionic conductivity as well as improving proton transportation [169]. Dinesh et al. used water-soluble graphene as an additive to magnesium air battery in order to decrease corrosion anode and increase overall negative potential [171]. GO is a great additive candidate in solid-state electrolytes, and it is proved that GO plays an important role in increasing the ionic conductivity of gel electrolytes as well as improving the mechanical strength of them [172]. Sohail et al. used modified and improved Hummer's method to fabricate GO electrolyte material, and it has been proved that GO sheets fabricated by both methods are suitable candidates to increase the thermal stability of electrolytes [173].

2.4 Future of Graphene

Since the discovery of graphene in 2004, there have been numerous studies and research on the properties and applications of graphene-based materials. Excellent electrical, thermal, mechanical, and optical properties of graphene are known since then. However, researchers are still investigating the structure of this single layer of carbon atoms in order to apply the significant characteristics in different research areas. An extensive range of applications has been introduced for graphene, from electronics and energy storage devices to membrane studies, water purifications, and biomedicals. A single sheet of graphene is stronger than steel and highly flexible at the same time, which makes it even more suitable for smart clothing and flexible screens. But the applications go beyond by doping graphene with oxygen-containing groups, nitrogen, and other functional groups. Furthermore, graphene is a great candidate to improve the mechanical, thermal, and electrical properties of composite materials. Scientists are still struggling with some of the problems such as coagulation, and agglomeration of graphene sheets, sharp edges that might disturb live cells [174], low aqueous dispersibility and large particle size of the sheets. Additionally, the fabrication of low-cost graphene with minimum defects in large quantities is still difficult. In conclusion, graphene has a great potential characteristic that can be applied in a variety of sciences. Yet, improving production as well as engineering properties will make graphene to reach its full capacity.

CHAPTER 3

COLLOIDAL BEHAVIOR OF GRAPHENE OXIDE

3.1 Introduction

Graphene-based materials have distinctive optical, mechanical and electrical properties which make them attractive for many applications [5,65,175-177]. Oxidation of graphite powder to graphene oxide (GO) followed by chemical reduction to reduced graphene oxide (rGO) is a well-established approach to generating graphene-based materials. Numerous methods of chemical reduction to rGO have been published where hydrazine hydrate [14], dimethylhydrazine [176], hydroquinone [176], $NaBH_4$ [178], HI [176,178] and Fe and Zn powder [176] have been used to reduce GO. Since the GO from different sources vary widely and contains a wide range of oxygen containing groups such as hydroxyl, carboxyl and epoxy [14,16,18,65,67,175-197], rGO represents a family of material with different physical/chemical properties. While there are several reports on different aspects and applications of GO and rGO [194-196,198,199], a systematic study of property variation in rGO containing different levels of oxygen is yet to be reported.

The level of reduction in rGO is also expected to alter aqueous dispersibility of these species. Besides chemical behavior, this also has ecological consequences. As the applications of GO and rGO proliferate, mass production and disposal of products containing these nanocarbon will increase with potential for environmental contamination and water pollution. Recent studies have shown that graphene can be toxic toward organisms including bacteria [200], nematodes zebra fish and humans [200,201]. Cytotoxicity toward bacteria through both membrane and oxidative stress has been demonstrated for

both GO and rGO and level of oxidation has been shown affect cytotoxicity [200,202]. While a hydrophobic rGO can be expected to settle out of aqueous media into solid phases such as river sediments, hydrophilic rGO will stay dispersed. Therefore, there is a need to develop an understanding of the fate of different rGOs in aqueous media, where there have been limited studies [67,190,191,197]. Theoretical predictions of GO aggregation kinetics and stability using Derjaguin– Landau– Verwey– Overbeek (DLVO) theory has been used to estimate the attachment efficiency [67,179,183], and an alternative Maxwell approach [203] taking into account has also been used to determine particle collision efficiencies and aggression kinetics of GO and rGOs. Time resolved dynamic light scattering has been used to study dispersibility of GO and rGOs [204], and the solubility of rGO from different methods have been measured in different solvents and correlated with solubility parameters [65].

An important consideration is that oxygen containing groups play an important role in determining chemical properties as well as dispersibility and aggregation of rGO in aqueous solutions. Since GO and rGO form different sources show a wide range of variability in both structure as well as the presence of functional groups, they cannot be compared directly. To address this issue, the objective of this work is the stepwise reduction of the same GO to generate rGO containing different levels of oxygen and study their chemical properties. Yet another objective is to study the colloidal behavior of the rGOs representing different levels of GO reduction.

3.2 Experiments

3.2.1 Materials

Graphene Oxide was purchased from Graphena Inc., Zinc was purchased from Fluka and all other chemicals were purchased from Sigma Aldrich with purity higher than 95%. Reduction of GO to rGO was carried out using a method published before[196], however the method was modified for step wise reduction. 200 mg of GO was dispersed in 50 mL water and sonicated for 10 min to form a homogeneous solution. 0.1 M Hydrochloric acid was added to adjust the pH to 2. The Zn power was then added and sonicated for 10 min to generate enough hydrogen that would lead to formation of rGO. Reducing the amount of Zn reduced the hydrogen generation and consequently the degree of reduction the addition of 200, 400 and 1000 mg Zinc led to the formation rGO containing 19.5, 33 and 8 percent oxygen, respectively. These are referred to as rGO-33, rGO-19.5 and rGO-8. The reduction of GO took place according to the Equations (3.1) and (3.2), and any remaining Zn was dissolved by adding additional HCl before filtration:

$$Zn + 2HCl \rightarrow ZnCl_2 + H_2 \quad (3.1)$$

$$GO + H_2 \rightarrow rGO + H_2O \quad (3.2)$$

3.2.2 Methods and Characterization

The GO and rGOs were analyzed using scanning electron microscope (SEM), Raman Spectroscopy, Thermo Gravimetric Analysis (TGA), and Fourier Transform Infrared spectroscopy (FTIR). SEM analysis was carried out on a LEO 1530 VP instrument equipped with an energy-dispersive X-Ray; TGA was performed on Pyris 1 system from

Perkin-Elmer Corp., and FTIR measurements were carried out in purified KBr pellets using a PerkinElmer (Spectrum One) instrument. TGA analysis was carryout by heating from 30°C to 700 °C under a flow of air at 10 mL/min, at a heating rate of 2 °C per min.

Stock solutions of GO and rGOs were prepared by sonication. Pre-weighed amounts of the GO and rGOs were added to MilliQ water to make a 40 mg/l stock solution. Different GO and rGO solutions were then prepared by diluting the stock solution. Stock solutions containing 400mM of sodium chloride and magnesium chloride were also prepared which were used for dispersibility studies. Dynamic Light Scattering (DLS) were carried out using 50 mg/1 dispersions of rGO were measured as a function of salt concentration at 25 ˚C using dynamic light scattering (Malvern Instruments Zetasizer Nano ZS90). The dynamic light scattering measurements were conducted at 90 °C with the incident laser beam and the autocorrelation function having been allowed to accumulate for more than 10 s with salt concentration ranging between 0.5 mM and 200 mM. Zeta potential of the Graphene oxide was measured on 10 mg l-1 dispersions at 25 ˚C on the Malvern Instruments Zetasizer nano ZS90. Hydrophobicity of GO and rGOs were determined by measuring the UV absorbance at 252 nm before and after partitioning in water extraction of a 50 mg l:1 dispersion of the GO with 1-Octanol.

3.3 Results and Discussion

To avoid the inter sample variation of GO from different sources, the same sample was reduced step wise using a gentle reduction technique. The resulting rGOs are listed in Table 3.1 and classified based on the oxygen content. Oxygen content were determined using EDAX. The SEM images of the different rGO are presented in Figure 3.1. In line with what

has been reported before, the GO sheets had smooth surface while the rGOs showed folded regimes and wrinkles.

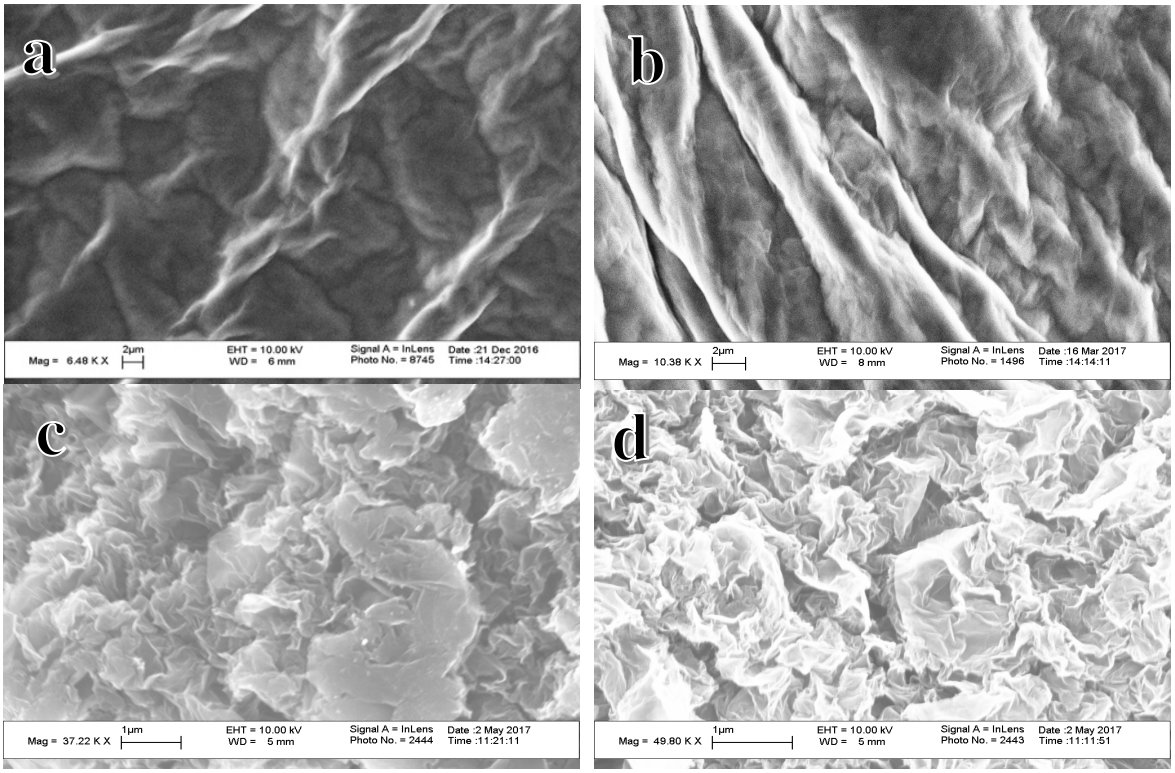

Figure 3.1 SEM images of **a)** GO, **b)** rGO-33 1, **c)** rGO-19.5, **d)** rGO-8.
Source: [205]

The chemical structure of GO before and after the reduction were studied by FTIR and the data is presented in Figure 3.2. The reduction of GO involves the elimination of oxygen containing groups and the restoration of conjugated π systems. Characteristic peaks including C–O (1060 cm-1), C–OH (1226 cm-1), O–H (1412 cm-1) and C=O (1733 cm-1), were observed in the GO spectrum, and these were significantly reduced in the rGO spectra. This clearly indicated the loss of oxygen groups form GO suggesting the formation of rGO.

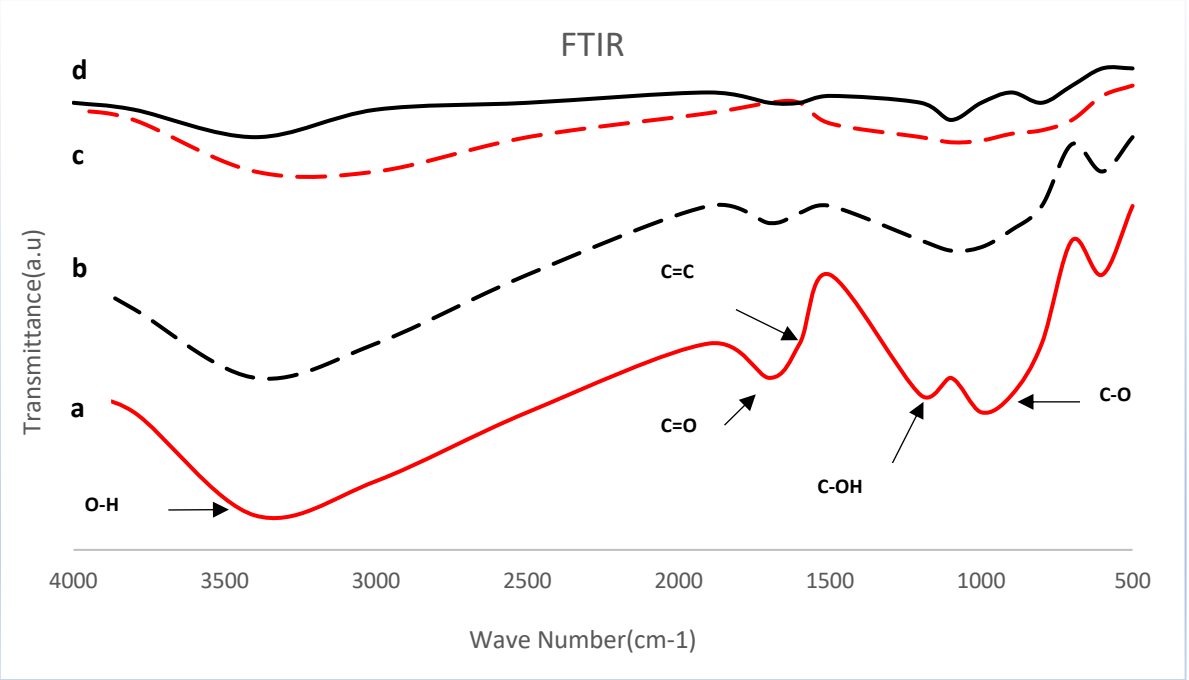

Figure 3.2 FTIR spectra of **a)** GO, **b)** rGO-33 1, **c)** rGO-19.5, **d)** rGO-8.
Source: [205]

Figure 3.3 shows the Raman spectra of the GO and rGO samples. Strong D-peak is suggestive of armchair conformation near the edges. After the reduction of GO, the G band shifted to 1580 cm^{-1} from 1600 cm^{-1} in line with what has been reported before [196]. The intensity of the D band increased with reduction and so did the I_D/I_G ratio. The crystallite sizes (L_a) of the sp^2 lattice of all the samples were calculated from the following Equation (3.3), where λ is the laser wavelength, and I_G and I_D are the intensities of the G- band and the D- band, respectively.

$$La = 2.4 \times 10^{-10} \times \lambda \times I_G/I_D \quad (3.3)$$

The intensity of D band increased during reduction while the intensity of G band decreased. As result L_a decreased in rGO. The values of La are given in Table 3.1, which shows that L_a decreased from 22.6 in original GO to 13.4 in rGO-8.

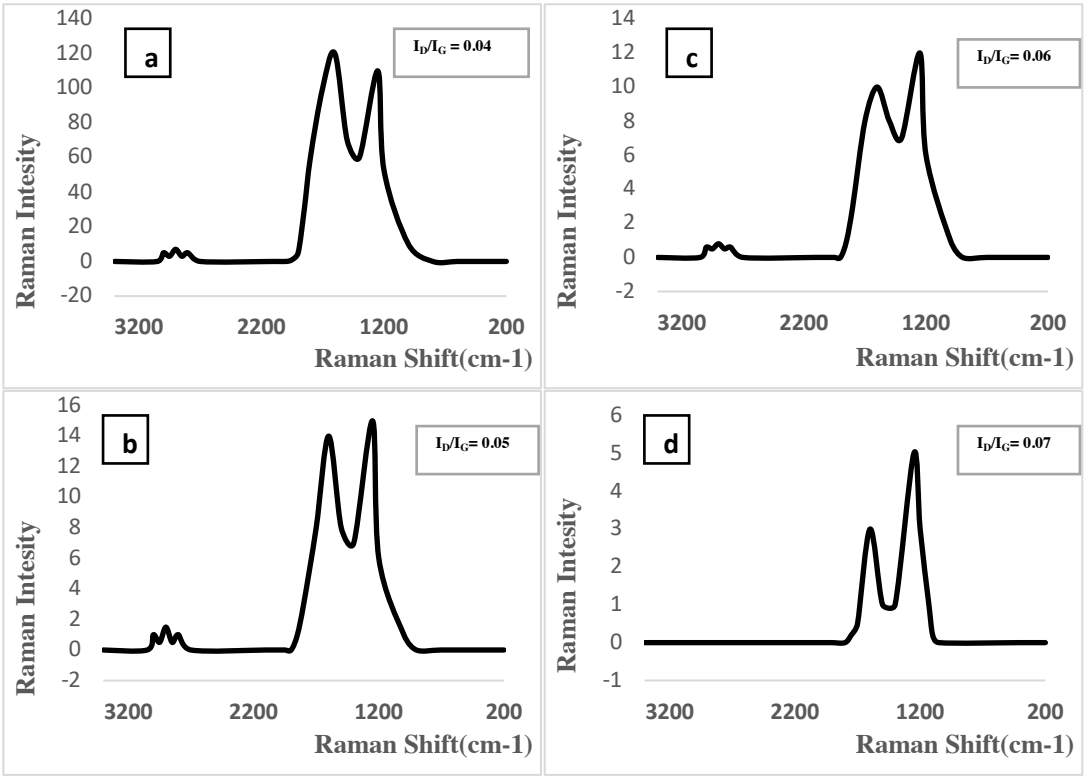

Figure 3.3 Raman spectra of **a)** GO, **b)** rGO-33, **c)** rGO-19.5, **d)** rGO-8 (The I_D/I_G ratio as abstract value for in-plane lattice defects).
Source: [205]

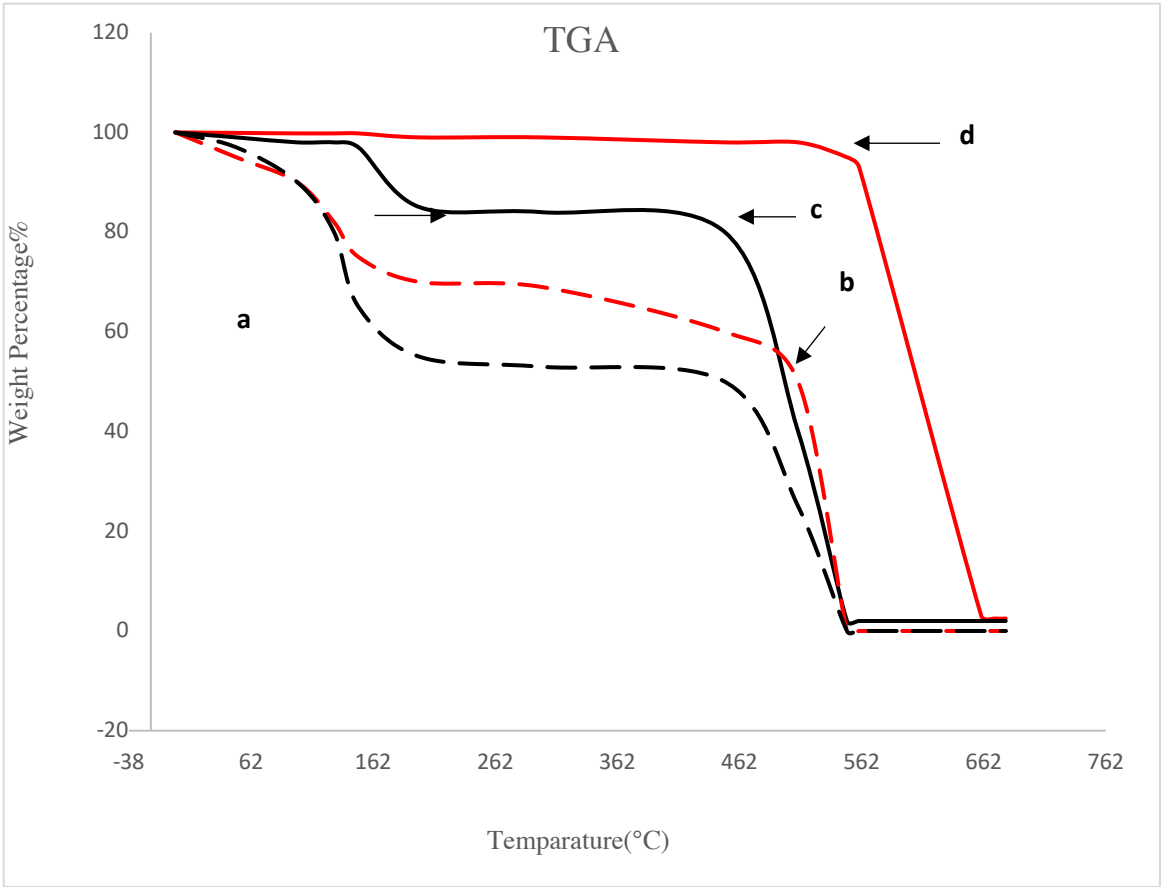

Figure 3.4 TGA curves of **a)** GO, **b)** rGO-33, **c)** rGO-19.5, **d)** rGO-8.
Source: [205]

The results from TGA analysis are presented in Figure 3.4. The two weight loss steps for GO were from the pyrolysis of oxygen containing functional groups and the second was from the oxidation of carbon. The former was around 160 °C and GO lost nearly 40% of its weight at 162 °C. The second step which is around 460 °C was related to the oxidation of sp^2 hybridzied carbon atoms. As the reduction progressed, the weight loss at 160 °C decreased with rGO-8 showing minimal decrease in weight at this temperature indicating that much of the oxygen containing groups had been removed. Deoxygnetioan also led to higher thermal stability of the carbon in rGO.

To measure solubility and dispersibility of GO and rGOs, pre-weighed amounts of GO and rGOs were added to DI water and let the solution settle for 2 hours. As shown in Table 3.1 solubility of graphene oxide reduces from 7.4 μg/ml to nearly zero for rGO-8. However, the rGO could be dispersed into a stable suspension via sonication. Dispersibility was measured by sonicating the suspension for 10 min and then the suspension was allowed to settle for 24 hours. As presented in in Table 3.1, here the dispersibility decreased from 8 μg/ml for GO to 2.5 μg/ml for rGO-8.

In the realm of aqueous behavior, the hydrophobicity of the different rGOs is an important consideration. Hydrophobicity index (HI) based on octanol water partitioning was used to determine dispersibility of GO in water [206]. The pictures of 1-Octanol/water partitioning are shown in Figure 3.5. HI was calculated based using a method published [34] before. It was computed using absorbance of GO and rGOs solutions at 252 nm in water prior to and following 1-Octanol extraction according the formula given below.

$$HI\ (\%) = \frac{(A_0 - A_i)}{A_0} \times 100 \tag{3.4}$$

As presented in Table 3.1, rGO showed lower HI with higher oxygen content. Hydrophilicity was high in highly carboxylated GO sheets which made it partition in the aqueous phase. HI increased from -3.89% to 5.2 % as the oxygen content decreased implying that it went from a highly hydrophilic GO to highly hydrophobic rGO which represented a dramatic change in aqueous dispersibility. HI of GO (-3.89%) is very close to reported HI for reported carboxylated carbon nanotubes (-4.15%).

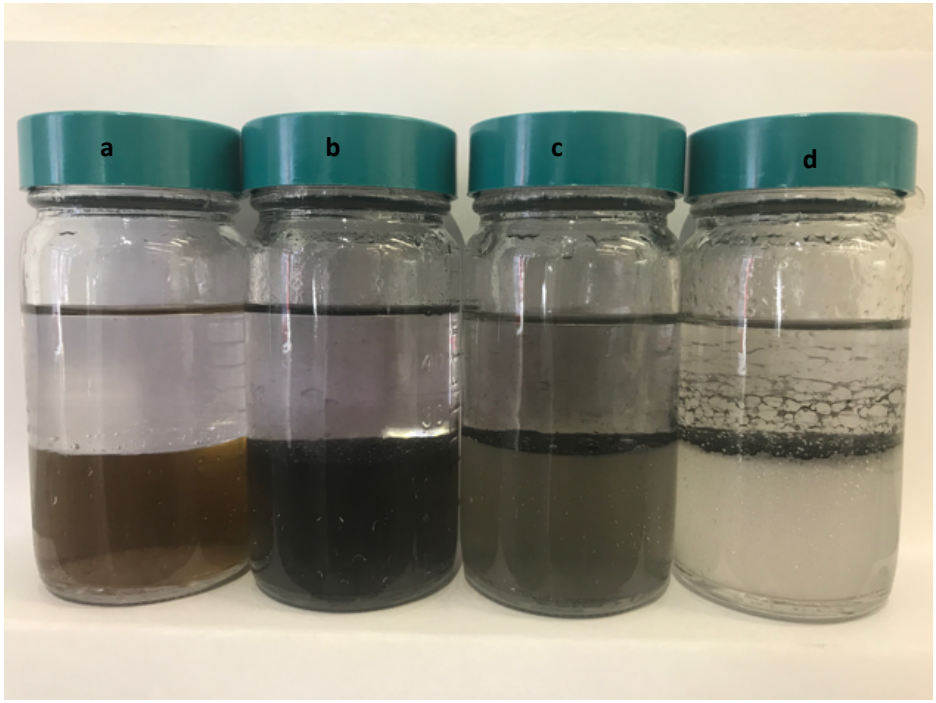

Figure 3.5 Photographs of 1-Octanol/water partitioning of **a)** GO, **b)** rGO-33, **c)** rGO-19.5, (d) rGO-8 after standing for an hour.
Source: [205]

In general, colloidal stability is attributed to balance between van der Waals forces that promote aggregation and electrostatic repulsion which is dispersive [204]. Zeta potential, particle size distribution and aggregation kinetics were used to study dispersibility of the different rGO. Due to its anisotropic shape, the two fundamental interacting modes between GO sheets are edge to edge and face to face. GO is known to form a good dispersion in water because of the electrostatic repulsion between ionized functionalities such as carboxylic groups that are mainly located at the edges. With the addition of salt, typically the monovalent Na^{+} has no specific interactions with the functional groups on GO surfaces and the aggregation follows conventional DLVO theory. In the presence of divalent Mg^{2+}, the mechanisms of GO aggregation kinetics could be

complicated because the divalent cations can also interact with surface functional groups of the GO sheets and even cross-link them, particularly at the edges [183,204,206]. Figures 3.6 and 3.7 show zeta potential and particle size of GO and rGOs as a function of ionic strength. As expected, the GO and rGO particles began to aggregate with increase in ionic strength. The addition of a divalent cation Mg^{2+} led to stronger aggregation of the GO sheets which is in line with the DLVO theory. As presented in Table 3.1, agglomerate size in the presence of 0.5 mmole of NaCl and MgCl2 increased as oxygen content increased. Particle size reduces from 642.3 to 327.9 nm in presence of 0.5 mmole/l NaCl and from 1274 to 358.3 nm in presence of equivalent $MgCl_2$ as oxygen containing groups are being removed. The zeta potential in NaCl was between 33.2 to 23.7 mV, which implied moderately stable dispersions, however the zeta potential in 0.5 mmole/l $MgCl_2$ was in the range of 9.66 to 0.92 mV, implying very unstable suspension.

The aggregation kinetics of the GO and rGO were studied using time resolved dynamic light scattering. The initial rate of agglomerate size is (r_h) is proportional to kno where k is the initial aggregation rate constant and no is the initial concentration of the solute. The attachment efficiency α which is the reciprocal of stability ratio of a dispersion were computed NaCl and $MgCl_2$ as [204]:

$$\alpha = \frac{(\frac{dr_h}{dt})_{t\to 0}}{(\frac{dr_h}{dt})^{f}_{t\to 0}} \tag{3.5}$$

Where $(\frac{dr_h}{dt})_{t\to 0}$ and $(\frac{dr_h}{dt})^{f}_{t\to 0}$ represent the slow and fast aggregation regimes, respectively [204]. The attachment efficiency was measured as the ratio of the initial slope of the aggregation profile to that obtained under fast aggregation conditions. These are plotted as a function of salt concentration for the GO and rGO and are presented in Figure 3.6 and 7. In line with previous studies, distinct unfavorable and favorable aggregation regimes demarcated by the critical coagulation concentration (CCC) (Figures 3.6 and 7) were observed. This indicated that the DLVO type interactions were the dominant mechanism for colloidal stability of GO and rGO. The CCC values are presented in Table1. Surface oxidation in rGO clearly played an important role and higher oxygen content led to higher CCC values. There was no significant change in CCC value for GO and rGO-33. Higher CCC for high oxygen containing groups was due to the fact that there was more interaction between oxygen containing group and electrolytes in solution. In general, the CCC value determined for GO and rGO is significantly lower than the reported CCC value for fullerene but is quiet similar to CNT [200].

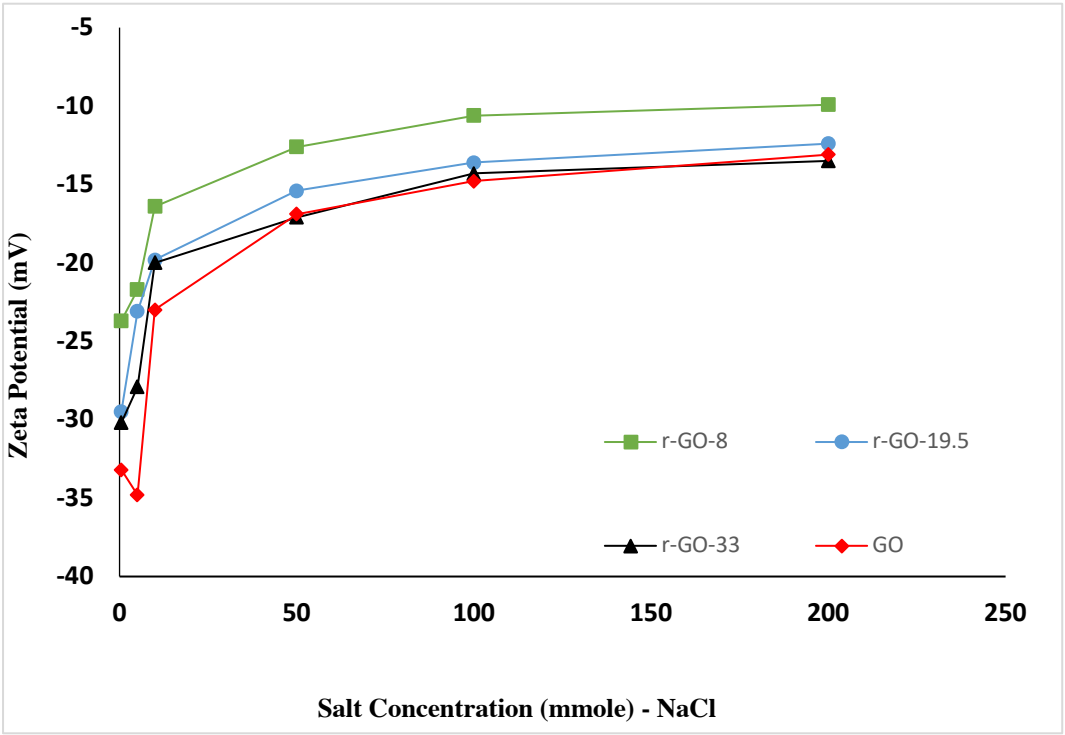

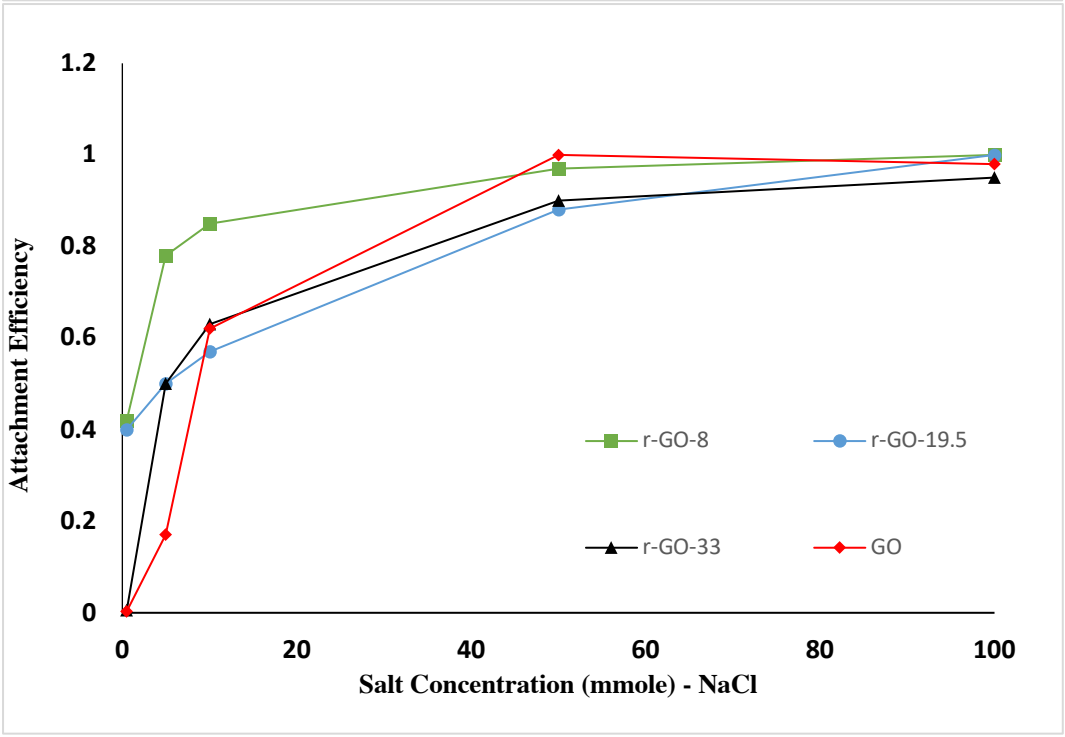

Figure 3.6 a) Zeta potential as a function of NaCl concentration, **b)** Attachment efficiency as a function of NaCl concentration. GO and rGOs concentration was maintained 4mg/l in DI water.
Source: [205]

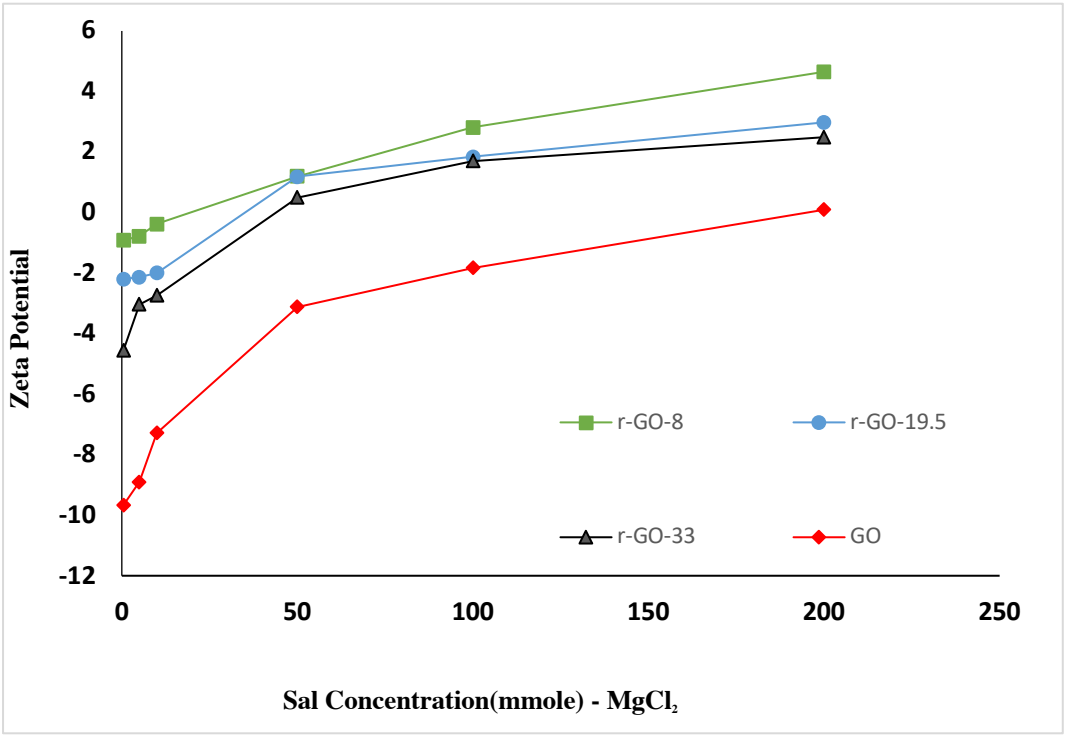

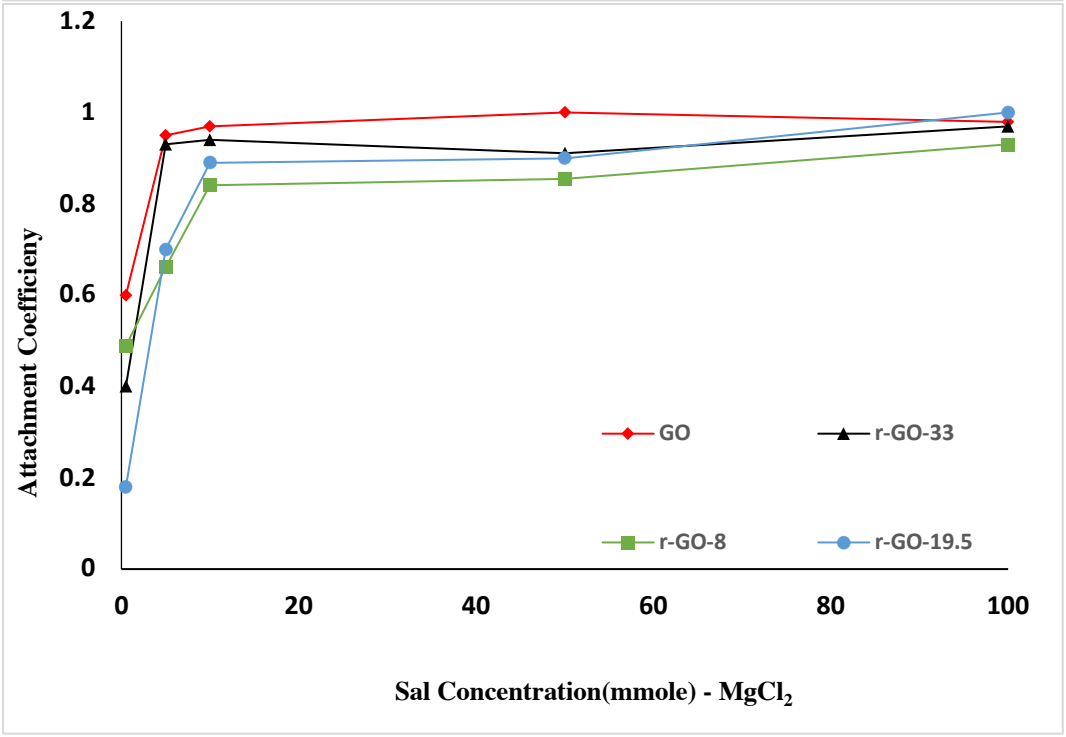

Figure 3.7 **a)** Zeta potential as a function of $MgCl_2$ concentration; **b)** Attachment efficiency as a function of $MgCl_2$ concentration. GO and rGOs concentration were maintained 4mg/l in DI water.
Source: [205]

Table 3.1 Properties of GO and rGOs Produced via Stepwise Reduction

Analysis/Sample	GO	rGO-33	rGO-19.5	rGO-8
Percent Carbon	**55%**	**66.2%**	**79.46%**	**90%**
Percent Oxygen	**45%**	**33%**	**19.5%**	**8%**
L_a	**22.6**	**18.5**	**16**	**13.4**
Particle size in 0.5 mmole/l NaCl	**642.3**	**385.5**	**376.7**	**327.9**
CCC in NaCl	**28**	**27**	**20**	**15**
Particle size in 0.5 mmole/l $MgCl_2$	**1274**	**608.2**	**551.1**	**358.3**
CCC in $MgCl_2$	**6**	**6**	**5**	**2**
Zeta potential in 0.5 mmole/l NaCl	**-33.2**	**-30.02**	**-29.5**	**-23.7**
Zeta potential in 0.5 mmole/l $MgCl_2$	**-9.66**	**-4.54**	**-2.2**	**-0.92**
Hydrophobicity Index	**-3.89%**	**0.98%**	**1.75%**	**5.2%**
Solubility(μg/ml)	**7.4**	**2.1**	**~0**	**~0**
Dispersibility(μg/ml)	**8**	**6.3**	**4.1**	**2.5**

Source: [205]

3.4 Conclusions

Controlled, step wise reduction of GO was carried out by nascent hydrogen generated from a reaction between metallic zinc and HCl. rGOs containing 33, 19.5 and 8% oxygen were synthesized and studied. FTIR confirmed the reduction of GO while Raman and SEM showed increase in defects and wrinkles in rGOs. Aqueous dispersibility and colloidal behavior as measured by size of agglomerates, zeta potential rGO were highly dependent on oxygen content. Higher oxygen content led to higher CCC values in both NaCl and $MgCl_2$.

CHAPTER 4

COLLOIDAL BEHAVIOR OF GRAPHENE OXIDE AND CARBON NANOTUBE HYBRIDS

4.1 Introduction

Oxidation of graphite powder to graphite oxide, and exfoliation of graphite oxide to graphene oxide (GO) is a well-established [207-210], commercially viable approach to generating graphene-based materials. Electrochemical exfoliation of graphite also reported as a low defect method to produce graphene [211]. The GO is characterized as a single graphitic aromatic monolayer (sp^2 bonded) and oxygenated aliphatic regions (sp^3 carbon atoms) containing hydroxyl, epoxy, carbonyl, and carboxyl functional groups [13,212,213]. The oxygen content in GO can be over 50%, which make it highly hydrophilic and water soluble[214,215], but it has low electrical conductivity. However, the GO can be reduced to rGO to increase its hydrophobicity and enhance electrical properties. The reduction can be tuned to alter properties so that it becomes a useful material for applications such as batteries, supercapacitors and other electronics. Numerous methods of chemical reduction to rGO have been published where hydrazine hydrate, dimethylhydrazine, hydroquinone, NaBH4, HI, Fe, and Zn powder have been used to reduce GO [13,205]. The level of reduction in rGO is critical for tuning its various properties, and we have reported the controlled reduction of GO to rGO via *in situ* reduction by nascent hydrogen [205].

Carbon nanotubes are rolled up graphene sheets that have high electrical conductivity but no water dispersibility [216]. Recently, the hybridization of CNTs with GO have been reported [123,133,217-220]. Graphene-CNT hybrids have been produced by a simple solution assembly where the CNTs have been suspended between the GO layers to

prevent graphene sheets from agglomerating. Also, there is synergistic effect between GO and CNTs which leads to better electrical conductivity, electro catalytic activity in the Graphene-CNT fibers of the Graphene-CNT hybrid. The combination of these two separate materials has the potential to open up a wide range of applications [123,133,217,221] including optoelectronic devices, supercapacitors and lithium batteries [222-224]. The hybrids have shown improvement in the dielectric constants compared to the pristine GO and CNT, and the CNT have worked as spacers between GO sheets resulted in better specific capacitance[123,208,212,219,225]. The incorporation of GO-CNT hybrids into the aerogel and polyamide composites have provided better mechanical properties and thermal stability and they have been used for heavy metal ion removal, detection of pollutants and filtration and membrane processes [119,226].

An important aspect of the GO-CNT hybrids is the aqueous dispersibility. While the GO is highly dispersible, the CNTs are insoluble. It has been reported that the GO serve as medium to suspend the CNTs [207,227,228]. The aqueous behavior of the GO-CNT hybrids is an important concept that is yet to be studied. Such understanding of GO-CNT and rGO-CNT hybrids is very important for processing of these materials and also as water pollutants when they may be released to the environment. Moreover, if the GO is reduced to rGO in the presence of CNTs during the chemical reduction, the CNTs will be entrapped among the GO layers and generate a layered structure with spacers rather than collapsing the layers on each other. The objective of this paper is to develop an understanding of the rGO-CNTs generated by controlled *in situ* reduction of GO and their aqueous behavior.

4.2 Experiments

4.2.1 Materials

Graphene Oxide was purchased from Graphena Inc., Carbon nanotubes were purchased from Cheaptubes, Zinc was purchased from Fluka and all other chemicals were purchased from Sigma Aldrich with purity higher than 95%. Pre-weighed amount of GO and CNT with 1:1 ratio was added together in aqueous solution and sonicated for 15 minutes. Stepwise reduction of GO to rGO in the presence of CNTs was carried out using a method published before[205]. 0.1 M Hydrochloric acid was added to GO-CNT aqueous solution to adjust the pH to 2. The Zn power was then added and sonicated for 1 min to generate enough hydrogen that would lead to formation of rGO. Any remaining Zn was dissolved by adding additional HCl before filtration. Chemical reaction of the experiment represented in formulas 4.1 and 2.

$$Zn + 2HCl \rightarrow ZnCl_2 + H_2 \quad (4.1)$$

$$GO + H_2 \rightarrow rGO + H_2O \quad (4.2)$$

Oxygen content of each sample was controlled by the reduction process. Amount of Zinc that was added to the solution was the limiting reagent to control the production of nascent hydrogen which removed oxygen containing groups in the hybrids. The various rGO-CNT hybrids thus formed are denominated as rGO-CNT-X where X represents the percentage of oxygen. Oxygen content of the hybrid was used to designate a sample. For example, while the GO contained nearly 52% oxygen, the CNT-GO hybrid contained half

that, and was named GO-CNT-26. Here we prepared three additional hybrids namely rGO-CNT-18, rGO-CNT-7, and rGO-CNT-2.

4.2.2 Methods

Figure 4.1 shows the incorporation CNTs between GO layers to form hybrid structures followed by subsequent formation of rGO-CNT-X when some of the oxygen groups were removed. The latter were formed during the *in situ* reduction of the GO in presence of CNTs, where the CNT were automatically incorporated between the rGO layers. As mentioned, the oxygen content of the rGO-CNT-X was controlled by limiting the generation of nascent hydrogen. Therefore, these hybrids were structurally different from ones formed by mixing rGO and CNTs.

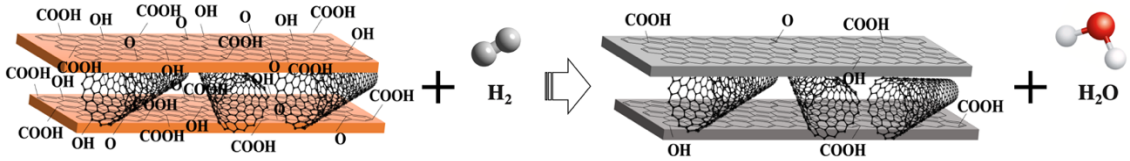

Figure 4.1 Graphical representation of prepared **a)** GO-CNT and **b)** rGO-CNT hybrids. *Source: [118]*

4.2.3 Characterization

Characterization of the GO-CNT and rGO-CNTs was carried out using Elemental Analysis (EA), Raman Spectroscopy, attenuated total reflection Fourier Transform Infrared spectroscopy (ATR-FTIR), scanning electron microscope (SEM), energy-dispersive X-Ray (EDAX), Thermo Gravimetric Analysis (TGA). Raman spectra achieved by DXR Raman microscope from Thermo Scientific and FTIR measurements were carried out using

an Agilent Cary 610/620 FTIR instrument. SEM analysis was carried out on a JSM-7900F instrument equipped with an energy-dispersive X-Ray. TGA was performed on Pyris 1 system from Perkin-Elmer Corp., and TGA analysis was carryout by heating from 30 to 800 °C under a flow of air at 10 mL/min, at a heating rate of 10 °C per min.

Stock solutions of hybrids were prepared by sonication. Pre-weighed amounts of the GO and CNT were added to MilliQ water to make a 40 mg/l stock solution. Different hybrids solutions were then prepared by diluting the stock solution. Stock solutions containing 400 mM of sodium chloride and magnesium chloride were also prepared which were used for dispersibility studies. Dynamic Light Scattering (DLS) were carried out using 50 mg/1 dispersions of rGO were measured as a function of salt concentration at 25 ˚C using dynamic light scattering (Malvern Instruments Zetasizer Nano ZS90). The dynamic light scattering measurements were conducted at 90 °C with the incident laser beam and the autocorrelation function having been allowed to accumulate for more than 10 s with salt concentration ranging between 0.5 mM and 200 mM. Zeta Potential was studied using 0.5 mM of NaCl and $MgCl_2$. Sonicated stock solutions were settled for 2 hours and 24 hours to measure solubility and dispersibility, respectively. At last, hydrophobicity of hybrids was determined by measuring the UV absorbance at 252 nm before and after partitioning in water extraction of a 50 mg l-1 dispersion of the hybrids with 1-Octanol.

4.3 Results and Discussion

Pure GO, CNT along with four different mixtures of GO-CNT were studied in this research. Summary of findings are listed in Table 4.1. In order to determine composition of the samples, elemental analysis (Carbon, Hydrogen, Nitrogen, Oxygen, Sulfur) was carried out. Carbon and Oxygen content of each hybrid and pristine GO and CNT is reported in Table 4.1. The concentrations of Hydrogen, Sulfur and Nitrogen in each sample was negligible. Figure 4.2 presents the Raman spectra for the samples. There are two main overlapping peaks in the Raman spectra for GO and CNT. G band at 1580 cm^{-1} and D band at 1350 cm^{-1} [229]. The crystallite sizes (L_a) of the sp^2 lattice of all the samples were calculated from the Equation (4.3), where λ is the laser wavelength, and I_G and I_D are the intensities of the G- band and the D- band, respectively.

$$L_a = 2.4 \times 10^{-10} \times \lambda \times {}^{I_G}/_{I_D} \tag{4.3}$$

L_a of the samples were presented in Table 4.1. The L_a of raw GO was 22.5 nm which was very close to the GO-CNT-26 hybrid which was 21.96 nm. It showed that GO characteristics were more affected by GO than CNT. Lattice spacing decreased after reduction of oxygen containing groups. After reduction, the intensity of the D band increased, and the intensity of the G band decreased. L_a of rGO-CNT-18 which was 18.31 showed that folding of GO sheets after reduction in presence of CNT did not happened much. Clearly, defects did not increase much in presence of CNT.

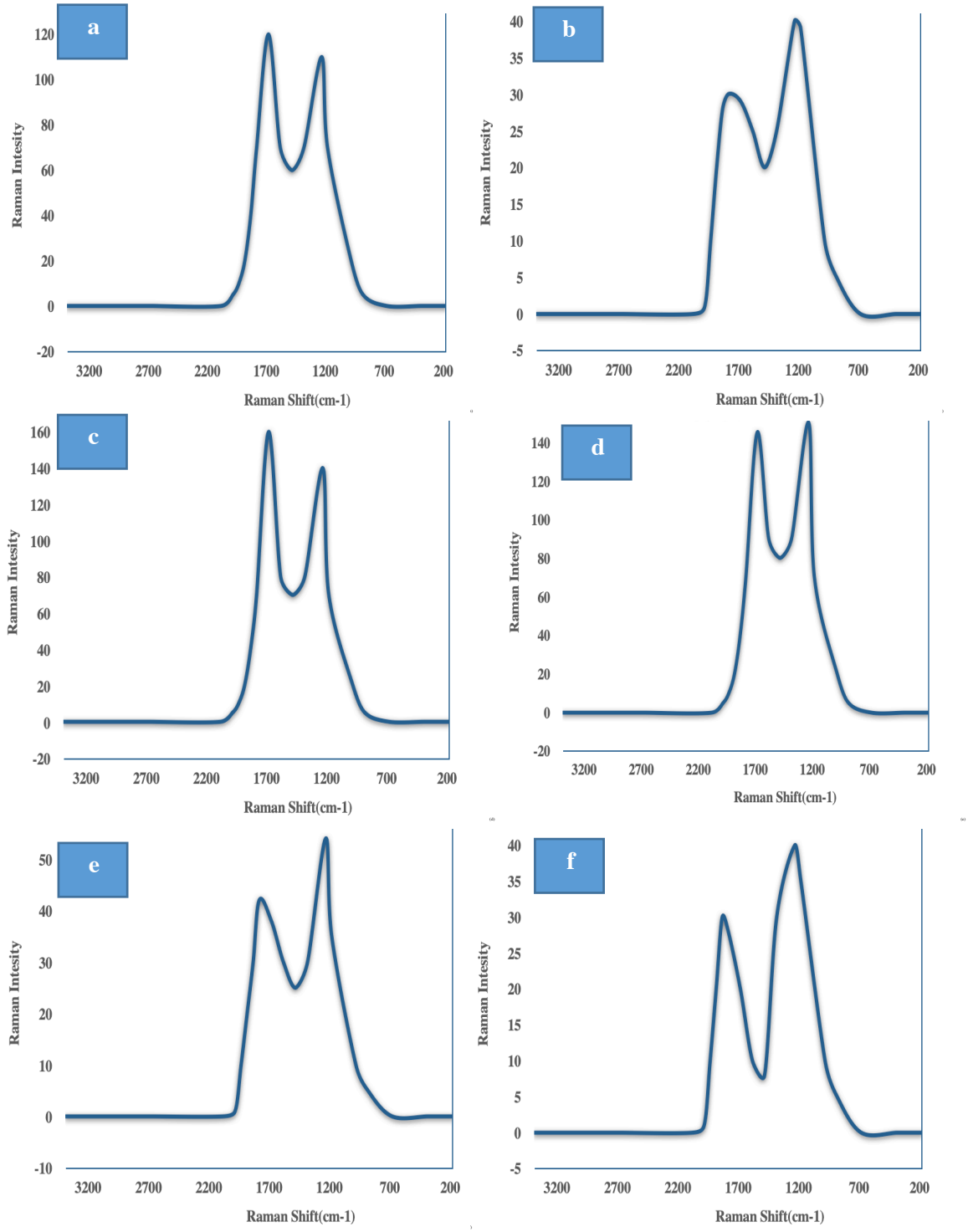

Figure 4.2 Raman spectra of **a)** GO, **b)** CNT, **c)** GO-CNT-26, **d)** rGO-CNT-18, **e)** rGO-CNT-7, **f)** rGO-CNT-2.
Source: [118]

Structure of samples was studied by FTIR and results are presented in Figure 3. Characteristic peaks for GO for C–O (1060 cm^{-1}), C–OH (1226 cm^{-1}), O–H (1412 cm^{-1}) and C=O (1733 cm^{-1}) were observed in the GO spectrum and GO-CNT-26 hybrid spectra [205,230]. These peaks were reduced after the formation of rGO in hybrid and are attributed to the removal of oxygen containing groups. The oxygen containing peaks were very low in rGO-CNT-18, rGO-CNT-7, and rGO-CNT-2.

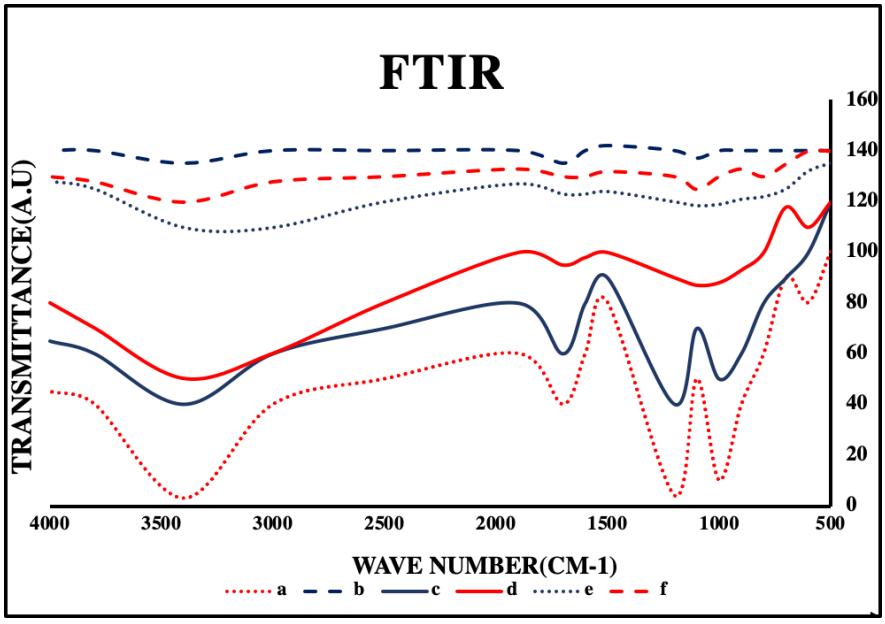

Figure 4.3 FTIR Spectra of **a)** GO, **b)** CNT, **c)** GO-CNT-26, **d)** rGO-CNT-18, **e)** rGO-CNT-7, **f)** rGO-CNT-2.
Source: [118]

Figure 4.4 shows SEM images of the samples. Figure 4.4 a) shows GO sheets while Figure 4.4 b) shows the pure CNTs. Figures 4.4 c) and f) display presence of the CNT and GO in the hybrids. Figure 4.4 c) represents the GO-CNT-26 hybrid formed by simple mixing which shows relatively uniform distribution of CNTs over the GO layers. In GO-CNT-26, the GO sheets were not as flat as they were before mixing. Figure 4.4 c) shows

overlapping of GO and CNT and interaction between the layers. In line with previous reports [205], the GO wrinkled and folded after being reduced to rGO. However, after reduction in the presence of CNTs, there were fewer wrinkles compared to the previous reports [205,231,232]. Existence of CNTs and their interaction with the GO layers prevented the latter's folding. Preparation method was designed to overcome problems with coagulation of GO sheets during chemical reduction.

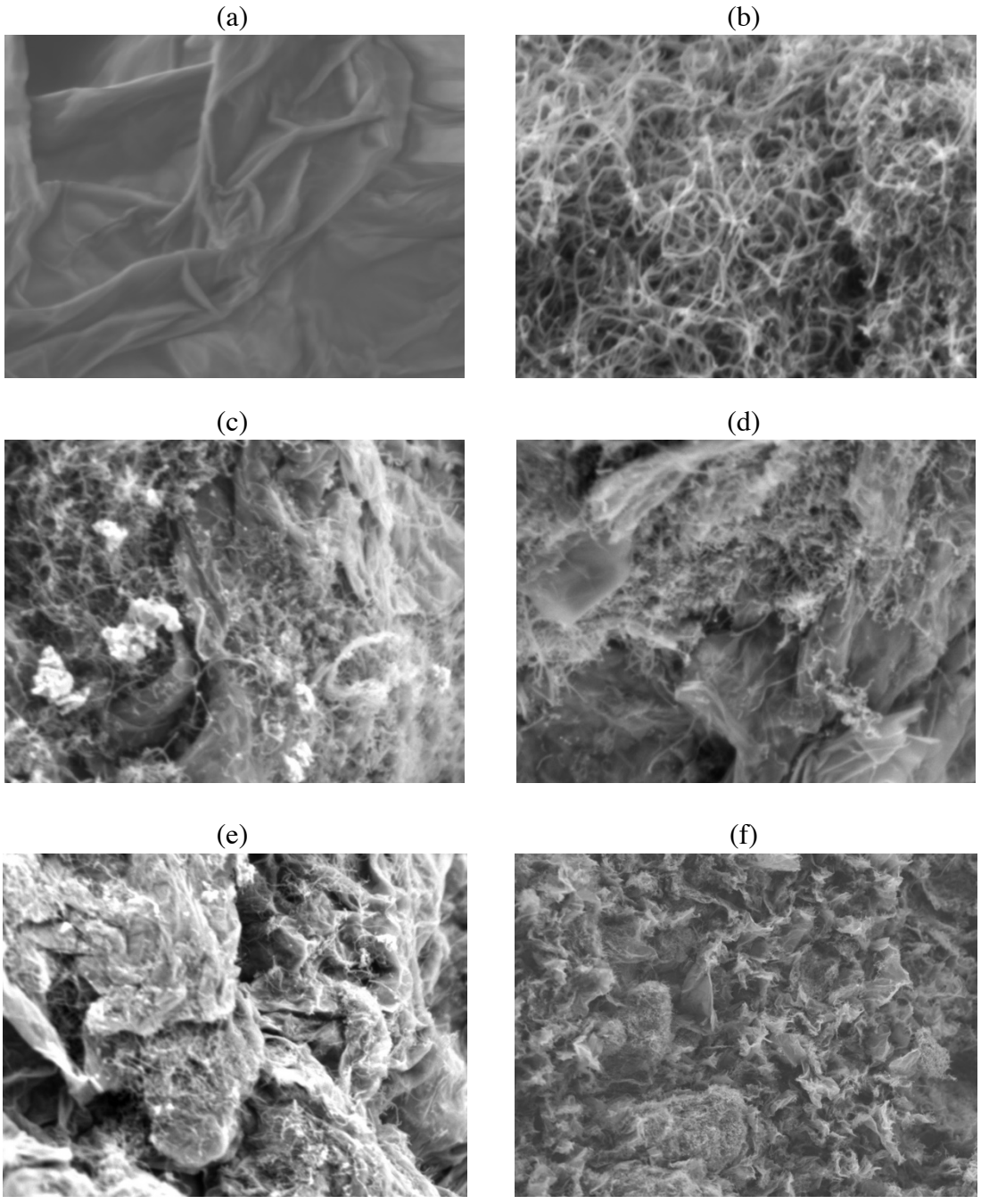

Figure 4.4 SEM images of **a)** GO, **b)** CNT, **c)** GO-CNT-26, **d)** rGO-CNT-18, **e)** rGO-CNT-7, **f)** rGO-CNT-2
Source: [118]

TGA analysis is shown in Figure 4.5. There were two main weight loss steps in the TGA analysis. The first weight loss was around 200 ºC for the removal of oxygen containing groups. This step was not noticeable in rGO-CNT-7 and rGO-CNT-2 which had very small amount of oxygen containing groups. The second weight loss was due to the oxidation of the carbon around 500 °C for pure GO and 600 °C for pure CNTs and the rGO-CNT hybrids were somewhere in between. The weight reduction temperature for the rGO-CNT-2 was nearly 700 °C which was higher than the raw CNT. After reduction, carbon showed higher thermal stability [230]. This data was in the same order as the Raman spectra that showed rGO-CNT-26 hybrid characteristics were closer to GO and rGO-CNT-2 characteristics were closer to the CNT.

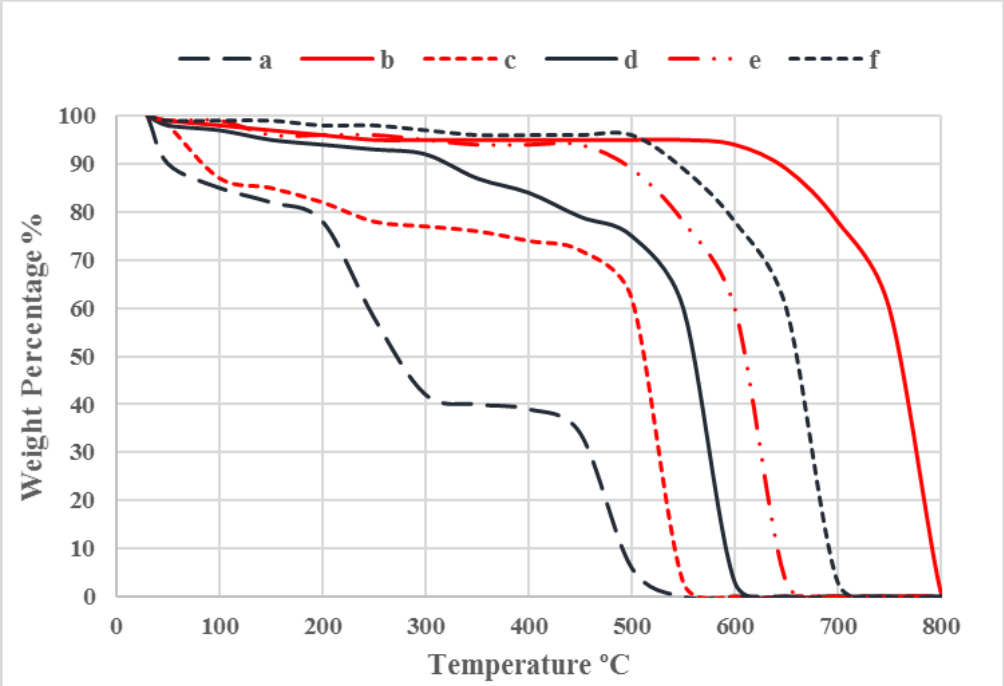

Figure 4.5 TGA of **a)** GO, **b)** CNT, **c)** GO-CNT-26, **d)** rGO-CNT-18, **e)** rGO-CNT-7, **f)** rGO-CNT-2.
Source: [118]

Pre-weighed amounts of the GO, CNT and rGO-CNTs were added to DI water and the solution was allowed to settle for 2 hours to measure the solubility and while dispersibility was measured by sonicating the suspension for 10 min and then the suspension was allowed to settle for 24 hours. Solubility and dispersibility of the samples are presented in Table1. The CNTs were insoluble, and the solubility of GO was 7.4 μg/ml, which reduced to 6.2 μg/ml after making the GO-CNT hybrid. This showed that GO was effective in dispersing the insoluble CNTs in the aqueous solution. Solubility decreased to near zero after reduction of GO in rGO-CNT-2. Dispersibility was in line with the solubility. Dispersibility decreased from 7.1 μg/ml for GO-CNT-26 to 0.5 μg/ml for rGO-CNT-2.

Hydrophobicity index (HI) was used to study the aqueous behavior of the hybrids using a method published before [205] [204,206]. 1-Octanol/Water partitioning followed by UV absorbance at 252 nm for quantification was used to calculate HI according to Equation (4.4) [204,206].

$$HI(\%) = \frac{(Ao - Ai)}{Ao} \times 100 \tag{4.4}$$

The 1-Octanol/water partitioning is shown in Figure 4.6 and the HI are presented in Table 1. The top part of the solution in Figure 4.6 is 1-Octanol and the bottom part is the water. From left to right in Figure 6, the samples became more hydrophobic after the reduction of oxygen containing groups. According to Table 4.1, HI of pure GO which was -3.89 % which was closer to GO-CNT-26 which showed an HI of -3.2 %. Removal of oxygen containing groups in the GO sheets led to higher hydrophobicity. rGO-CNT-2 was

highly hydrophobic with HI of 7.4 %. All the GO and GO-CNT-26 were dispersed in the water part. However, rGO-CNT-18 and rGO-CNT-7 were dispersed in both phases while rGO-CNT-2 and pure CNT were dispersed into the 1-Octanol.

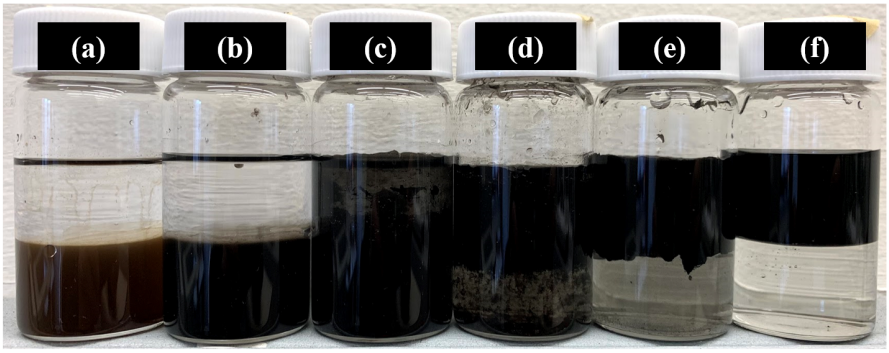

Figure 4.6 1-Octanol/water partitioning of **a)** GO, **b)** GO-CNT-26**, c)** rGO-CNT-18, **d)** rGO-CNT-7, **e)** rGO-CNT-2, **f)** CNT.
Source: [118]

The difference between the hybrids generated here and physical mixtures of CNT and GO is demonstrated as follows. rGO-CNT-23 was prepared by *in situ* reduction and an equivalent CNT-GO mixture was by physical mixing of the two components; both had same oxygen content. Figure 4.7 shows the 1-Octanol/water partitioning of rGO-CNT-23 and the CNT-rGO mixture. In case of the mixture, the CNTs partitioned in the 1-Ocatonl phase and the rGO in the aqueous phase. However, the in case of the rGO-CNT-23, the CNTs were embedded between the GO layers and the hybrid partitioned completely into the aqueous phase. This demonstrates the uniqueness of the rGO-CNT-23 generated via the *in situ* reduction technique.

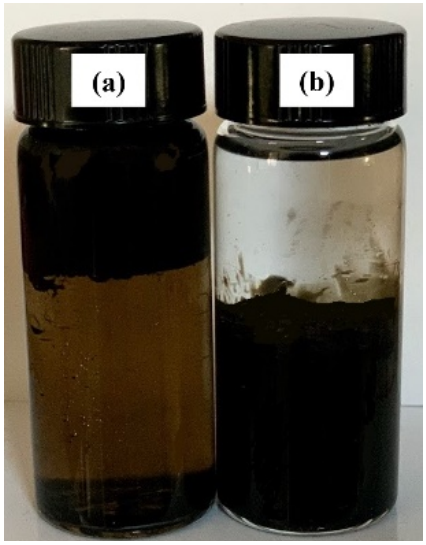

Figure 4.7 1-Octanol/water Partitioning for **a)** rGO-CNT mixture, **b)** *in situ* reduced rGO-CNT-23 hybrid.
Source: [118]

Aggregation kinetics of the samples was studied using dynamic light scattering. Colloidal stability is a balance between van der Waals forces which promotes aggregation and electrostatic repulsion. After addition of salts to the aqueous solution, Na^{+} and Mg^{2+} had no specific interactions with the oxygen containing groups of the GO and the aggregation followed conventional DLVO theory. GO sheets and CNT have anisotropic shapes and interaction between sheets and tubes can be from edge to edge or face to face. For the hybrids, these interactions are different than raw materials and they changed after the reduction to rGO. DLS measurement were made after sonication for an hour. As shown in Table 4.1, particle size increased with the addition of salts due to the coagulation of particles. From 642.3 nm for GO and 884 nm of CNT, it went up to 3025 nm for rGO-CNT-7 hybrid in presence of 0.5 mmole/l NaCl, and from 1274 nm of GO and 1423 nm of CNT, it goes up to 4558 nm for GO-CNT-7 hybrids in presence of 0.5 mmole/l $MgCl_2$. It

shows that particle size of the hybrids was much higher than raw GO and CNT and it increased after reduction of the GO. rGO-CNT-2 hybrids tended to fold, precipitate and settled down.

Attachment efficiency (α) which represents stability ratio of a dispersion, has been calculated by Equation (4.4). In the Equation (4.5), r_h is the radius of radius of an equivalent hard sphere diffusing at the same rate as the molecule under observation. Where $(drh/dt)t \to 0$ and $(drh/dt)t \to 0(f)$ represent the slow and fast aggregation regimes, respectively.

$$\propto = \frac{(drh/dt)t \to 0}{(drh/dt)t \to 0(f)} \tag{4.5}$$

The attachment efficiency was measured as the ratio of the initial slope of the aggregation profile to that obtained under fast aggregation conditions. Figures 4.8 and 4.9 plotted the attachment efficiency as a function of salt concentration. Critical Coagulation Concentration (CCC) was reached by the plotted Figures which is the border of the fast regime and the slow regime. CCC value is the transition point between fast and sloe regime which has been pointed in Figures 4.8 and 4.9. CCC values of the rGO-CNT-26,18 and 7 hybrids have been decreased and the coagulation occurred at lower concentrations since the particle size was much higher than the pristine materials. In contrast, the CCC value of rGO-CNT-2 could not be measured in presence of NaCl and $MgCl_2$ which is due to the sedimentation of rGO-CNT-2 samples during the experiment. Decreasing of CCC value after removing the oxygen containing groups in hybrids was due to the more interaction

between oxygen containing groups and electrolytes in solution. In general, the CCC value was significantly lower for hybrids than raw CNT and GO.

The Zeta potential measurements are presented in Table 4.1. Zeta potential for hybrids in presence of 0.5 mmole/l NaCl ranged from 26.3 to 10.4 mV, which implied decreasing stability of dispersions on removal of the oxygen containing groups. Addition of CNT to GO affected the zeta potential of pristine GO slightly. However, the zeta potential of the reduced hybrids in presence of 0.5 mmole/1 $MgCl_2$ was in the range of 8.2 to 0.8 mV, implying decrease in stability.

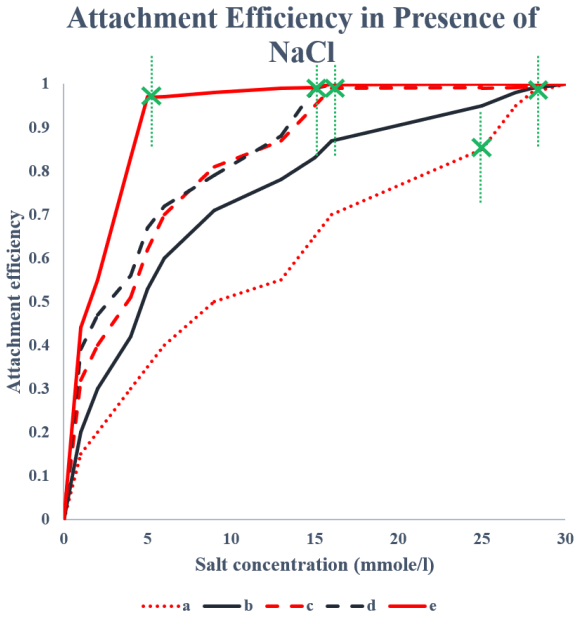

Figure 4.8 Attachment efficiency as a function of salt concentration of **a)** GO, **b)** CNT, **c)** GO-CNT-26, **d)** rGO-CNT-18, **e)** rGO-CNT-7 in presence of NaCl.
Source: [118]

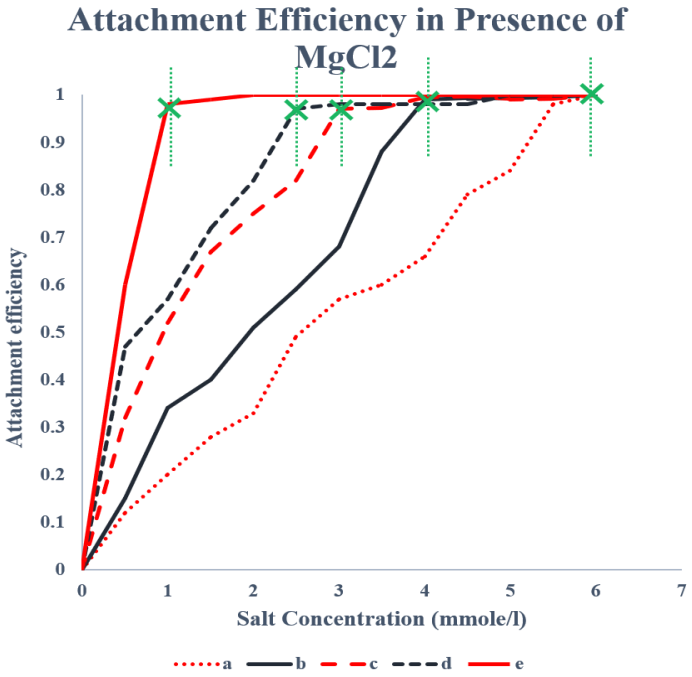

Figure 4.9 Attachment efficiency as a function of salt concentration of **a)** GO, **b)** CNT, **c)** GO-CNT-26, **d)** rGO-CNT-18, **e)** rGO-CNT-7 in presence of $MgCl_2$.
Source: [118]

Table 4.1 Summary of Data for Pristine GO, CNT and GO-CNT Hybrid and rGO-CNT Hybrids

Analysis/Sample	Pure GO	Pure CNT	GO-CNT-26	rGO-CNT-18	rGO-CNT-7	rGO-CNT-2
Carbon percentage	**46.5%**	**99.2%**	**74.25%**	**81.1%**	**93.2%**	**98.1%**
Oxygen percentage	**52.5%**	**0.3%**	**25.15%**	**17.9%**	**6.2%**	**1.8%**
L_a(nm)	**22.5**	**13.02**	**21.96**	**18.31**	**14.67**	**12.23**
Particle size in 0.5 mmole/1 NaCl (nm)	**642.3**	**884**	**1774**	**2315**	**3025**	**NA**
CCC in NaCl	**28**	**25**	**16**	**15**	**6**	**NA**
Zeta Potential in Presence of 0.5 mmole/l NaCl (mV)	**28**	**10.1**	**26.3**	**19.5**	**15.2**	**10.4**
Particle size in 0.5 mmole/1 $MgCl_2$ (nm)	**1274**	**1423**	**2166**	**2366**	**4558**	**NA**
CCC in $MgCl_2$	**6**	**4**	**3**	**2.5**	**1**	**NA**
Hydrophobicity Index	**-3.9%**	**8.7%**	**-3.2%**	**1.2%**	**4.5%**	**7.4%**
Zeta Potential in Presence of 0.5 mmole/l $MgCl_2$ (mV)	**-9.6**	**-0.7**	**-8.2**	**-5.2**	**-2.7**	**-0.8**
Solubility(µg/ml)	**7.4**	**~0**	**6.2**	**2.7**	**~0**	**~0**
Dispersibility(µg/ml)	**8**	**0.9**	**7.1**	**5.5**	**3.1**	**0.5**

Source: [118]

4.4 Conclusions

Nascent hydrogen was used to reduce the GO in GO-CNT hybrids and the process could be controlled to form hybrids with oxygen content ranging from 26 to 2 percent. The GO-CNT-26 hybrid was highly soluble, and solubility dropped to near zero at high degree of reduction. In addition, highly hydrophilic GO-CNT-26 hybrid increased in hydrophobicity as it was further reduced. Dispersibility also decreased from 7.1 μg/ml in GO-CNT-26 to 0.5 μg/ml in rGO-CNT-2. CCC value of the rGO-CNT-18 and rGO-CNT-7 hybrids in presence of NaCl and $MgCl_2$ decreased as well. CCC value for rGO-CNT-2 was not measurable, since it was highly hydrophobic and particle size was too high to be dispersed during the analysis. In general, GO at low level of reduction the hybrid behaved more like GO and as the reduction was increased it began to behave more like the CNTs.

CHAPTER 5

CARBON NANOMATERIALS DOPED POLYACRYLAMIDE GEL ELECTORLYTES FOR HIGH PERFORMANCE SUPERCAPACITORS

5.1 Introduction

Development of new generation portable and flexible electronics has increases the demand for lightweight, flexible, long cycle life, high performance, and safe energy storage devices [233-236]. Supercapacitors (SC) are essential energy storage devices [237,238] that play a crucial role in increasing battery life and energy efficiency [141,239-241]. Additionally, SCs are candidates to replace rechargeable batteries due to their high-speed charge-discharge capabilities, high power densities, low costs, and long cycle life [242]. Along with enhancing electrode capacitance, there has been much interest in improving the electrochemical potential of electrolytes [243,244].

SC electrolytes can be liquid, gel, and solid [245]. Liquid electrolytes have low dynamic viscosity and high conductivity compared to gel and solid electrolytes [246]. However, their shortcomings are safety, high costs of packaging, narrower operating temperature windows, and lower decomposition voltages [168,247-250]. It is also difficult to package in flexible and conformal devices. Flexible electrodes along with solid-state electrolytes have been used in flexible devices [251]. While they have good mechanical properties and are very suited for flexible devices, the solid electrolytes typically show low ionic conductivity and overall performance. Gel polymer electrolytes (GE) are great compromise between the liquid and solid, have relatively good mechanical properties, lightweight, can be packaged easily, and can have higher ionic conductivity than the solids [252-256].

Designing composites with optimal thermal, mechanical, and electrochemical properties is an important consideration in the new generation GE development [257]. Variety of aqueous, non-aqueous, redox and ionic liquid GEs have been reported. [168,258]. Polymers such as poly(acrylonitrile) (PAN) [259], poly(vinyl alcohol) (PVA) [260], polyaniline (PANI) [261], poly(ethylene oxide) (PEO) [262], poly(methyl methacrylate) (PMMA) [263], and poly(vinylidene fluoride) (PVDF) [264] have been studied for gel polymer electrolyte applications. Another important parameter in GE synthesis is the electrolyte selection such as acidic, alkali and neutral. PVA is the most commonly used GEs with KOH electrolyte but has several limitations such as low ionic conductivity and mechanical strength, and limited work has been reported for neutral electrolytes such as lithium chloride (LiCl) [258,265]. At this point, there is a need to explore other gel electrolytes especially for neutral electrolytes such as Li^+ which have lower corrosion and lowering the water content. Polyacrylamide (PAM) is a promising candidate for gel electrolytes with higher ionic conductivity due to its porous nature and improved mechanical properties [266]. PAM along with lithium sulphate ($LiSO_4$) is potentially a good combination for fabricating neutral PGE with as Li with its small radius can show faster diffusion.

Typical GEs suffer from low ionic migration compared to liquid electrolytes and it is crucial to design new generation of GEs with proper ionic conductivity , mechanical strength and thermal stability for better performance SCs. Carbon-based nanomaterials have excellent thermal, electrical, and mechanical properties and are among the most commonly used additives to improve electrolytes as well as electrodes [244,260,267]. The incorporation of carboxyl functionalized carbon nanotubes (fCNTs) and graphene oxide

(GO) into PGEs have shown to alter ionic conductivity and mechanical properties in PVA aqueous alkali, PAM non-aqueous and PVDF ionic liquid gel electrolytes [170,265,268]. Moreover, using carbon-nanomaterials in electrolytes also can increase electrode/electrolyte compatibility. Objective of this study was to develop a novel neutral PAM-based GEs incorporated with nanocarbons in order to improve thermal, mechanical and electrochemical properties.

5.2 Materials and Methods

Acrylamide (AA), N, N';-methylene bisacrylamide (MBA), potassium persulfate, lithium sulfate, potassium permanganate, polyethylene oxide (PEO), carbon black, poly(3,4-ethylene dioxythiophene)-poly(styrene sulfonate) (PEDOT: PSS, 1.3 wt%), hydrochloric acid and sulfuric acid with the purity of 99+% were purchased from Sigma Aldrich. Carbon nanotubes (CNTs), graphene oxide (GO), and carbon clothe purchased from Cheaptubes, Graphenea, and the Fuel Cell Store, respectively.

5.2.1 Preparation of fCNT, fCNT/GO Composite

fCNT and fCNT/GO composite were prepared by a method designed before [110,270]. Pristine CNTs were added to a 1:1 volume ratio concentrated HCl and H_2SO_4 and reacted under 100°C for 40 minutes. Products were dried in a vacuum oven overnight after being filtered and triple washed. Oxygen content in fCNTs was measured to be 18%. fCNT/GO composite was synthesized by mixing two components and sonicating at room temperature for 3 hours.

5.2.2 Synthesis of Polyacrylamide Gel Polymer Electrolytes

The plain gel was synthesized by mixing a weighted amount of AA, MBA, and $LiSO_4$ in MilliQ water and stirred at 80°C for 1 hour. This was followed by adding $K_2S_2O_8$ aqueous solution and stirring for 1 minute. The gel was then generated within a few minutes. Concentration of each component was fixed at 5.5% AA, 0.5% MBA, 18.5% $LiSO_4$, 0.5% $K_2S_2O_8$ and 75% water. To incorporate carbon nanomaterials in the gel, one step was added to the procedure. 1 mL of 0.1 mg/ml aqueous solutions of fCNTs, GO, fCNT/GO (0.6%) were sonicated with AA for 3 hours prior to the first step of the synthesis. The rest of the process was kept the same as described before.

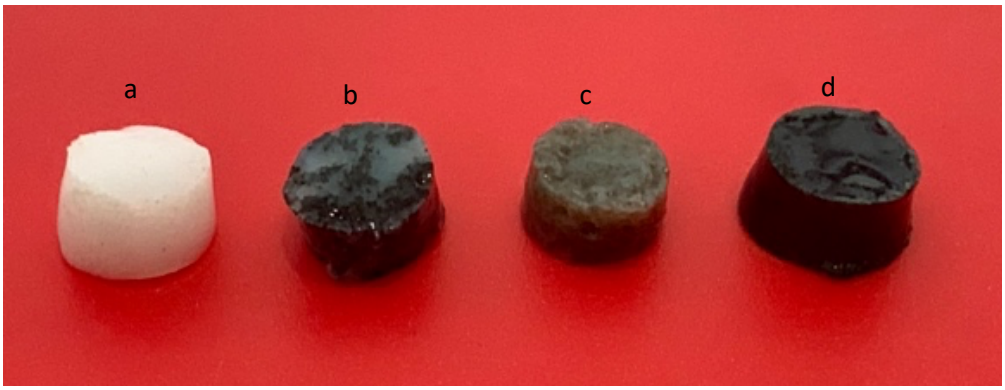

Figure 5.1 Image of **a)** PPGE, **b)** fCNT-PGE, **c)** GO-PGE, **d)** fCNT/GO-PGE.

5.2.3 Electrode Preparation and Device Assembly

Manganese dioxide (MnO_2) was synthesized as a base material for the electrodes. 25 mmol of 2.5 molar potassium permanganate solution and 9 mL concentrated hydrochloric acid was mixed and stirred overnight at room temperature. The procedure was followed by filtration and washing insoluble MnO_2 using MiliQ water. The reaction for the experiment is presented below:

$$2KMnO_{4(aq)} + 8HCl_{(aq)} \rightarrow 2KCl_{(aq)} + 2MnO_{2(s)} + 4H_2O + 3Cl_{2(g)} \quad (5.1)$$

Electrode paste composition was 85 % MnO_2, 5 % PEO, and 10 % carbon black. Total amount of 1 g dry powder was added into the 2.4 g PEDOT: PSS solution, mixed and applied on a conductive carbon cloth. Total electrode materials were set to 6 mg for further experiments.

Prepared electrodes were placed in the three-dimensional printed cases for measurements and tests. 3D printed casing design and the assembled product are presented in supplementary materials.

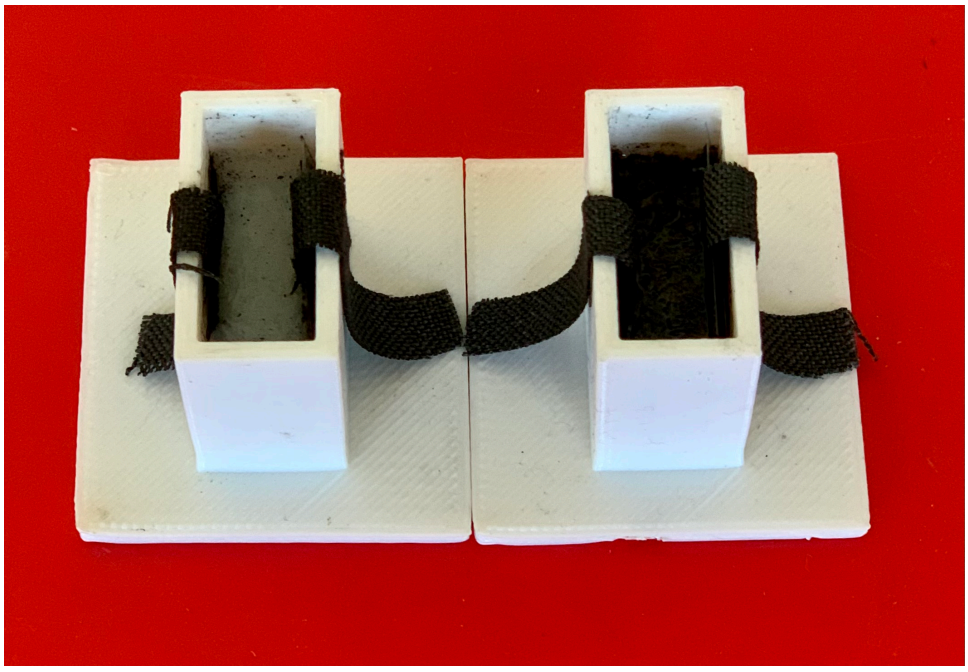

Figure 5.2 Image of PGEs casted in 3D printed casing.

5.2.4 Characterization and Electrochemical Measurements

The morphology of gel electrolytes was studied by JSM-7900F scanning electron microscope (SEM) from JEOL and Thermo Scientific DXRxi Raman imaging microscope. Thermal stability was investigated by Thermo Gravimetric Analyzer (TGA) and Differential Scanning Calorimeter (DSC) from Perkin Elmer. The rheological behaviors and mechanical properties of samples were studied by an oscillatory rheometer (Kinexus, Malvern Instruments, U.K.). Electrochemical impedance spectroscopy (EIS) and cyclic voltammetry (CV) were carried out on the Gamry instrument. Galvanostatic charge-discharge measurements were performed on an MTI Battery Analyzer.

5.3 Results and Discussion

5.3.1 Morphology of PGEs

Morphology of the dried PGEs and electrode material was observed under a Scanning Electron Microscope (SEM). Figure 5.3 a shows a flat structure of the dried PGE without any additive. Figures 5.3 b, c and d show the structure of the doped PGE by carbon nanomaterials, presenting submerging of fCNTs, GO, fCNT/GO in the gel structures. fCNTs tend to tangle and get clustered, same as GO layers that stack and agglomerate causing the uneven diffusion of nanomaterials through the PGE. On the other hand, in the fCNT/GO hybrid, there are π-π stacking interactions between fCNTs and graphene layers which increases synergistic effects in the hybrids and improve overall properties [271] as well as suspension distribution in gel scaffold [118]. Figures 5.3 e) and f) show fabricated MnO_2 as active material in SCs. Roughness and wrinkles on the synthesized MnO_2 increases the surface area and improves the overall performance of SCs. To clarify the

distribution of carbon nanomaterials in the PGE structure, Raman chemical imaging has been performed. Multivariate Curve Resolution (MCR) is an advanced method to investigate the composition of the chemicals [272] and the observed images of PGEs are presented in Figure 5.4. Each color on the MCR image represents a component in the PGE, and each component's identification is based on the Raman spectrum. Figure 5.4 a) shows the uniform structure of the PGE matrix, and the black color shows saturation of the individual Raman spectrum. Figures 5.4 b) and c) show an accumulation of fCNTs (blue) and GO (green) in the gel structure, respectively. From chemical composition images, it is observed that the distribution of the doped materials is uniform, and all the components are diffused evenly throughout the fCNT/GO-PGE in Figure 5.4 d).

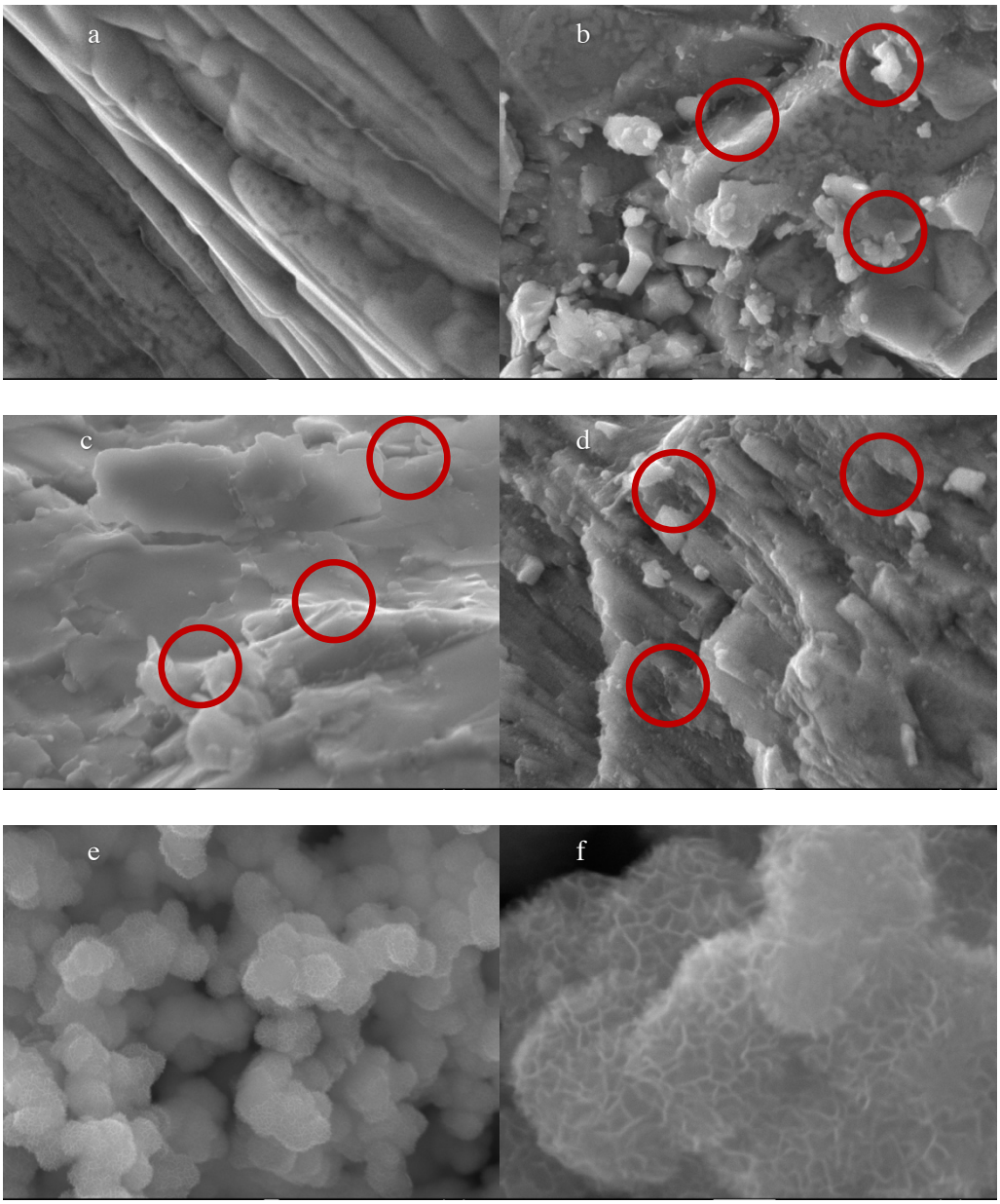

Figure 5.3 SEM images of **a)** PGE, **b)** fCNT-PGE, **c)** GO-PGE, **d)** fCNT/GO-PGE, **e)** and **f)** Generated MnO_2 for electrode materials.

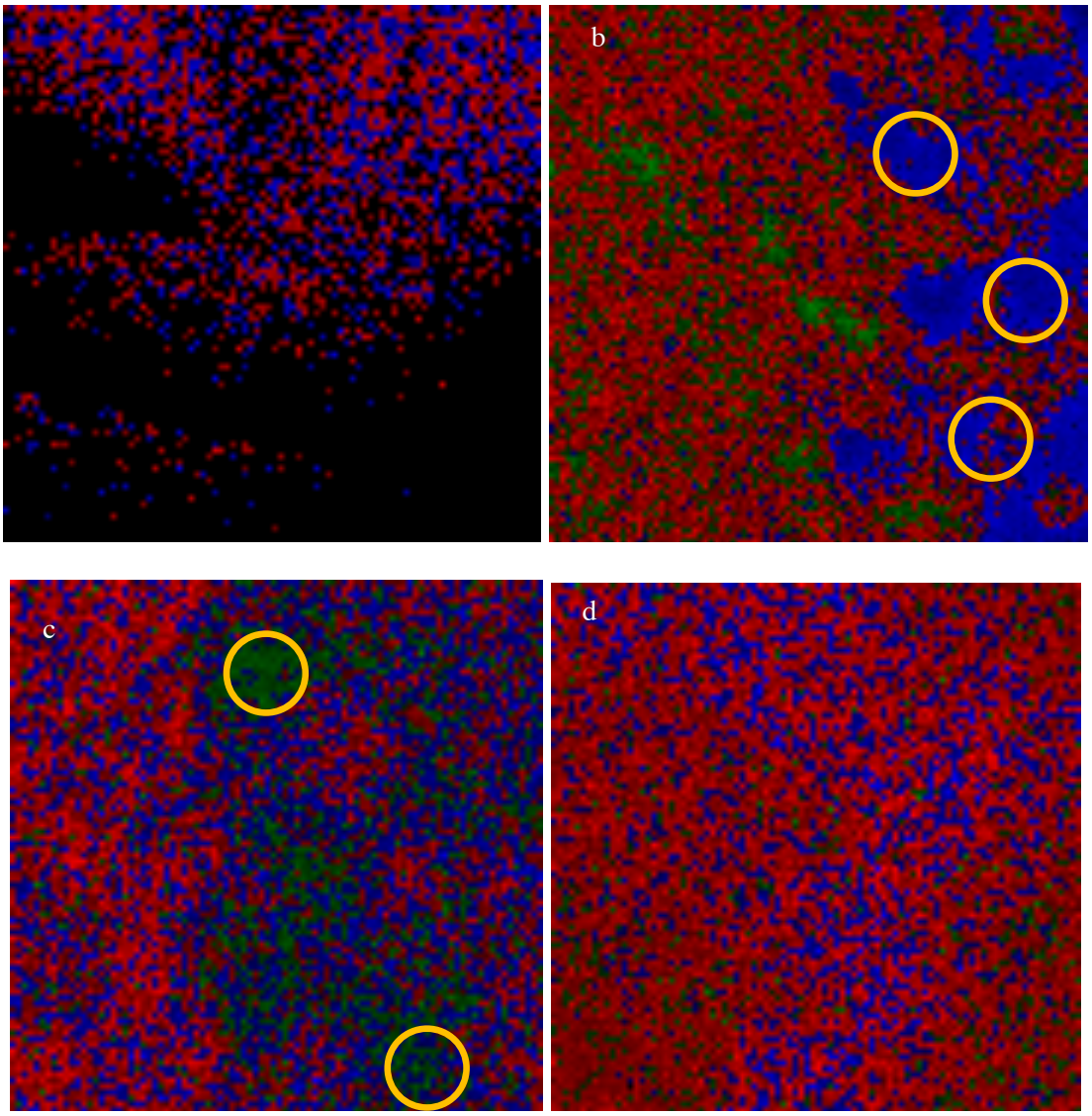

Figure 5.4 MCR images of **a)** PGE, **b)** fCNT-PGE (Blue color corresponds fCNTs), **c)** GO-PGE (Green color corresponds GO), **d)** fCNT/GO-PGE.

5.3.2 Thermal Stability Analysis

The thermal stability of GE plays an important in SCs stability and cycle life. Produced heat and temperature rise happens during the charge-discharge process, followed by electrolyte decomposition and device failure, or even safety issues. Also, the performance of SCs should remain stable in high-temperature environments [247,273].

The thermal stability of PGEs evaluated by a Thermo Gravimetric Analyzer (TGA) is presented in Figure 5.5. According to Figure 5.5, thermal degradation occurs in 3 steps. The first weight loss is happening by moisture removal in the gels. In the next stage, the co-polymer vaporizes from 150 °C to 430 °C. It is shown that the addition of GOs and fCNTs enhances the thermal stability of the PGE slightly. Since GO sheets have higher oxygen content (~45%), the weight loss at 100 °C is higher than other PGEs. fCNT/GO-PGE shows the most increased thermal stability among tested samples which will cause the lowest capacitance degradation.

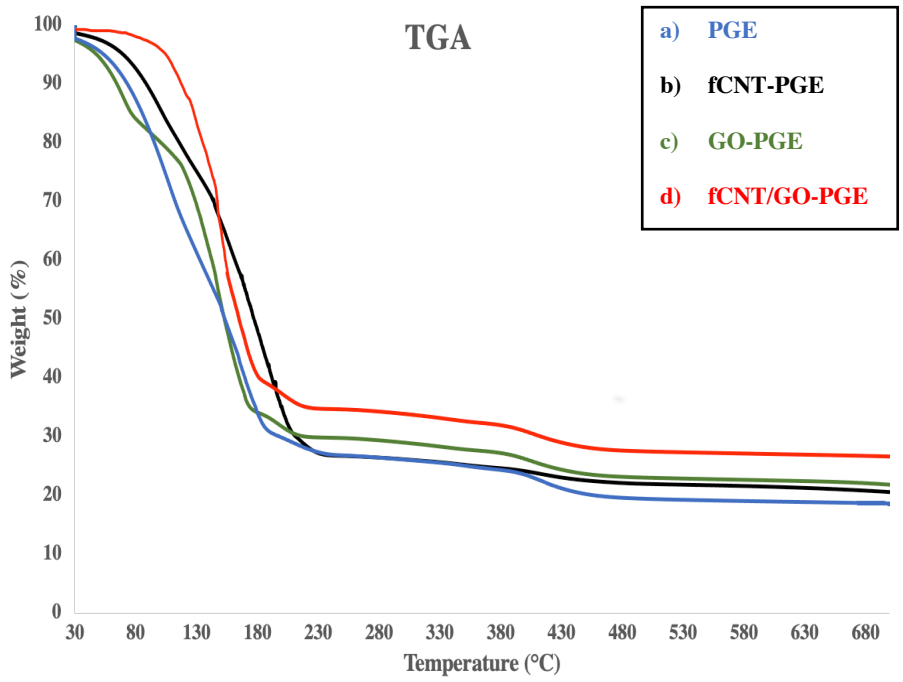

Figure 5.5 TGA graphs of **a)** PGE, **b)** fCNT-PGE, **c)** GO-PGE, **d)** fCNT/GO-PGE.

Differential Scanning Calorimeter (DSC) measurements were performed from 30 °C to 300 °C in the presence of N_2 gas. DSC is a useful measurement in terms of

thermodynamic properties of the gel electrolytes. Glass transition temperature (T_g) and the melting enthalpy (ΔH_m) based on DSC curves are presented in Table 5.1. According to Table 5.1, T_g of the electrolytes increased by adding carbon nanomaterials due to the hydrogen bonds intermolecular attraction in oxygen-containing groups of carbon derivatives and polymer chains followed by reducing chain mobility. Since GO contains more oxygen-containing functional groups than fCNTs, the hydrogen bonds of the gel composition and the oxygen-containing groups are higher in GO-PGE than the fCNT composite. More effective hydrogen bonds in the electrolyte structures bring a higher T_g for fCNT/GO-PGE compared to other electrolytes. Reduction of ΔH_m from 177 to 91.39 J/g indicates decreasing crystallinity of PGEs after doping with carbon nanomaterials. Lower alignments in polymer chains form canals for better ion diffusion.

Table 5.1 Thermal and Mechanical Properties of Gels Incorporated by Carbon Nanomaterials

Gel Electrolytes	$T_g(°C)$	$\Delta H_m(\frac{J}{g})$	***Elastic Modulus (kPa)***	***Loss Factor*** $(tan\delta)$
PGE	93.7	177.44	2.3	0.06
fCNT-PGE	118.5	169.44	1.5	0.05
GO-PGE	121.2	138.38	4.9	0.40
fCNT/GO-PGE	130.8	91.39	4.3	0.43

5.3.3 Viscoelastic Properties of PGEs

The rheological behaviors of samples were studied by a rotational viscometer. Dynamic strain sweep test was performed under the constant strain amplitude of 1 Hz at room

temperature to investigate the effect of shear stress on the viscoelastic behavior of the PGEs. Storage (elastic) modulus (G') and the loss (viscous) modulus (G") were collected and presented as a function of strain percentage in Figure 5.6. Increment of G' in GO-PGE and fCNT/GO-PGE shows the transformation of viscous gel to a more rigid and elastic composite. This alteration is also because oxygen-containing groups in GO and fCNT/GO form hydrogen bonds with polymer chains and improve the mechanical strength of the gel [265].

On the contrary, fCNTs that contain fewer carboxyl groups than GO agglomerates more in the PGE complex, forming defect areas. Nanomaterial agglomeration causes a lack of connection between the fCNTs and polymer matrix. The ratio of G″ to G′ introduced as loss factor (tan δ) is presented in Table 5.1. Tan δ describes the solid and liquid characteristics of the PGEs, and at the point that it becomes equal to 1, G″ crosses the G′ curve. According to Figure 5.6, in fCNT-PGE, the externally applied force is more than intermolecular forces, and irreversible collapse occurs [274]. A lower loss factor for PGE and fCNT-PGE represents a more solid-like structure, and a higher loss factor for GO-PGE and fCNT-PGE presents a more gel-like sticky structure. Adhesive properties are appropriate properties in SCs applications in order to increase the contact of PGE and electrode materials.

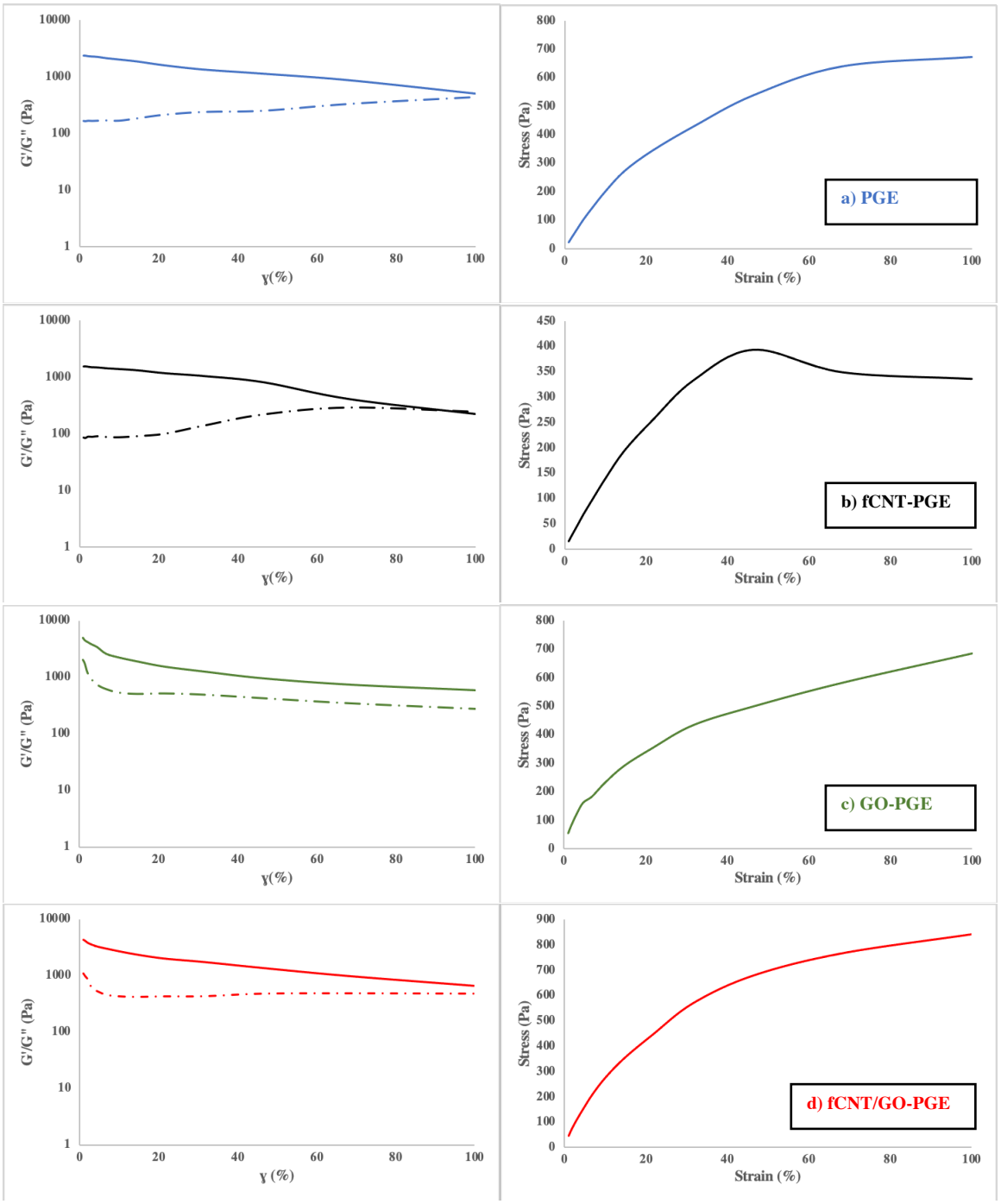

Figure 5.6 Strain sweep and strain stress curves of **a)** PGE, **b)** fCNT-PGE, **c)** GO-PGE, **d)** fCNT/GO-PGE.

5.3.4 EIS and CV Analysis for Gel Electrolytes

Electrochemical impedance spectroscopy (EIS), which is an alternating current (AC) based measurement, has been performed to reach detailed information about PGEs [275]. The efficiency of SCs strongly depends on ion redox and ionic conductivity of the electrolytes. Two probe analysis was carried out by connecting working/sense electrode (anode) and counter/reference electrode (cathode) to graphite sheets placed in a three dimensional printed case filled with gel electrolytes. Measurements were performed under 10 mHz to 100 kHz with 0.1 mV amplitude and 0 DC voltage, and oscillating current response through the sample was collected. Nyquist and bode plots are presented in Figures 5.7 a) and b) to compare prepared PGE, and the summary of the data is presented in Table 5.2. Interception in the high-frequency region and x-axis in Nyquist plot (Real Z versus Imaginary Z) shows bulk resistance (R_b) of the PGE. In general, Nyquist plots are separated into three regions, including semicircle at high frequencies, which is the interfacial charge transfer region, diffusion, and capacitive region. According to Figure 5.6 a), the semicircle of Nyquist plots for the gel electrolytes are not noticeable. The particular reason for this matter is the very small charge transfer resistance at the graphite electrode interface and gel electrolytes [276,277].

The ionic conductivity, which can be extracted from the Nyquist plot, is a critical parameter in electrolyte properties. As bulk resistance increases, the conducting nature will decrease. Ionic conductivity (σ) of gels is calculated by using Equation (5.2), and the resulted values listed in Table 5.2:

$$\sigma = \frac{L}{R_b A} \tag{5.2}$$

Where L is the thickness of electrolyte and A is the surface area that graphite sheets and gels contact. Ionic conductivity of the gel electrolytes is listed as 41.2, 58.8, 60, and 132 $m S cm^{-1}$ respectively for pure gel, fCNT-PGE, GO-PGE, and fCNT/GO-PGE.

The reason for conductivity increment is that the Li^{+} with a small ionic radius diffuses between GO layers and increases the final ionic conductivity. The charge transfer of fCNT/GO-PGE is three times higher than pure PAM gel electrolyte, and also higher than fCNT-PGE and GO-PGE since the distribution of carbon nanomaterials is uniform in this gel electrolyte. In addition, the presence of uniformly distributed carbon nanomaterial expands catalytic areas in gel scaffold, and diffusion of ions occurs faster.

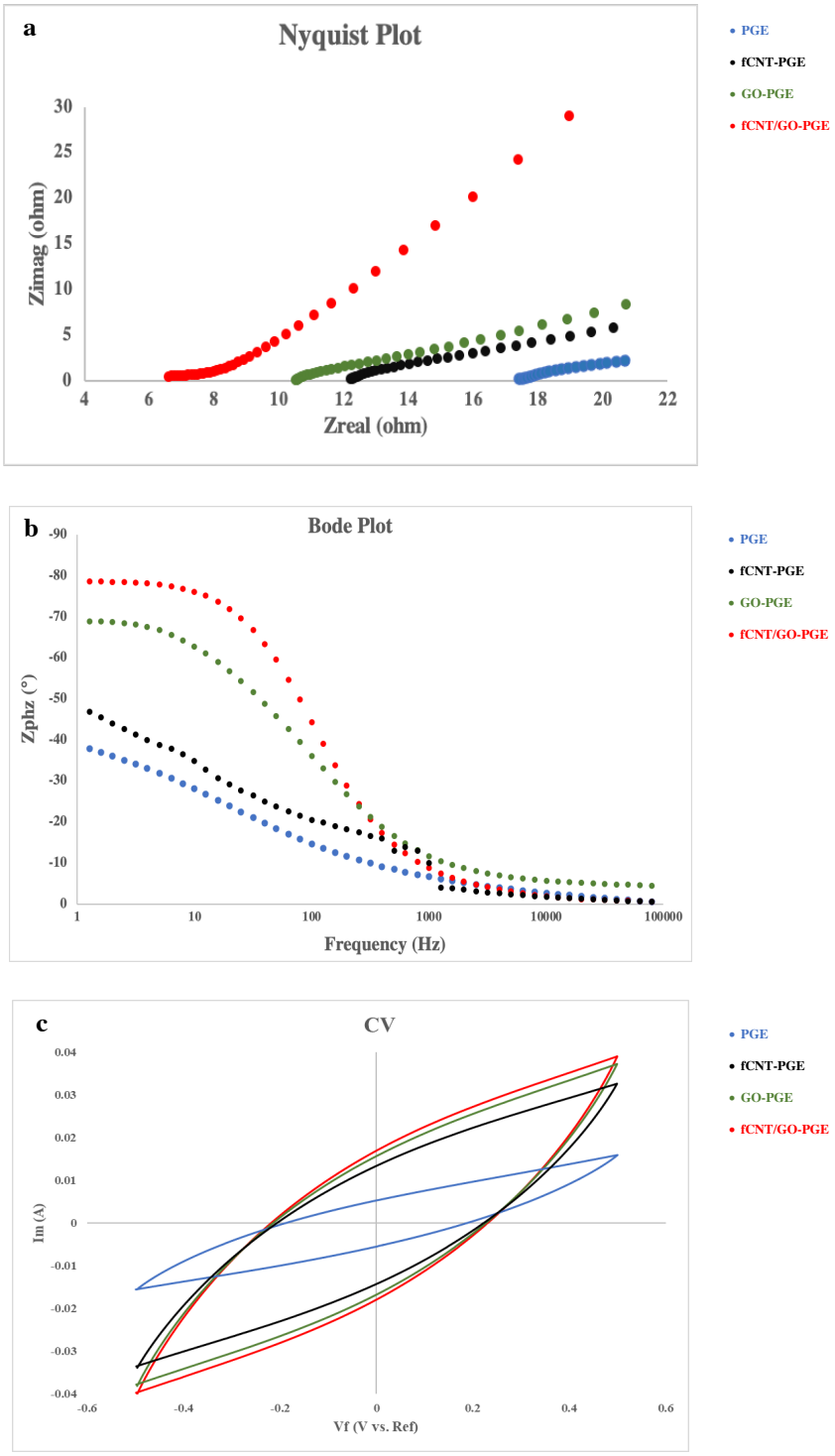

Figure 5.7 **a**) Nyquist plots, **b)** Bode plots, and **c)** Cyclic voltammetry at 100 mV s^{-1} of PGE, fCNT-PGE, GO-PGE and fCNT/GO-PGE.

Table 5.2 Electrochemical Properties of Gels Incorporated by Carbon Nanomaterials

Gel Electrolytes	*Bulk Resistance R_b (Ω)*	*Ionic conductivity σ ($mS\ cm^{-1}$)*	*Phase (°)*	*Average electrons lifetime τ (mS)*	*Specific Capacitance (Fg^{-1})*
PGE	16	41	45	0.016	39.5
fCNT-PGE	11	59	56	0.005	65.5
GO-PGE	10	64	70	0.004	77.6
fCNT/GO -PGE	5	132	83	0.001	83.3

Bode plot is a frequency-based plot of EIS measurements, and the phase vs. frequency diagram includes three different areas: capacitive behavior at lower frequency followed by diffusion and interfacial charge transfer [277]. The collected angle difference between the charging voltage and the current is presented as phase degree and presented in Table 5.2. The negative angle degree is related to the leading current from voltage by 90 degrees [278]. Another parameter that is calculated from the bode plot is the average electrons lifetime (τ) by adding peak frequency (f_p) in Equation (5.3) [279].

$$T = \frac{1}{2\,\pi f_p} \tag{5.3}$$

Since τ is as low as 0.001 mS for fCNT/GO-PGE, ions transfer faster, and it is in line with the higher ionic conductivity for fCNT/GO-PGE compared to other PGEs.

Electrochemical properties of gel electrolytes were determined by running cyclic voltammetry (CV) at 5, 10, 50, and 100 mV s^{-1} at room temperature. Symmetrical carbon

cloth electrodes have been used as anode and cathode to establish cyclic voltammograms for a scan rate of 100 mV s^{-1} presented in Figure 5.7. The gel electrolytes incorporated by carbon nanomaterials show better performance than PGE in all scan rates, which is due to the enhancement of ion transfer in the presence of fCNTs, GO and fCNT/GO in PGEs. Moreover, the semi-rectangular shape of CV rises from the reversibility of the reaction.

5.3.5 Galvanostatic Charge-Discharge Studies

Prepared electrodes and PGEs were examined by galvanostatic discharge measurements performed on an MTI Battery Analyzer and cycled between 0 and 1.5 V. Galvanostatic charge/discharge curves are presented in Figure 6. Capacitance was calculated from Equation (5.4) and listed in Table 5.2:

$$C_{sp} : Specific\ capacitance\ (F.g^{-1}) = \frac{I}{\frac{dV}{dt} \times m} \tag{5.4}$$

Where I is discharge current (A cm^2), dv/dt is the slope of the discharge curve, and m is the mass of electrode material (g).

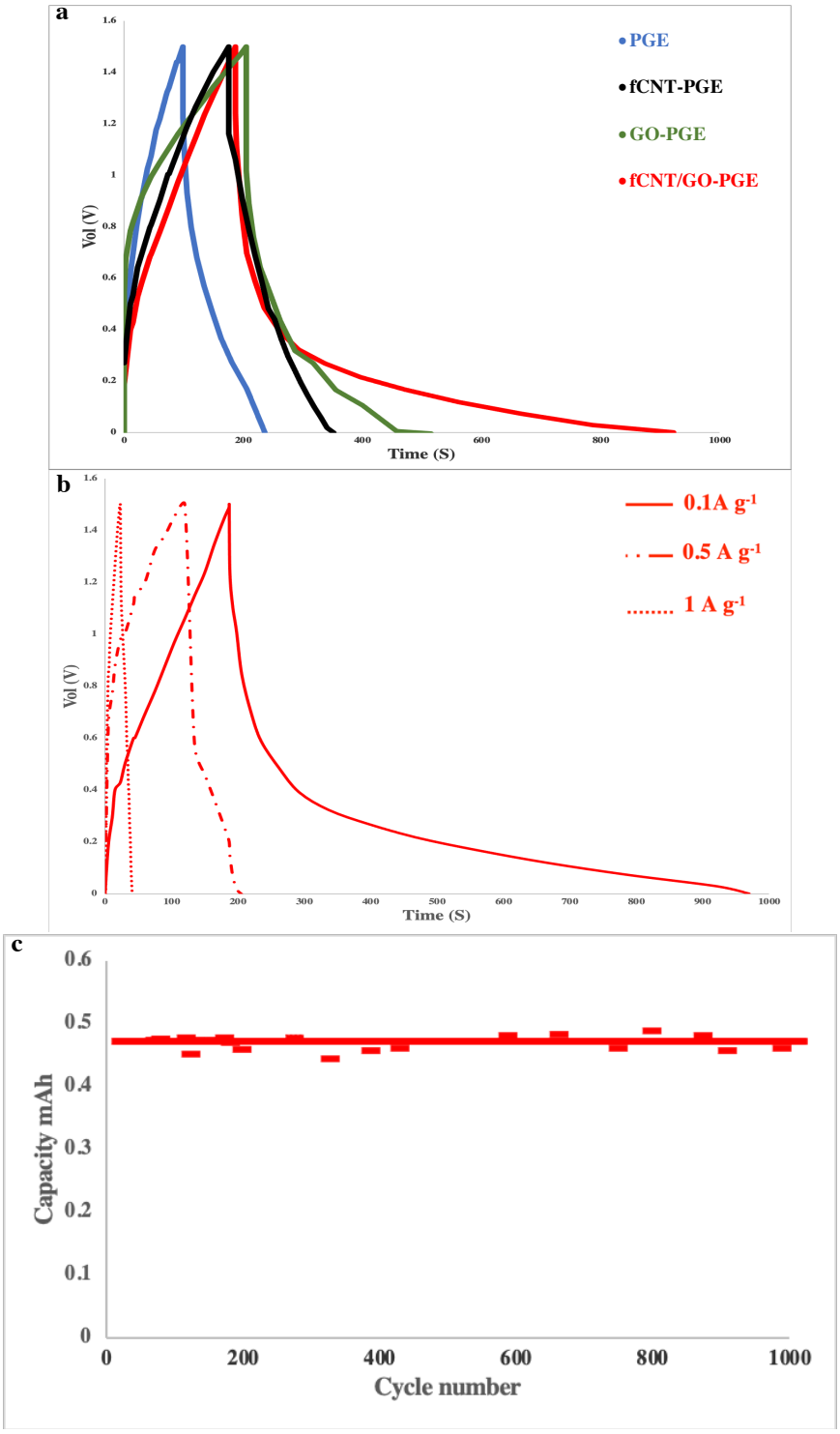

Figure 5.8 Electrochemical performance of PGE based SCs. **a)** Galvanostatic Charge-Discharge curves under the current density of 0.1 A g^{-1}, **b)** Galvanostatic Charge-Discharge curves of fCNT/GO-PGE SC under the current density of 0.1, 0.5 and 1 A g^{-1}, **c)** Cycling performance of fCNT/GO-PGE SC a current density of 0.1 A g^{-1}.

Calculated capacitance values are 39.5, 65.5, 77.6, and 83.3 F g^{-1} for PGE, fCNT-PGE, GO-PGE, and fCNT/GO-PGE, respectively. The specific capacitance of SCs improved by adding carbon nanomaterials due to the increment of ionic conductivity in PGEs. The addition of carbon nanomaterials in the PGE framework facilitates ion migration between the electrodes by generating pores. fCNT/GO benefits from multiple parameters and shows the best electrolyte properties. fCNT/GO hybrid with a homogenous structure has uniform distribution and less aggregation of additives in composites. On the other hand, more gel-like properties of fCNT/GO-PGE provide better adhesion and fewer voids at the electrode-electrolyte interface. Charge-discharge measurements for 1 A g^{-1} and 0.5A g^{-1}, as well as the capacity of SC at 0.1 A g^{-1} current for 1000 cycles for fCNT/GO-PGE, are reported in Figures 5.8 b) and c).

5.4 Conclusions

In conclusion, advanced gel electrolytes doped by carbon nanomaterials were prepared, and their thermal, mechanical, and electrochemical properties were studied. PGE, fCNT-PGE, GO-PGE, and fCNT/GO-PGE electrolytes were compared in different aspects. It was found that the incorporation of 0.6% carbon nanomaterials altered the thermal and mechanical properties of PGE. T_g of the samples increased from 93.7 to 130.8 °C for PGE to fCNT/GO-PGE. Using fCNTs along with GO in composite structure increased the synergetic effect and uniform distribution of integrated materials. Rheological properties of PGEs were studied, and elastic modulus was doubled in fCNT/GO-PGE compared to PGE owing to the hydrogen bonds formed between carboxyl groups in nanomaterials and gel structure.

Additionally, from EIS measurements, ionic conductivity doubled by using fCNT/GO in the PGE structure. This was due to the formation of ionic channels in the gel composition. The presence of fCNTs prevented aggregation of GO sheets and increased overall performance compared to fCNT-PGE or GO-PGE. Moreover, the performance of SCs with generated PGEs was studied, and it showed that the specific capacitance of SCs risen from 39.5 to 83.3 Fg^{-1}. In general, doping of nano carbons, especially the combination of carboxylated nanotubes and graphene oxides, brought improvement to thermal, mechanical, and electrochemical properties of PAM-based gel electrolytes. These gel electrolytes also have great potential for flexible electrochemical devices.

CHAPTER 6

SUMMARY OF FINDINGS AND RECOMMENDATIONS

This dissertation is a detailed study on effect of oxygen containing functional groups of graphene oxide and graphene oxide carbon nanotube hybrids on their solubility, dispersibility, hydrophobicity and colloidal behavior.

Graphene oxide was successfully reduced in a step-wise pattern by addition of calculated amount of zinc powder in an acidic environment. It was concluded that removing oxygen containing groups increases the hydrophobicity and decreases the solubility and dispersibility of rGOs.

Additionally, carbon nanotubes and graphene oxide hybrids was fabricated and reduced accordingly. Presence of CNTs during the reduction process decreases the coagulation and of rGO sheets. It was concluded that as reduction level of rGO increases, solubility and dispersibility of the hybrids decreases and they become more hydrophobic.

Finally, carboxylated CNT, GO and fCNT-GO hybrids was incorporated into polyacrylamide gel electrolytes for supercapacitor applications. It was demonstrated that carbon-nanomaterials specifically fCNT-GO hybrid are effective additives in gel electrolyte applications to improve ionic conductivity, as well as mechanical strength and thermal stability.

This dissertation demonstrated the importance of oxygen containing functional groups on final properties of graphene oxide. In future, studies should be focused on other properties of rGOs such as electrical properties which are important in electronic devices application. Moreover, effectiveness of CNT presence in rGO procedure opens a new

variety of structural for other variation of the CNT-GO hybrids, such as fCNT-GO, CNT-rGO and fCNT and rGO. Different variation of hybrids should be compared in order to increase applications as well as detailed environmental fate studies. Additionally, rGO-CNT with the lowest oxygen content and high electrical conductivity is a great candidate for electrode materials in battery design. Synergetic effect of rGO-CNT will increase the conductivity of the final electrode materials in lithium ion or zinc air batteries. Finally, molecular dynamic (MD) is an effective method to determine properties of graphene derivatives computationally. Using an MD simulation to understand the aqueous behavior of rGOs and effect of oxygen content in rGOs will give a better visualization of the reduction effects.

REFERENCES

1. Dresselhaus, M.S.; Terrones, M. Carbon-based nanomaterials from a historical perspective. *Proceedings of the IEEE* **2013**, *101*, 1522-1535, doi:10.1109/JPROC.2013.2261271.

2. Li, Y.; Li, Z.; Lei, L.; Lan, T.; Li, Y.; Li, P.; Lin, X.; Liu, R.; Huang, Z.; Fen, X.; et al. Chemical vapor deposition-grown carbon nanotubes/graphene hybrids for electrochemical energy storage and conversion. *FlatChem* **2019**, *15*, 100091, doi:https://doi.org/10.1016/j.flatc.2019.100091.

3. De la Calle, I.; Romero-Rivas, V. Chapter 9 - The role of nanomaterials in analytical chemistry: trace metal analysis. *Applications of nanomaterials*, Mohan Bhagyaraj, S., Oluwafemi, O.S., Kalarikkal, N., Thomas, S., Eds.; Cambridge, MA: Woodhead Publishing: 2018; pp. 251-301.

4. Iijima, S. Helical microtubules of graphitic carbon. *Nature* **1991**, *354*, 56-58, doi:10.1038/354056a0.

5. Geim, A.K.; Novoselov, K.S. The rise of graphene. *Nature Materials* **2007**, *6*, 183-191.

6. Rao, N.; Singh, R.; Bashambu, L. Carbon-based nanomaterials: Synthesis and prospective applications. *Materials Today: Proceedings* **2020**, doi:https://doi.org/10.1016/j.matpr.2020.10.593.

7. Su, H.; Lai, Z.; Kan, E.; Zhu, X. Hp-C17: A novel carbon allotrope with an all-sp3 network. *Physics Letters A* **2020**, *384*, 126379, doi:https://doi.org/10.1016/j.physleta.2020.126379.

8. Hong, X.; Shi, W.; Zheng, H.; Liang, D. Effective carbon nanotubes/graphene hybrid films for electron field emission application. *Vacuum* **2019**, *169*, 108917, doi:https://doi.org/10.1016/j.vacuum.2019.108917.

9. Park, S.; An, J.; Potts, J.R.; Velamakanni, A.; Murali, S.; Ruoff, R.S. Hydrazine-reduction of graphite- and graphene oxide. *Carbon* **2011**, *49*, 3019-3023, doi:https://doi.org/10.1016/j.carbon.2011.02.071.

10. Mogera, U.; Kulkarni, G.U. A new twist in graphene research: Twisted graphene. *Carbon* **2020**, *156*, 470-487, doi:https://doi.org/10.1016/j.carbon.2019.09.053.

11. Wang, Y.; Li, Z.; Wang, J.; Li, J.; Lin, Y. Graphene and graphene oxide: biofunctionalization and applications in biotechnology. *Trends in Biotechnology* **2011**, *29*, 205-212, doi:https://doi.org/10.1016/j.tibtech.2011.01.008.

12. Bhuyan, M.S.A.; Uddin, M.N.; Islam, M.M.; Bipasha, F.A.; Hossain, S.S. Synthesis of graphene. *International Nano Letters* **2016**, *6*, 65-83, doi:10.1007/s40089-015-0176-1.

13. Zhu, Y.; Murali, S.; Cai, W.; Li, X.; Suk, J.W.; Potts, J.R.; Ruoff, R.S. Graphene and graphene oxide: synthesis, properties, and applications. *Advanced Materials* **2010**, *22*, 3906-3924, doi:10.1002/adma.201001068.

14. Choi, J.; Tu, N.D.K.; Lee, S.-S.; Lee, H.; Kim, J.S.; Kim, H. Controlled oxidation level of reduced graphene oxides and its effect on thermoelectric properties. *Macromolecular Research* **2014**, *22*, 1104-1108, doi:10.1007/s13233-014-2160-4.

15. Mypati, S.; Sellathurai, A.; Kontopoulou, M.; Docoslis, A.; Barz, D.P.J. High concentration graphene nanoplatelet dispersions in water stabilized by graphene oxide. *Carbon* **2020**, doi:https://doi.org/10.1016/j.carbon.2020.12.068.

16. Pei, S.; Cheng, H.-M. The reduction of graphene oxide. *Carbon* **2012**, *50*, 3210-3228, doi:https://doi.org/10.1016/j.carbon.2011.11.010.

17. Marcano, D.C.; Kosynkin, D.V.; Berlin, J.M.; Sinitskii, A.; Sun, Z.; Slesarev, A.; Alemany, L.B.; Lu, W.; Tour, J.M. Improved synthesis of graphene oxide. *ACS Nano* **2010**, *4*, 4806-4814, doi:10.1021/nn1006368.

18. Paredes, J.I.; Villar-Rodil, S.; Martínez-Alonso, A.; Tascón, J.M.D. Graphene oxide dispersions in organic solvents. *Langmuir* **2008**, *24*, 10560-10564, doi:10.1021/la801744a.

19. Geim, A.K.; Novoselov, K.S. The rise of graphene. *Nature Materials* **2007**, *6*, 183-191, doi:10.1038/nmat1849.

20. Xu, T.; Yang, D.; Fan, Z.; Li, X.; Liu, Y.; Guo, C.; Zhang, M.; Yu, Z.-Z. Reduced graphene oxide/carbon nanotube hybrid fibers with narrowly distributed mesopores for flexible supercapacitors with high volumetric capacitances and satisfactory durability. *Carbon* **2019**, *152*, 134-143, doi:https://doi.org/10.1016/j.carbon.2019.06.005.

21. Du, W.; Wu, H.; Chen, H.; Xu, G.; Li, C. Graphene oxide in aqueous and nonaqueous media: Dispersion behaviour and solution chemistry. *Carbon* **2020**, *158*, 568-579, doi:https://doi.org/10.1016/j.carbon.2019.11.027.

22. Choi, W.; Lahiri, I.; Seelaboyina, R.; Kang, Y.S. Synthesis of graphene and its applications: A Review. *Critical Reviews in Solid State and Materials Sciences* **2010**, *35*, 52-71, doi:10.1080/10408430903505036.

23. Sundararajan, S.; Bhushan, B. Development of AFM-based techniques to measure mechanical properties of nanoscale structures. *Sensors and Actuators A: Physical* **2002**, *101*, 338-351, doi:https://doi.org/10.1016/S0924-4247(02)00268-6.

24. Zhou, C.; Li, F.; Hu, J.; Ren, M.; Wei, J.; Yu, Q. Enhanced mechanical properties of cement paste by hybrid graphene oxide/carbon nanotubes. *Construction and Building Materials* **2017**, *134*, 336-345, doi:https://doi.org/10.1016/j.conbuildmat.2016.12.147.

25. Suresh Balaji, S.; Sandhiya, M.; Sathish, M. Enhanced electrochemical performance of supercritical fluid aided P-doped graphene nanoflakes by I3−/I− redox couple. *Journal of Energy Storage* **2021**, *33*, 102085, doi:https://doi.org/10.1016/j.est.2020.102085.

26. Hossain, S.; Abdalla, A.M.; Suhaili, S.B.H.; Kamal, I.; Shaikh, S.P.S.; Dawood, M.K.; Azad, A.K. Nanostructured graphene materials utilization in fuel cells and batteries: A review. *Journal of Energy Storage* **2020**, *29*, 101386, doi:https://doi.org/10.1016/j.est.2020.101386.

27. Jia, Y.; Zhao, Y.-S.; Yang, X.-X.; Ren, M.-X.; Wang, Y.-Q.; Lei, B.-Y.; Zhao, D.-L. Sulfur encapsulated in nitrogen-doped graphene aerogel as a cathode material for high performance lithium-sulfur batteries. *International Journal of Hydrogen Energy* **2020**, doi:https://doi.org/10.1016/j.ijhydene.2020.11.199.

28. Huang, L.; Diao, D.; Cao, Y. Electrochemical corrosion behaviors of N-doped graphene sheets embedded carbon films in acid. *Applied Surface Science* **2020**, 148781, doi:https://doi.org/10.1016/j.apsusc.2020.148781.

29. Luo, G.-Y.; Gu, Y.-J.; Liu, Y.; Chen, Z.-L.; Huo, Y.-l.; Wu, F.-Z.; Mai, Y.; Dai, X.-Y.; Deng, Y. Electrochemical performance of in situ LiFePO4 modified by N-doped graphene for Li-ion batteries. *Ceramics International* **2021**, doi:https://doi.org/10.1016/j.ceramint.2020.12.259.

30. Altuntepe, A.; Zan, R. Permanent boron doped graphene with high homogeneity using phenylboronic acid. *Journal of Molecular Structure* **2020**, 129629, doi:https://doi.org/10.1016/j.molstruc.2020.129629.

31. Qu, Y.; Ding, J.; Fu, H.; Chen, H.; Peng, J. Investigation on tunable electronic properties of semiconducting graphene induced by boron and sulfur doping. *Applied Surface Science* **2021**, *542*, 148763, doi:https://doi.org/10.1016/j.apsusc.2020.148763.

32. Tewatia, K.; Sharma, A.; Sharma, M.; Kumar, A. Synthesis of graphene oxide and its reduction by green reducing agent. *Materials Today: Proceedings* **2020**, doi:https://doi.org/10.1016/j.matpr.2020.09.294.

33. Nebol'sin, V.A.; Galstyan, V.; Silina, Y.E. Graphene oxide and its chemical nature: Multi-stage interactions between the oxygen and graphene. *Surfaces and Interfaces* **2020**, *21*, 100763, doi:https://doi.org/10.1016/j.surfin.2020.100763.

34. Ge, W.; Ma, Q.; Wang, W.; Jia, F.; Song, S. Synthesis of three-dimensional reduced graphene oxide aerogels as electrode material for supercapacitor application. *Chemical Physics* **2021**, 111096, doi:https://doi.org/10.1016/j.chemphys.2021.111096.

35. Miyata, T.; Gohda, S.; Fujii, T.; Ono, H.; Itoh, H.; Nishina, Y.; Kashimura, K. Pure electric and magnetic fields applied to reduced graphene oxide for defect repair and oxygen removal. *Carbon* **2021**, *171*, 10-15, doi:https://doi.org/10.1016/j.carbon.2020.08.044.

36. Quezada-Renteria, J.A.; Ania, C.O.; Chazaro-Ruiz, L.F.; Rangel-Mendez, J.R. Influence of protons on reduction degree and defect formation in electrochemically reduced graphene oxide. *Carbon* **2019**, *149*, 722-732, doi:https://doi.org/10.1016/j.carbon.2019.04.109.

37. Chen, D.; Feng, H.; Li, J. Graphene Oxide: Preparation, Functionalization, and Electrochemical Applications. *Chemical Reviews* **2012**, *112*, 6027-6053, doi:10.1021/cr300115g.

38. Yadav, S.; Devi, A. Recent advancements of metal oxides/nitrogen-doped graphene nanocomposites for supercapacitor electrode materials. *Journal of Energy Storage* **2020**, *30*, 101486, doi:https://doi.org/10.1016/j.est.2020.101486.

39. Wang, S.-Y.; Wang, C.-F.; Lv, Y.-K.; Shen, S.-G. Fabrication of fluorescent biosensing platform based on graphene oxide-DNA and their application in biomolecule detection. *TrAC Trends in Analytical Chemistry* **2018**, *106*, 53-61, doi:https://doi.org/10.1016/j.trac.2018.07.004.

40. Lee, K.S.; Phiri, I.; Park, C.W.; Ko, J.M. A facile and green approach for the synthesis of bacteria-doped graphene oxide for supercapacitor electrodes. *Materials Letters* **2020**, *275*, 128133, doi:https://doi.org/10.1016/j.matlet.2020.128133.

41. Compton, O.C.; Nguyen, S.T. Graphene oxide, highly reduced graphene oxide, and graphene: Versatile building blocks for carbon-based materials. *Small* **2010**, *6*, 711-723, doi:https://doi.org/10.1002/smll.200901934.

42. Perrozzi, F.; Prezioso, S.; Ottaviano, L. Graphene oxide: from fundamentals to applications. *Journal of Physics: Condensed Matter* **2014**, *27*, 013002, doi:10.1088/0953-8984/27/1/013002.

43. Islam, M.S.; Renner, F.; Azizighannad, S.; Mitra, S. Direct incorporation of nano graphene oxide (nGO) into hydrophobic drug crystals for enhanced aqueous dissolution. *Colloids and Surfaces B: Biointerfaces* **2020**, *189*, 110827, doi:https://doi.org/10.1016/j.colsurfb.2020.110827.

44. Biswas, A.; Bayer, I.S.; Biris, A.S.; Wang, T.; Dervishi, E.; Faupel, F. Advances in top–down and bottom–up surface nanofabrication: Techniques, applications & future prospects. *Advances in Colloid and Interface Science* **2012**, *170*, 2-27, doi:https://doi.org/10.1016/j.cis.2011.11.001.

45. Son, M.; Ham, M.-H. Low-temperature synthesis of graphene by chemical vapor deposition and its applications. *FlatChem* **2017**, *5*, 40-49, doi:https://doi.org/10.1016/j.flatc.2017.07.002.

46. Tetlow, H.; Posthuma de Boer, J.; Ford, I.J.; Vvedensky, D.D.; Coraux, J.; Kantorovich, L. Growth of epitaxial graphene: Theory and experiment. *Physics Reports* **2014**, *542*, 195-295, doi:https://doi.org/10.1016/j.physrep.2014.03.003.

47. Ding, Y.; Zhu, J.; Wang, S.; Yang, M.; Yang, S.; Yang, L.; Zhao, X.; Xu, F.; Wang, Z.; Li, Y. Dependence of reduction degree on electromagnetic absorption of graphene nanoribbon unzipped from carbon nanotube. *Journal of Colloid and Interface Science* **2019**, *552*, 196-203, doi:https://doi.org/10.1016/j.jcis.2019.05.033.

48. Mondal, S.; Ghosh, S.; Raj, C.R. Unzipping of single-walled carbon nanotube for the development of electrocatalytically active hybrid catalyst of graphitic carbon and Pd nanoparticles. *ACS Omega* **2018**, *3*, 622-630, doi:10.1021/acsomega.7b01913.

49. Rangel, N.L.; Sotelo, J.C.; Seminario, J.M. Mechanism of carbon nanotubes unzipping into graphene ribbons. *Journal of Chemical Physics* **2009**, *131*, 031105, doi:10.1063/1.3170926.

50. Yoo, M.J.; Park, H.B. Effect of hydrogen peroxide on properties of graphene oxide in Hummers method. *Carbon* **2019**, *141*, 515-522, doi:https://doi.org/10.1016/j.carbon.2018.10.009.

51. Saikia, B.K.; Benoy, S.M.; Bora, M.; Tamuly, J.; Pandey, M.; Bhattacharya, D. A brief review on supercapacitor energy storage devices and utilization of natural carbon resources as their electrode materials. *Fuel* **2020**, *282*, 118796, doi:https://doi.org/10.1016/j.fuel.2020.118796.

52. Alkhouzaam, A.; Qiblawey, H.; Khraisheh, M.; Atieh, M.; Al-Ghouti, M. Synthesis of graphene oxides particle of high oxidation degree using a modified Hummers method. *Ceramics International* **2020**, *46*, 23997-24007, doi:https://doi.org/10.1016/j.ceramint.2020.06.177.

53. Whitener, K.E.; Sheehan, P.E. Graphene synthesis. *Diamond and Related Materials* **2014**, *46*, 25-34, doi:https://doi.org/10.1016/j.diamond.2014.04.006.

54. Agarwal, V.; Zetterlund, P.B. Strategies for reduction of graphene oxide – A comprehensive review. *Chemical Engineering Journal* **2021**, *405*, 127018, doi:https://doi.org/10.1016/j.cej.2020.127018.

55. Wang, J.; Salihi, E.C.; Šiller, L. Green reduction of graphene oxide using alanine. *Materials Science and Engineering: C* **2017**, *72*, 1-6, doi:https://doi.org/10.1016/j.msec.2016.11.017.

56. Feng, H.; Cheng, R.; Zhao, X.; Duan, X.; Li, J. A low-temperature method to produce highly reduced graphene oxide. *Nature Communications* **2013**, *4*, 1539, doi:10.1038/ncomms2555.

57. Yang, Z.-z.; Zheng, Q.-b.; Qiu, H.-x.; Li, J.; Yang, J.-h. A simple method for the reduction of graphene oxide by sodium borohydride with CaCl2 as a catalyst. *New Carbon Materials* **2015**, *30*, 41-47, doi:https://doi.org/10.1016/S1872-5805(15)60174-3.

58. Leo, I.M.; Soto, E.; Vaquero, F.; Mota, N.; Garcia, B.; Liuzzi, D.; Guil-López, R.; Navarro, R.M.; Fierro, J.L.G. Influence of the reduction of graphene oxide with hydroiodic acid on the structure and photoactivity of CdS–rGO hybrids. *Topics in Catalysis* **2017**, *60*, 1183-1195, doi:10.1007/s11244-017-0799-8.

59. Rabchinskii, M.K.; Dideikin, A.T.; Kirilenko, D.A.; Baidakova, M.V.; Shnitov, V.V.; Roth, F.; Konyakhin, S.V.; Besedina, N.A.; Pavlov, S.I.; Kuricyn, R.A.; et al. Facile reduction of graphene oxide suspensions and films using glass wafers. *Scientific Reports* **2018**, *8*, 14154, doi:10.1038/s41598-018-32488-x.

60. Zhou, X.; Zhang, J.; Wu, H.; Yang, H.; Zhang, J.; Guo, S. Reducing graphene oxide via hydroxylamine: A simple and efficient route to graphene. *The Journal of Physical Chemistry C* **2011**, *115*, 11957-11961, doi:10.1021/jp202575j.

61. Shin, H.-J.; Kim, K.K.; Benayad, A.; Yoon, S.-M.; Park, H.K.; Jung, I.-S.; Jin, M.H.; Jeong, H.-K.; Kim, J.M.; Choi, J.-Y.; et al. Efficient reduction of graphite oxide by sodium borohydride and its effect on electrical conductance. *Advanced Functional Materials* **2009**, *19*, 1987-1992, doi:https://doi.org/10.1002/adfm.200900167.

62. Williams, G.; Seger, B.; Kamat, P.V. TiO2-graphene nanocomposites. UV-assisted photocatalytic reduction of graphene oxide. *ACS Nano* **2008**, *2*, 1487-1491, doi:10.1021/nn800251f.

63. Shao, Y.; Wang, J.; Engelhard, M.; Wang, C.; Lin, Y. Facile and controllable electrochemical reduction of graphene oxide and its applications. *Journal of Materials Chemistry* **2010**, *20*, 743-748, doi:10.1039/B917975E.

64. Chen, W.; Yan, L.; Bangal, P.R. Preparation of graphene by the rapid and mild thermal reduction of graphene oxide induced by microwaves. *Carbon* **2010**, *48*, 1146-1152, doi:https://doi.org/10.1016/j.carbon.2009.11.037.

65. Konios, D.; Stylianakis, M.M.; Stratakis, E.; Kymakis, E. Dispersion behaviour of graphene oxide and reduced graphene oxide. *Journal of Colloid and Interface Science* **2014**, *430*, 108-112, doi:http://dx.doi.org/10.1016/j.jcis.2014.05.033.

66. Park, S.; An, J.; Jung, I.; Piner, R.D.; An, S.J.; Li, X.; Velamakanni, A.; Ruoff, R.S. Colloidal suspensions of highly reduced graphene oxide in a wide variety of organic solvents. *Nano Letters* **2009**, *9*, 1593-1597, doi:10.1021/nl803798y.

67. Wu, L.; Liu, L.; Gao, B.; Muñoz-Carpena, R.; Zhang, M.; Chen, H.; Zhou, Z.; Wang, H. Aggregation kinetics of graphene oxides in aqueous solutions: Experiments, mechanisms, and modeling. *Langmuir* **2013**, *29*, 15174-15181, doi:10.1021/la404134x.

68. Chen, J.; Dai, F.; Zhang, L.; Xu, J.; Liu, W.; Zeng, S.; Xu, C.; Chen, L.; Dai, C. Molecular insights into the dispersion stability of graphene oxide in mixed solvents: Theoretical simulations and experimental verification. *Journal of Colloid and Interface Science* **2020**, *571*, 109-117, doi:https://doi.org/10.1016/j.jcis.2020.03.036.

69. Li, Q.; Xiao, Y.; Shi, X.; Song, S. Rapid evaporation of water on graphene/graphene-oxide: A molecular dynamics study. *Nanomaterials* **2017**, *7*, 265.

70. Weiss, N.O.; Zhou, H.; Liao, L.; Liu, Y.; Jiang, S.; Huang, Y.; Duan, X. Graphene: An emerging electronic material. *Advanced Materials* **2012**, *24*, 5782-5825, doi:https://doi.org/10.1002/adma.201201482.

71. Justino, C.I.L.; Gomes, A.R.; Freitas, A.C.; Duarte, A.C.; Rocha-Santos, T.A.P. Graphene based sensors and biosensors. *TrAC Trends in Analytical Chemistry* **2017**, *91*, 53-66, doi:https://doi.org/10.1016/j.trac.2017.04.003.

72. Wang, M.; Niu, Y.; Zhou, J.; Wen, H.; Zhang, Z.; Luo, D.; Gao, D.; Yang, J.; Liang, D.; Li, Y. The dispersion and aggregation of graphene oxide in aqueous media. *Nanoscale* **2016**, *8*, 14587-14592, doi:10.1039/C6NR03503E.

73. Ghany, N.A.A.; Elsherif, S.A.; Handal, H.T. Revolution of graphene for different applications: State-of-the-art. *Surfaces and Interfaces* **2017**, *9*, 93-106, doi:https://doi.org/10.1016/j.surfin.2017.08.004.

74. Bolotin, K.I.; Sikes, K.J.; Jiang, Z.; Klima, M.; Fudenberg, G.; Hone, J.; Kim, P.; Stormer, H.L. Ultrahigh electron mobility in suspended graphene. *Solid State Communications* **2008**, *146*, 351-355, doi:https://doi.org/10.1016/j.ssc.2008.02.024.

75. Rao, C.N.R.; Gopalakrishnan, K.; Govindaraj, A. Synthesis, properties and applications of graphene doped with boron, nitrogen and other elements. *Nano Today* **2014**, *9*, 324-343, doi:https://doi.org/10.1016/j.nantod.2014.04.010.

76. Jeong, H.M.; Lee, J.W.; Shin, W.H.; Choi, Y.J.; Shin, H.J.; Kang, J.K.; Choi, J.W. Nitrogen-doped graphene for high-performance ultracapacitors and the importance of nitrogen-doped sites at basal planes. *Nano Letters* **2011**, *11*, 2472-2477, doi:10.1021/nl2009058.

77. Martins, T.B.; Miwa, R.H.; da Silva, A.J.R.; Fazzio, A. Electronic and Transport properties of boron-doped graphene nanoribbons. *Physical Review Letters* **2007**, *98*, 196803, doi:10.1103/PhysRevLett.98.196803.

78. Yang, Z.; Yao, Z.; Li, G.; Fang, G.; Nie, H.; Liu, Z.; Zhou, X.; Chen, X.a.; Huang, S. Sulfur-doped graphene as an efficient metal-free cathode catalyst for oxygen reduction. *ACS Nano* **2012**, *6*, 205-211, doi:10.1021/nn203393d.

79. Xue, M.; Chen, G.; Yang, H.; Zhu, Y.; Wang, D.; He, J.; Cao, T. Superconductivity in potassium-doped few-layer graphene. *Journal of the American Chemical Society* **2012**, *134*, 6536-6539, doi:10.1021/ja3003217.

80. Bianchi, M.; Rienks, E.D.L.; Lizzit, S.; Baraldi, A.; Balog, R.; Hornekær, L.; Hofmann, P. Electron-phonon coupling in potassium-doped graphene: Angle-resolved photoemission spectroscopy. *Physical Review B* **2010**, *81*, 041403, doi:10.1103/PhysRevB.81.041403.

81. Mudusu, D.; Nandanapalli, K.R.; Lee, S.; Hahn, Y.-B. Recent advances in graphene monolayers growth and their biological applications: A review. *Advances in Colloid and Interface Science* **2020**, *283*, 102225, doi:https://doi.org/10.1016/j.cis.2020.102225.

82. Liu, S.; Zeng, T.H.; Hofmann, M.; Burcombe, E.; Wei, J.; Jiang, R.; Kong, J.; Chen, Y. Antibacterial activity of graphite, graphite oxide, graphene oxide, and reduced graphene oxide: Membrane and oxidative stress. *ACS Nano* **2011**, *5*, 6971-6980, doi:10.1021/nn202451x.

83. Hegab, H.M.; ElMekawy, A.; Zou, L.; Mulcahy, D.; Saint, C.P.; Ginic-Markovic, M. The controversial antibacterial activity of graphene-based materials. *Carbon* **2016**, *105*, 362-376, doi:https://doi.org/10.1016/j.carbon.2016.04.046.

84. Ji, H.; Sun, H.; Qu, X. Antibacterial applications of graphene-based nanomaterials: Recent achievements and challenges. *Advanced Drug Delivery Reviews* **2016**, *105*, 176-189, doi:https://doi.org/10.1016/j.addr.2016.04.009.

85. Liu, Y.; Wen, J.; Gao, Y.; Li, T.; Wang, H.; Yan, H.; Niu, B.; Guo, R. Antibacterial graphene oxide coatings on polymer substrate. *Applied Surface Science* **2018**, *436*, 624-630, doi:https://doi.org/10.1016/j.apsusc.2017.12.006.

86. Liu, J.; Ma, Q.; Huang, Z.; Liu, G.; Zhang, H. Recent progress in graphene-based noble-metal nanocomposites for electrocatalytic applications. *Advanced Materials* **2019**, *31*, 1800696, doi:https://doi.org/10.1002/adma.201800696.

87. Tang, B.; Hu, G.; Gao, H.; Hai, L. Application of graphene as filler to improve thermal transport property of epoxy resin for thermal interface materials. *International Journal of Heat and Mass Transfer* **2015**, *85*, 420-429, doi:https://doi.org/10.1016/j.ijheatmasstransfer.2015.01.141.

88. Yu, J.; Huang, X.; Wu, C.; Jiang, P. Permittivity, thermal conductivity and thermal stability of poly(vinylidene fluoride)/graphene nanocomposites. *IEEE Transactions on Dielectrics and Electrical Insulation* **2011**, *18*, 478-484, doi:10.1109/TDEI.2011.5739452.

89. Han, Y.; Xu, Z.; Gao, C. Ultrathin graphene nanofiltration membrane for water purification. *Advanced Functional Materials* **2013**, *23*, 3693-3700, doi:https://doi.org/10.1002/adfm.201202601.

90. Joshi, R.; Alwarappan, S.; Yoshimura, M.; Sahajwalla, V.; Nisina, Y. Graphene Oxide: the new membrane material; 2015; Volume 1, p. 1.

91. Zhang, M.; Guan, K.; Ji, Y.; Liu, G.; Jin, W.; Xu, N. Controllable ion transport by surface-charged graphene oxide membrane. *Nature Communications* **2019**, *10*, 1253, doi:10.1038/s41467-019-09286-8.

92. Baig, M.I.; Ingole, P.G.; Jeon, J.-d.; Hong, S.U.; Choi, W.K.; Lee, H.K. Water vapor transport properties of interfacially polymerized thin film nanocomposite membranes modified with graphene oxide and GO-TiO2 nanofillers. *Chemical Engineering Journal* **2019**, *373*, 1190-1202, doi:https://doi.org/10.1016/j.cej.2019.05.122.

93. Zeynali, R.; Ghasemzadeh, K.; Sarand, A.B.; Kheiri, F.; Basile, A. Performance evaluation of graphene oxide (GO) nanocomposite membrane for hydrogen separation: Effect of dip coating sol concentration. *Separation and Purification Technology* **2018**, *200*, 169-176, doi:https://doi.org/10.1016/j.seppur.2018.02.032.

94. Liang, F.; Liu, Q.; Zhao, J.; Guan, K.; Mao, Y.; Liu, G.; Gu, X.; Jin, W. Ultrafast water-selective permeation through graphene oxide membrane with water transport promoters. *AIChE Journal* **2020**, *66*, e16812, doi:https://doi.org/10.1002/aic.16812.

95. Gao, W.; Wu, G.; Janicke, M.T.; Cullen, D.A.; Mukundan, R.; Baldwin, J.K.; Brosha, E.L.; Galande, C.; Ajayan, P.M.; More, K.L.; et al. Ozonated graphene oxide film as a proton-exchange membrane. *Angewandte Chemie International Edition* **2014**, *53*, 3588-3593, doi:https://doi.org/10.1002/anie.201310908.

96. Bhadra, M.; Roy, S.; Mitra, S. Desalination across a graphene oxide membrane via direct contact membrane distillation. *Desalination* **2016**, *378*, 37-43, doi:https://doi.org/10.1016/j.desal.2015.09.026.

97. Zhao, Y.; Li, X.-g.; Zhou, X.; Zhang, Y.-n. Review on the graphene based optical fiber chemical and biological sensors. *Sensors and Actuators B: Chemical* **2016**, *231*, 324-340, doi:https://doi.org/10.1016/j.snb.2016.03.026.

98. Wu, Z.; Chen, X.; Zhu, S.; Zhou, Z.; Yao, Y.; Quan, W.; Liu, B. Enhanced sensitivity of ammonia sensor using graphene/polyaniline nanocomposite. *Sensors and Actuators B: Chemical* **2013**, *178*, 485-493, doi:https://doi.org/10.1016/j.snb.2013.01.014.

99. Yasri, N.G.; Sundramoorthy, A.K.; Chang, W.-J.; Gunasekaran, S. Highly selective mercury detection at partially oxidized graphene/poly(3,4-ethylenedioxythiophene):poly(styrenesulfonate) nanocomposite film-modified electrode. *Frontiers in Materials* **2014**, *1*, doi:10.3389/fmats.2014.00033.

100. Li, J.; Guo, S.; Zhai, Y.; Wang, E. Nafion–graphene nanocomposite film as enhanced sensing platform for ultrasensitive determination of cadmium. *Electrochemistry Communications* **2009**, *11*, 1085-1088, doi:https://doi.org/10.1016/j.elecom.2009.03.025.

101. Xu, F.; Deng, M.; Liu, Y.; Ling, X.; Deng, X.; Wang, L. Facile preparation of poly (diallyldimethylammonium chloride) modified reduced graphene oxide for sensitive detection of nitrite. *Electrochemistry Communications* **2014**, *47*, 33-36, doi:https://doi.org/10.1016/j.elecom.2014.07.016.

102. Mitchell, E.; Candler, J.; De Souza, F.; Gupta, R.K.; Gupta, B.K.; Dong, L.F. High performance supercapacitor based on multilayer of polyaniline and graphene oxide. *Synthetic Metals* **2015**, *199*, 214-218, doi:https://doi.org/10.1016/j.synthmet.2014.11.028.

103. Mohan, V.B.; Lau, K.-t.; Hui, D.; Bhattacharyya, D. Graphene-based materials and their composites: A review on production, applications and product limitations. *Composites Part B: Engineering* **2018**, *142*, 200-220, doi:https://doi.org/10.1016/j.compositesb.2018.01.013.

104. Yin, J.; Dong, Z.; Liu, Y.; Wang, H.; Li, A.; Zhuo, Z.; Feng, W.; Fan, W. Toxicity of reduced graphene oxide modified by metals in microalgae: Effect of the surface properties of algal cells and nanomaterials. *Carbon* **2020**, *169*, 182-192, doi:https://doi.org/10.1016/j.carbon.2020.07.057.

105. Zhu, X.; Xu, Y.; Cheng, Z.; Wang, Y.; Lu, Z.; Zhang, G. First principles study of atmospheric pollutants adsorption on non-defect and monatomic defect graphene. *Diamond and Related Materials* **2021**, *112*, 108252, doi:https://doi.org/10.1016/j.diamond.2021.108252.

106. Zhang, D.; Liang, R.; Yang, H.; Song, Y.; Yang, L.; Zhang, C.; Liu, A. Formation of helical polyphenyl nanostructures on carbon nanotubes. *Inorganic Chemistry Communications* **2021**, *126*, 108491, doi:https://doi.org/10.1016/j.inoche.2021.108491.

107. Jain, N.; Jee Kanu, N. The potential application of carbon nanotubes in water Treatment: A state-of-the-art-review. *Materials Today: Proceedings* **2021**, doi:https://doi.org/10.1016/j.matpr.2021.01.331.

108. Gao, X.; Yin, W.; Liu, X. Carbon nanotubes-based electrode for Zn ion batteries. *Materials Research Bulletin* **2021**, *138*, 111246, doi:https://doi.org/10.1016/j.materresbull.2021.111246.

109. Patil, J.; Patil, H.; Sankpal, R.; Rathod, D.; Patil, K.; Kubade, P.R.; Kulkarni, H.B. Studies on mechanical and thermal performance of carbon nanotubes/polypropylene nanocomposites. *Materials Today: Proceedings* **2020**, doi:https://doi.org/10.1016/j.matpr.2020.11.452.

110. Wu, Z.; Wang, Z.; Yu, F.; Thakkar, M.; Mitra, S. Variation in chemical, colloidal and electrochemical properties of carbon nanotubes with the degree of carboxylation. *Journal of Nanoparticle Research* **2017**, *19*, doi:10.1007/s11051-016-3697-2.

111. Zhang, X.; Huang, Q.; Liu, M.; Tian, J.; Zeng, G.; Li, Z.; Wang, K.; Zhang, Q.; Wan, Q.; Deng, F.; et al. Preparation of amine functionalized carbon nanotubes via a bioinspired strategy and their application in Cu2+ removal. *Applied Surface Science* **2015**, *343*, 19-27, doi:https://doi.org/10.1016/j.apsusc.2015.03.081.

112. Maleki, A.; Hamesadeghi, U.; Daraei, H.; Hayati, B.; Najafi, F.; McKay, G.; Rezaee, R. Amine functionalized multi-walled carbon nanotubes: Single and binary systems for high capacity dye removal. *Chemical Engineering Journal* **2017**, *313*, 826-835, doi:https://doi.org/10.1016/j.cej.2016.10.058.

113. Liu, Y.; Zhang, Q.; Zhang, R.; Wang, B.; Hao, R.; Zhang, W.; Sang, S. Manipulating the electronic properties of CNT by doping metal. *Materials Science and Engineering: B* **2020**, *262*, 114803, doi:https://doi.org/10.1016/j.mseb.2020.114803.

114. Wan, N.; Sun, L.-t.; Ding, S.-n.; Xu, T.; Hu, X.-h.; Sun, J.; Bi, H.-c. Synthesis of graphene–CNT hybrids via joule heating: Structural characterization and electrical transport. *Carbon* **2013**, *53*, 260-268, doi:https://doi.org/10.1016/j.carbon.2012.10.057.

115. Liu, Y.; He, D.; Dubrunfaut, O.; Zhang, A.; Zhang, H.; Pichon, L.; Bai, J. GO-CNTs hybrids reinforced epoxy composites with porous structure as microwave absorbers. *Composites Science and Technology* **2020**, *200*, 108450, doi:https://doi.org/10.1016/j.compscitech.2020.108450.

116. Li, Y.; Yang, T.; Yu, T.; Zheng, L.; Liao, K. Synergistic effect of hybrid carbon nantube–graphene oxide as a nanofiller in enhancing the mechanical properties of PVA composites. *Journal of Materials Chemistry* **2011**, *21*, 10844-10851, doi:10.1039/C1JM11359C.

117. Qiu, L.; Yang, X.; Gou, X.; Yang, W.; Ma, Z.-F.; Wallace, G.G.; Li, D. Dispersing carbon nanotubes with graphene oxide in water and synergistic effects between graphene derivatives. *Chemistry – A European Journal* **2010**, *16*, 10653-10658, doi:10.1002/chem.201001771.

118. Azizighannad, S.; Mitra, S. Controlled synthesis of reduced graphene oxide-carbon nanotube hybrids and their aqueous behavior. *Journal of Nanoparticle Research* **2020**, *22*, 130, doi:10.1007/s11051-020-04874-y.

119. Wei Fan, L.Z., Tianxi Liu. Graphene-carbon nanotube hybrids for energy and environmental applications; *SpringerBriefs in Molecular Science*: 2017.

120. Dong, X.; Li, B.; Wei, A.; Cao, X.; Chan-Park, M.B.; Zhang, H.; Li, L.-J.; Huang, W.; Chen, P. One-step growth of graphene–carbon nanotube hybrid materials by chemical vapor deposition. *Carbon* **2011**, *49*, 2944-2949, doi:https://doi.org/10.1016/j.carbon.2011.03.009.

121. Fan, Z.; Yan, J.; Zhi, L.; Zhang, Q.; Wei, T.; Feng, J.; Zhang, M.; Qian, W.; Wei, F. A three-dimensional carbon nanotube/graphene sandwich and its application as electrode in supercapacitors. *Advanced Materials* **2010**, *22*, 3723-3728, doi:https://doi.org/10.1002/adma.201001029.

122. Yang, Q.; Pang, S.-K.; Yung, K.-C. Electrochemically reduced graphene oxide/carbon nanotubes composites as binder-free supercapacitor electrodes. *Journal of Power Sources* **2016**, *311*, 144-152, doi:https://doi.org/10.1016/j.jpowsour.2016.02.016.

123. Zhang, M.; Jia, Y.; Li, H.; Wang, J. A facile method to synthesise reduced graphene oxide/carbon nanotube hybrid fibers as binder-free electrodes for supercapacitors. *Synthetic Metals* **2017**, *232*, 66-71, doi:https://doi.org/10.1016/j.synthmet.2017.07.010.

124. Kumar, P.; Woon, K.L.; Wong, W.S.; Mohamed Saheed, M.S.; Burhanudin, Z.A. Hybrid film of single-layer graphene and carbon nanotube as transparent conductive electrode for organic light emitting diode. *Synthetic Metals* **2019**, *257*, 116186, doi:https://doi.org/10.1016/j.synthmet.2019.116186.

125. Zang, X.; Jiang, Y.; Sanghadasa, M.; Lin, L. Chemical vapor deposition of 3D graphene/carbon nanotubes networks for hybrid supercapacitors. *Sensors and Actuators A: Physical* **2020**, *304*, 111886, doi:https://doi.org/10.1016/j.sna.2020.111886.

126. Tran, X.T.; Hussain, M.; Kim, H.T. Facile and fast synthesis of a reduced graphene oxide/carbon nanotube/iron/silver hybrid and its enhanced performance in catalytic reduction of 4–nitrophenol. *Solid State Sciences* **2020**, *100*, 106107, doi:https://doi.org/10.1016/j.solidstatesciences.2019.106107.

127. Sui, Z.; Meng, Q.; Zhang, X.; Ma, R.; Cao, B. Green synthesis of carbon nanotube–graphene hybrid aerogels and their use as versatile agents for water purification. *Journal of Materials Chemistry* **2012**, *22*, 8767-8771, doi:10.1039/C2JM00055E.

128. Sharma, V.K.; McDonald, T.J.; Kim, H.; Garg, V.K. Magnetic graphene–carbon nanotube iron nanocomposites as adsorbents and antibacterial agents for water purification. *Advances in Colloid and Interface Science* **2015**, *225*, 229-240, doi:https://doi.org/10.1016/j.cis.2015.10.006.

129. Dey, B.; Ahmad, M.W.; Almezeni, A.; Sarkhel, G.; Bag, D.S.; Choudhury, A. Enhancing electrical, mechanical, and thermal properties of polybenzimidazole by 3D carbon nanotube@graphene oxide hybrid. *Composites Communications* **2020**, *17*, 87-96, doi:https://doi.org/10.1016/j.coco.2019.11.012.

130. Zhan, W.; Ni, L.; Gu, Z.; Cui, F.; Jiang, J.; Chen, L. The influences of graphene and carbon nanotubes on properties of waterborne intumescent fire resistive coating. *Powder Technology* **2021**, *385*, 572-579, doi:https://doi.org/10.1016/j.powtec.2021.03.018.

131. Liu, Z.; Qian, Z.; Song, J.; Zhang, Y. Conducting and stretchable composites using sandwiched graphene-carbon nanotube hybrids and styrene-butadiene rubber. *Carbon* **2019**, *149*, 181-189, doi:https://doi.org/10.1016/j.carbon.2019.04.037.

132. Nyanor, P.; El-Kady, O.; Yehia, H.M.; Hamada, A.S.; Nakamura, K.; Hassan, M.A. Effect of carbon nanotube (CNT) content on the hardness, wear resistance and thermal expansion of in-situ reduced graphene oxide (rGO)-reinforced aluminum matrix composites. *Metals and Materials International* **2019**, doi:10.1007/s12540-019-00445-6.

133. Wimalasiri, Y.; Zou, L. Carbon nanotube/graphene composite for enhanced capacitive deionization performance. *Carbon* **2013**, *59*, 464-471, doi:https://doi.org/10.1016/j.carbon.2013.03.040.

134. Li, X.; Ma, L.; Zhang, H.; Wang, S.; Jiang, Z.; Guo, R.; Wu, H.; Cao, X.; Yang, J.; Wang, B. Synergistic effect of combining carbon nanotubes and graphene oxide in mixed matrix membranes for efficient CO2 separation. *Journal of Membrane Science* **2015**, *479*, 1-10, doi:https://doi.org/10.1016/j.memsci.2015.01.014.

135. Alvarez, G.E.; Marcovecchio, M.G.; Aguirre, P.A. Optimization of the integration among traditional fossil fuels, clean energies, renewable sources, and energy storages: An MILP model for the coupled electric power, hydraulic, and natural gas systems. *Computers & Industrial Engineering* **2020**, *139*, 106141, doi:https://doi.org/10.1016/j.cie.2019.106141.

136. Olabi, A.G.; Abdelkareem, M.A.; Wilberforce, T.; Sayed, E.T. Application of graphene in energy storage device – A review. *Renewable and Sustainable Energy Reviews* **2021**, *135*, 110026, doi:https://doi.org/10.1016/j.rser.2020.110026.

137. Koohi-Fayegh, S.; Rosen, M.A. A review of energy storage types, applications and recent developments. *Journal of Energy Storage* **2020**, *27*, 101047, doi:https://doi.org/10.1016/j.est.2019.101047.

138. Kumar, H.; Sharma, R.; Yadav, A.; Kumari, R. Recent advancement made in the field of reduced graphene oxide-based nanocomposites used in the energy storage devices: A review. *Journal of Energy Storage* **2021**, *33*, 102032, doi:https://doi.org/10.1016/j.est.2020.102032.

139. Ho, J.; Jow, T.R.; Boggs, S. Historical introduction to capacitor technology. *IEEE Electrical Insulation Magazine* **2010**, *26*, 20-25, doi:10.1109/MEI.2010.5383924.

140. Pandolfo, A.G.; Hollenkamp, A.F. Carbon properties and their role in supercapacitors. *Journal of Power Sources* **2006**, *157*, 11-27, doi:https://doi.org/10.1016/j.jpowsour.2006.02.065.

141. Yang, W.; Ni, M.; Ren, X.; Tian, Y.; Li, N.; Su, Y.; Zhang, X. Graphene in supercapacitor applications. *Current Opinion in Colloid & Interface Science* **2015**, *20*, 416-428, doi:https://doi.org/10.1016/j.cocis.2015.10.009.

142. Dehghani-Sanij, A.R.; Tharumalingam, E.; Dusseault, M.B.; Fraser, R. Study of energy storage systems and environmental challenges of batteries. *Renewable and Sustainable Energy Reviews* **2019**, *104*, 192-208, doi:https://doi.org/10.1016/j.rser.2019.01.023.

143. Li, M.; Lu, J.; Chen, Z.; Amine, K. 30 years of lithium-ion batteries. *Advanced Materials* **2018**, *30*, 1800561, doi:https://doi.org/10.1002/adma.201800561.

144. Blomgren, G.E. The development and future of lithium ion batteries. *Journal of The Electrochemical Society* **2016**, *164*, A5019-A5025, doi:10.1149/2.0251701jes.

145. Wakihara, M. Recent developments in lithium ion batteries. *Materials Science and Engineering: R: Reports* **2001**, *33*, 109-134, doi:https://doi.org/10.1016/S0927-796X(01)00030-4.

146. Wang, Z.; Wu, Z.; Bramnik, N.; Mitra, S. Fabrication of high-performance flexible alkaline batteries by implementing multiwalled carbon nanotubes and copolymer separator. *Advanced Materials* **2014**, *26*, 970-976, doi:https://doi.org/10.1002/adma.201304020.

147. Köhler, U.; Antonius, C.; Bäuerlein, P. Advances in alkaline batteries. *Journal of Power Sources* **2004**, *127*, 45-52, doi:https://doi.org/10.1016/j.jpowsour.2003.09.006.

148. Liu, Z.; Mo, F.; Li, H.; Zhu, M.; Wang, Z.; Liang, G.; Zhi, C. Advances in flexible and wearable energy-storage textiles. *Small Methods* **2018**, *2*, 1800124, doi:https://doi.org/10.1002/smtd.201800124.

149. Abdelkareem, M.A.; Elsaid, K.; Wilberforce, T.; Kamil, M.; Sayed, E.T.; Olabi, A. Environmental aspects of fuel cells: A review. *Science of The Total Environment* **2021**, *752*, 141803, doi:https://doi.org/10.1016/j.scitotenv.2020.141803.

150. Ramezanizadeh, M.; Alhuyi Nazari, M.; Hossein Ahmadi, M.; Chen, L. A review on the approaches applied for cooling fuel cells. *International Journal of Heat and Mass Transfer* **2019**, *139*, 517-525, doi:https://doi.org/10.1016/j.ijheatmasstransfer.2019.05.032.

151. Li, Y.; Yang, J.; Song, J. Nano energy system model and nanoscale effect of graphene battery in renewable energy electric vehicle. *Renewable and Sustainable Energy Reviews* **2017**, *69*, 652-663, doi:https://doi.org/10.1016/j.rser.2016.11.118.

152. Van Mierlo, J.; Maggetto, G. Fuel cell or battery: Electric cars are the future. *Fuel Cells* **2007**, *7*, 165-173, doi:https://doi.org/10.1002/fuce.200600052.

153. Zhanadilov, O.; Mentbayeva, A.; Beisbayeva, Z.; Amze, M.; Bakenov, Z. PAM-based hydrogel electrolyte for hybrid rechargeable aqueous (Zn and Li-ion) battery. *Materials Today: Proceedings* **2021**, doi:https://doi.org/10.1016/j.matpr.2020.11.989.

154. Wan, H.; Hu, X. New strategy to prepare nitrogen self-doped graphene nanosheets by magnesiothermic reduction and its application in lithium ion batteries. *International Journal of Hydrogen Energy* **2019**, *44*, 24369-24376, doi:https://doi.org/10.1016/j.ijhydene.2019.07.207.

155. Yen, P.-J.; Ilango, P.R.; Chiang, Y.-C.; Wu, C.-W.; Hsu, Y.-C.; Chueh, Y.-L.; Wei, K.-H. Tunable nitrogen-doped graphene sheets produced with in situ electrochemical cathodic plasma at room temperature for lithium-ion batteries. *Materials Today Energy* **2019**, *12*, 336-347, doi:https://doi.org/10.1016/j.mtener.2019.01.003.

156. Kucinskis, G.; Bajars, G.; Kleperis, J. Graphene in lithium ion battery cathode materials: A review. *Journal of Power Sources* **2013**, *240*, 66-79, doi:https://doi.org/10.1016/j.jpowsour.2013.03.160.

157. Cheng, F.Y.; Chen, J.; Gou, X.L.; Shen, P.W. High-power alkaline Zn–MnO2 batteries using γ-MnO2 nanowires/nanotubes and electrolytic zinc powder. *Advanced Materials* **2005**, *17*, 2753-2756, doi:https://doi.org/10.1002/adma.200500663.

158. McDowall, J. Conventional battery technologies-present and future. In Proceedings of the 2000 Power Engineering Society Summer Meeting (Cat. No.00CH37134), 16-20 July 2000, 2000; pp. 1538-1540 vol. 1533.

159. Kim, H.; Park, K.-Y.; Hong, J.; Kang, K. All-graphene-battery: bridging the gap between supercapacitors and lithium ion batteries. *Scientific Reports* **2014**, *4*, 5278, doi:10.1038/srep05278.

160. Shaker, M.; Riahifar, R.; Li, Y. A review on the superb contribution of carbon and graphene quantum dots to electrochemical capacitors' performance: Synthesis and application. *FlatChem* **2020**, *22*, 100171, doi:https://doi.org/10.1016/j.flatc.2020.100171.

161. Tan, Y.B.; Lee, J.-M. Graphene for supercapacitor applications. *Journal of Materials Chemistry A* **2013**, *1*, 14814-14843, doi:10.1039/C3TA12193C.

162. Wang, Y.; Shi, Z.; Huang, Y.; Ma, Y.; Wang, C.; Chen, M.; Chen, Y. Supercapacitor devices based on graphene materials. *The Journal of Physical Chemistry C* **2009**, *113*, 13103-13107, doi:10.1021/jp902214f.

163. Tang, W.; Peng, L.; Yuan, C.; Wang, J.; Mo, S.; Zhao, C.; Yu, Y.; Min, Y.; Epstein, A.J. Facile synthesis of 3D reduced graphene oxide and its polyaniline composite for super capacitor application. *Synthetic Metals* **2015**, *202*, 140-146, doi:https://doi.org/10.1016/j.synthmet.2015.01.031.

164. Oyedotun, K.O.; Manyala, N. Graphene foam–based electrochemical capacitors. *Current Opinion in Electrochemistry* **2020**, *21*, 125-131, doi:https://doi.org/10.1016/j.coelec.2019.12.010.

165. Ge, W.; Ma, Q.; Ai, Z.; Wang, W.; Jia, F.; Song, S. Three-dimensional reduced graphene oxide/montmorillonite nanosheet aerogels as electrode material for supercapacitor application. *Applied Clay Science* **2021**, *206*, 106022, doi:https://doi.org/10.1016/j.clay.2021.106022.

166. Chen, Y.; Zhang, X.; Zhang, D.; Yu, P.; Ma, Y. High performance supercapacitors based on reduced graphene oxide in aqueous and ionic liquid electrolytes. *Carbon* **2011**, *49*, 573-580, doi:https://doi.org/10.1016/j.carbon.2010.09.060.

167. Rag S, A.; Selvakumar, M.; De, S.; Chidangil, S.; Bhat, S. Laser induced graphene with biopolymer electrolyte for supercapacitor applications. *Materials Today: Proceedings* **2020**, doi:https://doi.org/10.1016/j.matpr.2020.08.791.

168. Dai, H.; Zhang, G.; Rawach, D.; Fu, C.; Wang, C.; Liu, X.; Dubois, M.; Lai, C.; Sun, S. Polymer gel electrolytes for flexible supercapacitors: Recent progress, challenges, and perspectives. *Energy Storage Materials* **2021**, *34*, 320-355, doi:https://doi.org/10.1016/j.ensm.2020.09.018.

169. Cao, L.; Wu, H.; Yang, P.; He, X.; Li, J.; Li, Y.; Xu, M.; Qiu, M.; Jiang, Z. Graphene oxide-based solid electrolytes with 3D prepercolating pathways for efficient proton transport. *Advanced Functional Materials* **2018**, *28*, 1804944, doi:https://doi.org/10.1002/adfm.201804944.

170. Karaman, E.S.; Wang, Z.; Chen, K.; Siddiqui, Z.; Cheng, Y.; Basuray, S.; Kumar, V.; Mitra, S. Functionalized carbon nanotube doped gel electrolytes with enhanced mechanical and electrical properties for battery applications. *Materials Chemistry and Physics* **2021**, *264*, 124448, doi:https://doi.org/10.1016/j.matchemphys.2021.124448.

171. Mayilvel Dinesh, M.; Saminathan, K.; Selvam, M.; Srither, S.R.; Rajendran, V.; Kaler, K.V.I.S. Water soluble graphene as electrolyte additive in magnesium-air battery system. *Journal of Power Sources* **2015**, *276*, 32-38, doi:https://doi.org/10.1016/j.jpowsour.2014.11.079.

172. Jia, W.; Li, Z.; Wu, Z.; Wang, L.; Wu, B.; Wang, Y.; Cao, Y.; Li, J. Graphene oxide as a filler to improve the performance of PAN-$LiClO_4$ flexible solid polymer electrolyte. *Solid State Ionics* **2018**, *315*, 7-13, doi:https://doi.org/10.1016/j.ssi.2017.11.026.

173. Sohail, M.; Saleem, M.; Ullah, S.; Saeed, N.; Afridi, A.; Khan, M.; Arif, M. Modified and improved Hummer's synthesis of graphene oxide for capacitors applications. *Modern Electronic Materials* **2017**, *3*, 110-116, doi:https://doi.org/10.1016/j.moem.2017.07.002.

174. Li, Y.; Yuan, H.; von dem Bussche, A.; Creighton, M.; Hurt, R.H.; Kane, A.B.; Gao, H. Graphene microsheets enter cells through spontaneous membrane penetration at edge asperities and corner sites. *Proceedings of the National Academy of Sciences* **2013**, *110*, 12295-12300, doi:10.1073/pnas.1222276110.

175. Thakur, S.; Karak, N. Alternative methods and nature-based reagents for the reduction of graphene oxide: A review. *Carbon* **2015**, *94*, 224-242, doi:http://dx.doi.org/10.1016/j.carbon.2015.06.030.

176. Chua, C.K.; Pumera, M. Chemical reduction of graphene oxide: a synthetic chemistry viewpoint. *Chemical Society Reviews* **2014**, *43*, 291-312, doi:10.1039/C3CS60303B.

177. Velasco-Soto, M.A.; Pérez-García, S.A.; Alvarez-Quintana, J.; Cao, Y.; Nyborg, L.; Licea-Jiménez, L. Selective band gap manipulation of graphene oxide by its reduction with mild reagents. *Carbon* **2015**, *93*, 967-973, doi:http://dx.doi.org/10.1016/j.carbon.2015.06.013.

178. Park, S.; Ruoff, R.S. Chemical methods for the production of graphenes. *Nature Nanotechnology* **2009**, *4*, 217-224.

179. Hua, Z.; Tang, Z.; Bai, X.; Zhang, J.; Yu, L.; Cheng, H. Aggregation and resuspension of graphene oxide in simulated natural surface aquatic environments. *Environmental Pollution* **2015**, *205*, 161-169, doi:http://dx.doi.org/10.1016/j.envpol.2015.05.039.

180. Doğan, H.Ö.; Ekinci, D.; Demir, Ü. Atomic scale imaging and spectroscopic characterization of electrochemically reduced graphene oxide. *Surface Science* **2013**, *611*, 54-59, doi:http://dx.doi.org/10.1016/j.susc.2013.01.014.

181. De Silva, K.K.H.; Huang, H.H.; Joshi, R.K.; Yoshimura, M. Chemical reduction of graphene oxide using green reductants. *Carbon* **2017**, *119*, 190-199, doi:http://dx.doi.org/10.1016/j.carbon.2017.04.025.

182. Chowdhury, I.; Duch, M.C.; Mansukhani, N.D.; Hersam, M.C.; Bouchard, D. Colloidal properties and stability of graphene oxide nanomaterials in the aquatic environment. *Environmental Science & Technology* **2013**, *47*, 6288-6296, doi:10.1021/es400483k.

183. Gudarzi, M.M. Colloidal stability of graphene xxide: Aggregation in two dimensions. *Langmuir* **2016**, *32*, 5058-5068, doi:10.1021/acs.langmuir.6b01012.

184. Han, S.; Hou, F.; Yuan, X.; Liu, J.; Yan, X.; Chen, S. Continuous hierarchical carbon nanotube/reduced graphene oxide hybrid films for supercapacitors. *Electrochimica Acta* **2017**, *225*, 566-573, doi:http://dx.doi.org/10.1016/j.electacta.2016.12.159.

185. Du, R.; Tian, X.; Yao, J.; Sun, Y.; Jin, J.; Zhang, Y.; Liu, Y. Controlled synthesis of three-dimensional reduced graphene oxide networks for application in electrode of supercapacitor. *Diamond and Related Materials* **2016**, *70*, 186-193, doi:http://dx.doi.org/10.1016/j.diamond.2016.11.003.

186. Mathkar, A.; Tozier, D.; Cox, P.; Ong, P.; Galande, C.; Balakrishnan, K.; Leela Mohana Reddy, A.; Ajayan, P.M. Controlled, stepwise reduction and band gap manipulation of graphene oxide. *The Journal of Physical Chemistry Letters* **2012**, *3*, 986-991, doi:10.1021/jz300096t.

187. Theophile, N.; Jeong, H.K. Electrochemical properties of poly(vinyl alcohol) and graphene oxide composite for supercapacitor applications. *Chemical Physics Letters* **2017**, *669*, 125-129, doi:http://dx.doi.org/10.1016/j.cplett.2016.12.029.

188. Pumera, M. Electrochemistry of graphene, graphene oxide and other graphenoids: Review. *Electrochemistry Communications* **2013**, *36*, 14-18, doi:http://dx.doi.org/10.1016/j.elecom.2013.08.028.

189. Toh, S.Y.; Loh, K.S.; Kamarudin, S.K.; Daud, W.R.W. Graphene production via electrochemical reduction of graphene oxide: Synthesis and characterisation. *Chemical Engineering Journal* **2014**, *251*, 422-434, doi:http://dx.doi.org/10.1016/j.cej.2014.04.004.

190. Zhao, J.; Liu, F.; Wang, Z.; Cao, X.; Xing, B. Heteroaggregation of graphene oxide with minerals in aqueous phase. *Environmental Science & Technology* **2015**, *49*, 2849-2857, doi:10.1021/es505605w.

191. Jang, G.G.; Song, B.; Moon, K.-s.; Wong, C.-P.; Keum, J.K.; Hu, M.Z. Particle size effect in porous film electrodes of ligand-modified graphene for enhanced supercapacitor performance. *Carbon* **2017**, *119*, 296-304, doi:https://doi.org/10.1016/j.carbon.2017.04.023.

192. Peng, W.; Li, H.; Liu, Y.; Song, S. A review on heavy metal ions adsorption from water by graphene oxide and its composites. *Journal of Molecular Liquids* **2017**, *230*, 496-504, doi:http://dx.doi.org/10.1016/j.molliq.2017.01.064.

193. Dai, J.; Wang, G.; Ma, L.; Wu, C. Study on the surface energies and dispersibility of graphene oxide and its derivatives. *Journal of Materials Science* **2015**, *50*, 3895-3907, doi:10.1007/s10853-015-8934-z.

194. Hong, B.J.; Compton, O.C.; An, Z.; Eryazici, I.; Nguyen, S.T. Successful stabilization of graphene oxide in electrolyte solutions: enhancement of biofunctionalization and cellular uptake. *ACS Nano* **2012**, *6*, 63-73, doi:10.1021/nn202355p.

195. Kavinkumar, T.; Manivannan, S. Synthesis, characterization and gas sensing properties of graphene oxide-multiwalled carbon nanotube composite. *Journal of Materials Science & Technology* **2016**, *32*, 626-632, doi:http://dx.doi.org/10.1016/j.jmst.2016.03.017.

196. Mei, X.; Ouyang, J. Ultrasonication-assisted ultrafast reduction of graphene oxide by zinc powder at room temperature. *Carbon* **2011**, *49*, 5389-5397, doi:http://dx.doi.org/10.1016/j.carbon.2011.08.019.

197. Konkena, B.; Vasudevan, S. Understanding aqueous dispersibility of graphene oxide and reduced graphene oxide through pKa measurements. *The Journal of Physical Chemistry Letters* **2012**, *3*, 867-872, doi:10.1021/jz300236w.

198. Jiao, T.; Guo, H.; Zhang, Q.; Peng, Q.; Tang, Y.; Yan, X.; Li, B. Reduced graphene oxide-based silver nanoparticle-containing composite hydrogel as highly efficient dye catalysts for wastewater treatment. *Scientific Reports* **2015**, *5*, 11873, doi:10.1038/srep11873.

199. Zhang, H.; Wang, S.; Lin, Y.; Feng, M.; Wu, Q. Stability, thermal conductivity, and rheological properties of controlled reduced graphene oxide dispersed nanofluids. *Applied Thermal Engineering* **2017**, *119*, 132-139, doi:https://doi.org/10.1016/j.applthermaleng.2017.03.064.

200. Zhao, J.; Wang, Z.; White, J.C.; Xing, B. Graphene in the aquatic environment: Adsorption, dispersion, toxicity and transformation. *Environmental Science & Technology* **2014**, *48*, 9995-10009, doi:10.1021/es5022679.

201. Liu, X.T.; Mu, X.Y.; Wu, X.L.; Meng, L.X.; Guan, W.B.; Ma, Y.Q.; Sun, H.; Wang, C.J.; Li, X.F. Toxicity of multi-walled carbon nanotubes, graphene oxide, and reduced graphene oxide to zebrafish embryos. *Biomedical and Environmental Sciences* **2014**, *27*, 676-683, doi:https://doi.org/10.3967/bes2014.103.

202. Yousefi, M.; Dadashpour, M.; Hejazi, M.; Hasanzadeh, M.; Behnam, B.; de la Guardia, M.; Shadjou, N.; Mokhtarzadeh, A. Anti-bacterial activity of graphene oxide as a new weapon nanomaterial to combat multidrug-resistance bacteria. *Materials Science and Engineering: C* **2017**, *74*, 568-581, doi:http://dx.doi.org/10.1016/j.msec.2016.12.125.

203. Hahn, M.W.; O'Melia, C.R. Deposition and reentrainment of brownian particles in porous media under unfavorable chemical conditions: Some concepts and applications. *Environmental Science & Technology* **2004**, *38*, 210-220, doi:10.1021/es030416n.

204. Ntim, S.A.; Sae-Khow, O.; Desai, C.; Witzmann, F.A.; Mitra, S. Size dependent aqueous dispersibility of carboxylated multiwall carbon nanotubes. *Journal of environmental monitoring : JEM* **2012**, *14*, 2772-2779, doi:10.1039/c2em30405h.

205. Azizighannad, S.; Mitra, S. Stepwise reduction of graphene oxide (GO) and its effects on chemical and colloidal Properties. *Scientific Reports* **2018**, *8*, 10083, doi:10.1038/s41598-018-28353-6.

206. Ntim, S.A.; Sae-Khow, O.; Witzmann, F.A.; Mitra, S. Effects of polymer wrapping and covalent functionalization on the stability of MWCNT in aqueous dispersions. *Journal of colloid and interface science* **2011**, *355*, 383-388, doi:10.1016/j.jcis.2010.12.052.

207. Tian, L.; Meziani, M.J.; Lu, F.; Kong, C.Y.; Cao, L.; Thorne, T.J.; Sun, Y.-P. Graphene oxides for homogeneous dispersion of carbon nanotubes. *ACS Applied Materials & Interfaces* **2010**, *2*, 3217-3222, doi:10.1021/am100687n.

208. Li, J.; Tang, J.; Yuan, J.; Zhang, K.; Yu, X.; Sun, Y.; Zhang, H.; Qin, L.-C. Porous carbon nanotube/graphene composites for high-performance supercapacitors. *Chemical Physics Letters* **2018**, *693*, 60-65, doi:https://doi.org/10.1016/j.cplett.2017.12.052.

209. Torres, D.; Pinilla, J.L.; Suelves, I. Unzipping of multi-wall carbon nanotubes with different diameter distributions: Effect on few-layer graphene oxide obtention. *Applied Surface Science* **2017**, *424*, 101-110, doi:https://doi.org/10.1016/j.apsusc.2017.01.273.

210. Tung, V.C.; Chen, L.-M.; Allen, M.J.; Wassei, J.K.; Nelson, K.; Kaner, R.B.; Yang, Y. Low-temperature solution processing of graphene–carbon nanotube hybrid Materials for high-performance transparent conductors. *Nano Letters* **2009**, *9*, 1949-1955, doi:10.1021/nl9001525.

211. Lee, C.-Y.; Mitchell, D.R.G.; Molino, P.; Fahy, A.; Wallace, G.G. Tunable solution-processable anodic exfoliated graphene. *Applied Materials Today* **2019**, *15*, 290-296, doi:https://doi.org/10.1016/j.apmt.2019.02.008.

212. Kavinkumar, T.; Manivannan, S. Improved dielectric behaviour of graphene oxide-multiwalled carbon nanotube nanocomposite. *Vacuum* **2018**, *148*, 149-157, doi:https://doi.org/10.1016/j.vacuum.2017.11.019.

213. Min, C.; Liu, D.; Shen, C.; Zhang, Q.; Song, H.; Li, S.; Shen, X.; Zhu, M.; Zhang, K. Unique synergistic effects of graphene oxide and carbon nanotube hybrids on the tribological properties of polyimide nanocomposites. *Tribology International* **2018**, *117*, 217-224, doi:https://doi.org/10.1016/j.triboint.2017.09.006.

214. Georgitsopoulou, S.; Petrai, O.; Georgakilas, V. Highly conductive functionalized reduced graphene oxide. *Surfaces and Interfaces* **2019**, *16*, 152-156, doi:https://doi.org/10.1016/j.surfin.2019.05.010.

215. Gao, Y.; Jing, H.W.; Chen, S.J.; Du, M.R.; Chen, W.Q.; Duan, W.H. Influence of ultrasonication on the dispersion and enhancing effect of graphene oxide–carbon nanotube hybrid nanoreinforcement in cementitious composite. *Composites Part B: Engineering* **2019**, *164*, 45-53, doi:https://doi.org/10.1016/j.compositesb.2018.11.066.

216. Chaudhery Mustansar Hussain, a.C.S.a.S.M. Modifying the sorption properties of multi-walled carbon nanotubesvia covalent functionalization. *Analyst* **2009**.

217. Rocha, D.P.; Silva, M.N.T.; Cardoso, R.M.; Castro, S.V.F.; Tormin, T.F.; Richter, E.M.; Nossol, E.; Munoz, R.A.A. Carbon nanotube/reduced graphene oxide thin-film nanocomposite formed at liquid-liquid interface: Characterization and potential electroanalytical applications. *Sensors and Actuators B: Chemical* **2018**, *269*, 293-303, doi:https://doi.org/10.1016/j.snb.2018.04.147.

218. Cong, L.; Li, X.; Ma, L.; Peng, Z.; Yang, C.; Han, P.; Wang, G.; Li, H.; Song, W.; Song, G. High-performance graphene oxide/carbon nanotubes aerogel-polystyrene composites: Preparation and mechanical properties. *Materials Letters* **2018**, *214*, 190-193, doi:https://doi.org/10.1016/j.matlet.2017.12.015.

219. Youn, H.-C.; Bak, S.-M.; Park, S.H.; Yoon, S.-B.; Chul Roh, K.; Kim, K.-B. *One*-Step Preparation of Reduced Graphene Oxide/Carbon Nanotube Hybrid Thin Film by Electrostatic Spray Deposition for Supercapacitor Applications; 2014; Volume 20, pp. 975-981.

220. Wang, K.; Pang, J.; Li, L.; Zhou, S.; Li, Y.; Zhang, T. Synthesis of hydrophobic carbon nanotubes/reduced graphene oxide composite films by flash light irradiation; 2018.

221. Zhi, M.; Xiang, C.; Li, J.; Li, M.; Wu, N. Nanostructured carbon–metal oxide composite electrodes for supercapacitors: a review. *Nanoscale* **2013**, *5*, 72-88, doi:10.1039/C2NR32040A.

222. Huang, J.; Yang, X.; Her, S.-C.; Liang, Y.-M. Carbon nanotube/graphene nanoplatelet hybrid film as a flexible multifunctional sensor. *Sensors* **2019**, *19*, doi:10.3390/s19020317.

223. Fang, R.; Chen, K.; Yin, L.; Sun, Z.; Li, F.; Cheng, H.-M. The regulating role of carbon nanotubes and graphene in lithium-ion and lithium–sulfur batteries. *Advanced Materials* **2019**, *31*, 1800863, doi:10.1002/adma.201800863.

224. Park, H.; Ambade, R.B.; Noh, S.H.; Eom, W.; Koh, K.H.; Ambade, S.B.; Lee, W.J.; Kim, S.H.; Han, T.H. Porous graphene-carbon nanotube scaffolds for fiber supercapacitors. *ACS Applied Materials & Interfaces* **2019**, *11*, 9011-9022, doi:10.1021/acsami.8b17908.

225. Ding, B.; Guo, D.; Wang, Y.; Wu, X.; Fan, Z. Functionalized graphene nanosheets decorated on carbon nanotubes networks for high performance supercapacitors. *Journal of Power Sources* **2018**, *398*, 113-119, doi:https://doi.org/10.1016/j.jpowsour.2018.07.063.

226. Yousefi, N.; Lu, X.; Elimelech, M.; Tufenkji, N. Environmental performance of graphene-based 3D macrostructures. *Nature Nanotechnology* **2019**, *14*, 107-119, doi:10.1038/s41565-018-0325-6.

227. Foley, M. Utilizing nanoscale materials as dispersants, surfactant or stabilizing molecules, methods of making the same , and products produces therefrom. US 10,049,783 B2, 2018.

228. Wang, E.; Dong, Y.; Islam, M.D.Z.; Yu, L.; Liu, F.; Chen, S.; Qi, X.; Zhu, Y.; Fu, Y.; Xu, Z.; et al. Effect of graphene oxide-carbon nanotube hybrid filler on the mechanical property and thermal response speed of shape memory epoxy composites. *Composites Science and Technology* **2019**, *169*, 209-216, doi:https://doi.org/10.1016/j.compscitech.2018.11.022.

229. Dresselhaus, M.S.; Jorio, A.; Hofmann, M.; Dresselhaus, G.; Saito, R. Perspectives on carbon nanotubes and graphene raman spectroscopy. *Nano Letters* **2010**, *10*, 751-758, doi:10.1021/nl904286r.

230. Wang, K.; Pang, J.; Li, L.; Zhou, S.; Li, Y.; Zhang, T. Synthesis of hydrophobic carbon nanotubes/reduced graphene oxide composite films by flash light irradiation. *Frontiers of Chemical Science and Engineering* **2018**, *12*, 376-382, doi:10.1007/s11705-018-1705-z.

231. Sharma, N.; Sharma, V.; Jain, Y.; Kumari, M.; Gupta, R.; Sharma, S.K.; Sachdev, K. Synthesis and characterization of graphene oxide (GO) and reduced graphene oxide (rGO) for gas sensing application. *Macromolecular Symposia* **2017**, *376*, 1700006, doi:10.1002/masy.201700006.

232. Smith, E.A.M.; Liu, Y.; Stirling, C.; Watson, D.J.; Slade, R.C.T.; Chen, J.; Crean, C. Plasma functionalisation of few-layer graphenes and carbon nanotubes for graphene microsupercapacitors. *Electrochimica Acta* **2019**, *317*, 348-357, doi:https://doi.org/10.1016/j.electacta.2019.05.080.

233. Zhu, M.; Wu, J.; Wang, Y.; Song, M.; Long, L.; Siyal, S.H.; Yang, X.; Sui, G. Recent advances in gel polymer electrolyte for high-performance lithium batteries. *Journal of Energy Chemistry* **2019**, *37*, 126-142, doi:https://doi.org/10.1016/j.jechem.2018.12.013.

234. Cheng, X.; Pan, J.; Zhao, Y.; Liao, M.; Peng, H. Gel polymer electrolytes for electrochemical energy storage. *Advanced Energy Materials* **2018**, *8*, 1702184, doi:https://doi.org/10.1002/aenm.201702184.

235. Tong, X.; Tian, Z.; Sun, J.; Tung, V.; Kaner, R.B.; Shao, Y. Self-healing flexible/stretchable energy storage devices. *Materials Today* **2021**, doi:https://doi.org/10.1016/j.mattod.2020.10.026.

236. Wang, X.; Lu, X.; Liu, B.; Chen, D.; Tong, Y.; Shen, G. Flexible energy-storage devices: Design consideration and recent progress. *Advanced Materials* **2014**, *26*, 4763-4782, doi:https://doi.org/10.1002/adma.201400910.

237. Wadekar, P.H.; Khose, R.V.; Pethsangave, D.A.; Some, S. The effect of bio-inspired co-electrolytes for enhancement of electrochemical properties of supercapacitors. *Energy and Environmental Materials* **2020**, *3*, 429-435, doi:https://doi.org/10.1002/eem2.12097.

238. Bi, S.; Banda, H.; Chen, M.; Niu, L.; Chen, M.; Wu, T.; Wang, J.; Wang, R.; Feng, J.; Chen, T.; et al. Molecular understanding of charge storage and charging dynamics in supercapacitors with MOF electrodes and ionic liquid electrolytes. *Nature Materials* **2020**, *19*, 552-558, doi:10.1038/s41563-019-0598-7.

239. Zhang, L.; Hu, X.; Wang, Z.; Sun, F.; Dorrell, D.G. A review of supercapacitor modeling, estimation, and applications: A control/management perspective. *Renewable and Sustainable Energy Reviews* **2018**, *81*, 1868-1878, doi:https://doi.org/10.1016/j.rser.2017.05.283.

240. Poonam; Sharma, K.; Arora, A.; Tripathi, S.K. Review of supercapacitors: Materials and devices. *Journal of Energy Storage* **2019**, *21*, 801-825, doi:https://doi.org/10.1016/j.est.2019.01.010.

241. Suriyakumar, S.; Bhardwaj, P.; Grace, A.N.; Stephan, A.M. Role of polymers in enhancing the performance of electrochemical Supercapacitors: A Review. *Batteries and Supercaps n/a*, doi:https://doi.org/10.1002/batt.202000272.

242. Zhou, D.; Wang, F.; Yang, J.; Fan, L.-z. Flexible solid-state self-charging supercapacitor based on symmetric electrodes and piezo-electrolyte. *Chemical Engineering Journal* **2021**, *406*, 126825, doi:https://doi.org/10.1016/j.cej.2020.126825.

243. Park, Y.; Choi, H.; Kim, M.-C.; Tran, N.A.T.; Cho, Y.; Sohn, J.I.; Hong, J.; Lee, Y.-W. Effect of ionic conductivity in polymer-gel electrolytes containing iodine-based redox mediators for efficient, flexible energy storage systems. *Journal of Industrial and Engineering Chemistry* **2021**, *94*, 384-389, doi:https://doi.org/10.1016/j.jiec.2020.11.009.

244. Miao, L.; Song, Z.; Zhu, D.; Li, L.; Gan, L.; Liu, M. Recent advances in carbon-based supercapacitors. *Materials Advances* **2020**, *1*, 945-966, doi:10.1039/D0MA00384K.

245. Nam, H.-S.; Kwon, J.S.; Kim, K.M.; Ko, J.M.; Kim, J.-D. Supercapacitive properties of a nanowire-structured MnO2 electrode in the gel electrolyte containing silica. *Electrochimica Acta* **2010**, *55*, 7443-7446, doi:https://doi.org/10.1016/j.electacta.2010.02.027.

246. Wang, Q.; Li, J.; Wang, D.; Niu, J.; Du, P.; Liu, J.; Liu, P. Enhanced electrochemical performance of polyaniline-based electrode for supercapacitors in mixed aqueous electrolyte. *Electrochimica Acta* **2020**, *349*, 136348, doi:https://doi.org/10.1016/j.electacta.2020.136348.

247. Pal, B.; Yang, S.; Ramesh, S.; Thangadurai, V.; Jose, R. Electrolyte selection for supercapacitive devices: a critical review. *Nanoscale Advances* **2019**, *1*, 3807-3835, doi:10.1039/C9NA00374F.

248. Seol, M.-L.; Nam, I.; Sadatian, E.; Dutta, N.; Han, J.-W.; Meyyappan, M. Printable gel polymer electrolytes for solid-state printed supercapacitors. *Materials* **2021**, *14*, doi:10.3390/ma14020316.

249. Lu, N.; Na, R.; Li, L.; Zhang, C.; Chen, Z.; Zhang, S.; Luan, J.; Wang, G. Rational Design of antifreezing organohydrogel electrolytes for flexible supercapacitors. *ACS Applied Energy Materials* **2020**, *3*, 1944-1951, doi:10.1021/acsaem.9b02379.

250. Lu, X.; Jiménez-Riobóo, R.J.; Leech, D.; Gutiérrez, M.C.; Ferrer, M.L.; del Monte, F. Aqueous-eutectic-in-salt electrolytes for high-energy-density supercapacitors with an operational temperature window of 100 °C, from –35 to +65 °C. *ACS Applied Materials & Interfaces* **2020**, *12*, 29181-29193, doi:10.1021/acsami.0c04011.

251. Redda, H.G.; Nikodimos, Y.; Su, W.-N.; Chen, R.-S.; Jiang, S.-K.; Abrha, L.H.; Hagos, T.M.; Bezabh, H.K.; Weldeyohannes, H.H.; Hwang, B.J. Enhancing the electrochemical performance of a flexible solid-state supercapacitor using a gel polymer electrolyte. *Materials Today Communications* **2021**, *26*, 102102, doi:https://doi.org/10.1016/j.mtcomm.2021.102102.

252. Chodankar, N.R.; Dubal, D.P.; Lokhande, A.C.; Lokhande, C.D. Ionically conducting PVA–LiClO4 gel electrolyte for high performance flexible solid state supercapacitors. *Journal of Colloid and Interface Science* **2015**, *460*, 370-376, doi:https://doi.org/10.1016/j.jcis.2015.08.046.

253. Sandhiya, M.; Vivekanand; Suresh Balaji, S.; Sathish, M. Na_2MoO_4-Incorporated polymer gel electrolyte for high energy density flexible supercapacitor. *ACS Applied Energy Materials* **2020**, *3*, 11368-11377, doi:10.1021/acsaem.0c02299.

254. Liu, J.; Khanam, Z.; Ahmed, S.; Wang, H.; Wang, T.; Song, S. A study of low-temperature solid-state supercapacitors based on Al-ion conducting polymer electrolyte and graphene electrodes. *Journal of Power Sources* **2021**, *488*, 229461, doi:https://doi.org/10.1016/j.jpowsour.2021.229461.

255. Li, G.; Zhang, X.; Sang, M.; Wang, X.; Zuo, D.; Xu, J.; Zhang, H. A supramolecular hydrogel electrolyte for high-performance supercapacitors. *Journal of Energy Storage* **2021**, *33*, 101931, doi:https://doi.org/10.1016/j.est.2020.101931.

256. Zhu, W.-C.; He, P.-Q.; Tien, H.-C.; Liu, H.-L.; Chen, W.-C.; Lv, W.; Lee, W.-Y. Solvent-enhanced transparent stretchable polymer nanocomposite electrode for supercapacitors. *ACS Applied Energy Materials* **2021**, doi:10.1021/acsaem.0c02781.

257. Wang, Z.; Zhu, M.; Pei, Z.; Xue, Q.; Li, H.; Huang, Y.; Zhi, C. Polymers for supercapacitors: Boosting the development of the flexible and wearable energy storage. *Materials Science and Engineering: R: Reports* **2020**, *139*, 100520, doi:https://doi.org/10.1016/j.mser.2019.100520.

258. Ghasemi, M.; Fahimi, Z.; Moradlou, O.; Sovizi, M.R. Porous gel polymer electrolyte for the solid state metal oxide supercapacitor with a wide potential window. *Journal of the Taiwan Institute of Chemical Engineers* **2021**, *118*, 223-231, doi:https://doi.org/10.1016/j.jtice.2020.12.020.

259. Wang, X.; Hao, X.; Xia, Y.; Liang, Y.; Xia, X.; Tu, J. A polyacrylonitrile (PAN)-based double-layer multifunctional gel polymer electrolyte for lithium-sulfur batteries. *Journal of Membrane Science* **2019**, *582*, 37-47, doi:https://doi.org/10.1016/j.memsci.2019.03.048.

260. Alipoori, S.; Mazinani, S.; Aboutalebi, S.H.; Sharif, F. Review of PVA-based gel polymer electrolytes in flexible solid-state supercapacitors: Opportunities and challenges. *Journal of Energy Storage* **2020**, *27*, 101072, doi:https://doi.org/10.1016/j.est.2019.101072.

261. Fu, X.; Li, T.; Qi, F.; Zhang, S.; Wen, J.; Shu, W.; Luo, P.; Zhang, R.; Hu, S.; Liu, Q. Designing high electrochemical surface area between polyaniline and hydrogel polymer electrolyte for flexible supercapacitors. *Applied Surface Science* **2020**, *507*, 145135, doi:https://doi.org/10.1016/j.apsusc.2019.145135.

262. Prasanth, R.; Shubha, N.; Hng, H.H.; Srinivasan, M. Effect of poly(ethylene oxide) on ionic conductivity and electrochemical properties of poly(vinylidenefluoride) based polymer gel electrolytes prepared by electrospinning for lithium ion batteries. *Journal of Power Sources* **2014**, *245*, 283-291, doi:https://doi.org/10.1016/j.jpowsour.2013.05.178.

263. Hosseinioun, A.; Paillard, E. In situ crosslinked PMMA gel electrolyte from a low viscosity precursor solution for cost-effective, long lasting and sustainable lithium-ion batteries. *Journal of Membrane Science* **2020**, *594*, 117456, doi:https://doi.org/10.1016/j.memsci.2019.117456.

264. Al Saad, M.A.M.; Khider Salman, R.; Allah Ibrahim, N.M. Investigation of the useability of polyester protective cover for PVDF-based polymer gel electrolytes. *Materials Today: Proceedings* **2021**, doi:https://doi.org/10.1016/j.matpr.2020.12.289.

265. Quan, Y.; Chen, M.; Zhou, W.; Tian, Q.; Chen, J. High-performance anti-freezing flexible Zn-MnO_2 battery based on polyacrylamide/graphene oxide/ethylene glycol gel electrolyte. *Frontiers in Chemistry* **2020**, *8*, doi:10.3389/fchem.2020.00603.

266. Miao, H.; Chen, B.; Li, S.; Wu, X.; Wang, Q.; Zhang, C.; Sun, Z.; Li, H. All-solid-state flexible zinc-air battery with polyacrylamide alkaline gel electrolyte. *Journal of Power Sources* **2020**, *450*, 227653, doi:https://doi.org/10.1016/j.jpowsour.2019.227653.

267. Wang, Z.; Wu, Z.; Di Benedetto, G.; Zunino, J.L.; Mitra, S. Microwave synthesis of highly oxidized and defective carbon nanotubes for enhancing the performance of supercapacitors. *Carbon* **2015**, *91*, 103-113, doi:https://doi.org/10.1016/j.carbon.2015.04.045.

268. Yang, X.; Zhang, F.; Zhang, L.; Zhang, T.; Huang, Y.; Chen, Y. A High-performance graphene oxide-doped ion gel as gel polymer electrolyte for all-solid-state supercapacitor applications. *Advanced Functional Materials* **2013**, *23*, 3353-3360, doi:https://doi.org/10.1002/adfm.201203556.

269. Li, J.; Qiao, J.; Lian, K. Hydroxide ion conducting polymer electrolytes and their applications in solid supercapacitors: A review. *Energy Storage Materials* **2020**, *24*, 6-21, doi:https://doi.org/10.1016/j.ensm.2019.08.012.

270. Chen, Y.; Mitra, S. Fast microwave-assisted purification, functionalization and dispersion of multi-walled carbon nanotubes. *Journal of Nanoscience and Nanotechnology* **2008**, *8*, 5770-5775, doi:10.1166/jnn.2008.215.

271. Zhao, M.-Q.; Liu, X.-F.; Zhang, Q.; Tian, G.-L.; Huang, J.-Q.; Zhu, W.; Wei, F. Graphene/single-walled carbon nanotube hybrids: one-step catalytic growth and applications for high-rate Li–S batteries. *ACS Nano* **2012**, *6*, 10759-10769, doi:10.1021/nn304037d.

272. Azizighannad, S.; Intrchom, W.; Mitra, S. Raman imaging of membrane fouling. *Separation and Purification Technology* **2020**, *242*, 116763, doi:https://doi.org/10.1016/j.seppur.2020.116763.

273. Lu, C.; Chen, X. All-Temperature flexible supercapacitors enabled by antifreezing and thermally stable hydrogel electrolyte. *Nano Letters* **2020**, *20*, 1907-1914, doi:10.1021/acs.nanolett.9b05148.

274. Selvanathan, V.; Yahya, R.; Alharbi, H.F.; Alharthi, N.H.; Alharthi, Y.S.; Ruslan, M.H.; Amin, N.; Akhtaruzzaman, M. Organosoluble starch derivative as quasi-solid electrolytes in DSSC: Unravelling the synergy between electrolyte rheology and photovoltaic properties. *Solar Energy* **2020**, *197*, 144-153, doi:https://doi.org/10.1016/j.solener.2019.12.074.

275. Zulkifli, A.M.; Said, N.I.; Bakr Aziz, S.; Dannoun, E.M.; Hisham, S.; Shah, S.; Abu Bakar, A.; Zainal, Z.H.; Tajuddin, H.A.; Mohammed Hadi, J.; et al. Characteristics of dye-sensitized solar cell assembled from modified chitosan-based gel polymer Electrolytes Incorporated with Potassium Iodide. *Molecules* **2020**, *25*, doi:10.3390/molecules25184115.

276. Yilmaz Erdogan, P.; Zengin, H.; Yavuz, A. Growth and cycling of polyaniline electrode in a deep eutectic solvent: A new electrolyte for supercapacitor applications. *Solid State Ionics* **2020**, *352*, 115362, doi:https://doi.org/10.1016/j.ssi.2020.115362.

277. Eftekhari, A. The mechanism of ultrafast supercapacitors. *Journal of Materials Chemistry A* **2018**, *6*, 2866-2876, doi:10.1039/C7TA10013B.

278. Ur Rehman, H.; Shuja, A.; Ali, M.; Murtaza, I.; Meng, H. Evaluation of defects and current kinetics for aging analysis of PEDOT:PSS based supercapacitors. *Journal of Energy Storage* **2020**, *28*, 101243, doi:https://doi.org/10.1016/j.est.2020.101243.

279. Duan, J.; Tang, Q.; Li, R.; He, B.; Yu, L.; Yang, P. Multifunctional graphene incorporated polyacrylamide conducting gel electrolytes for efficient quasi-solid-state quantum dot-sensitized solar cells. *Journal of Power Sources* **2015**, *284*, 369-376, doi:https://doi.org/10.1016/j.jpowsour.2015.03.060.